eman ta zabal zazu

Universidad del País Vasco **Euskal Herriko Unibertsitatea**

Obtention and functionalization

of

cellulose nanofibers

from

Agave tequilana Weber var. azul
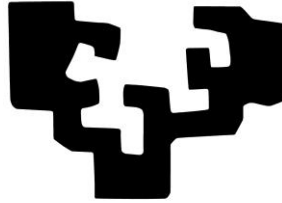
Eduardo ROBLES

Donostia 2017

eman ta zabal zazu

Universidad
del País Vasco

Euskal Herriko
Unibertsitatea

Obtention and Functionalization of Cellulose Nanofibers from *agave tequilana* Weber var. azul

A dissertation presented by

Eduardo Robles Barrios

In Fulfillment of the Requirements for the Degree
Doctor of Philosophy in Renewable Materials Engineering
by the University of the Basque Country UPV/EHU

Under the supervision of

Dr. Jalel Labidi

Chemical and Environmental Engineering Department
Engineering School of Gipuzkoa

Donostia-San Sebastián
2017

It was a summer of 2010, I was attending as an auditor to some lectures at the National Autonomous University of México when I received a letter from Dr. Jalel Labidi with the pertinent information to apply for a Masters course at the University of the Basque Country, UPV/EHU. Attached was a salute in a post-it which I still keep for myself as this signified for me the start of an exciting adventure, I am glad and proud that I had the chance to cover this path under his guidance. I studied engineering mechanics, therefore I had to learn again a lot of things in order to reach the same level that some of my mates had. It was not easy, but I won't lie, it was not hard, as I had the economical and moral support of my parents: Judit and Tocho. To them I owe everything I have and everything I could ever achieve, to them I owe my interest in life and things, and this curiosity that took me here. They made this possible, this is why, this work is dedicated to them, with its voids and mistakes, with the hurries in which was redacted, but with the love I profess to my work, with the passion that aflame my heart every time I have the chance to talk about it, and of course in the following pages, to write about it.

Ipan Donostitlàn, (1-ollin, 4-tecpatl)

Præfatio

Blue agave is one of the most important cultivars in Mexico, being the most important of the agave family which, on its behalf, is the second most important crop farmed throughout Mesoamerica, only after the whole growing-system called *milpa* (in Nahuatl: maize field) which itself constitutes or has constituted the base of Mesoamerican diet. Therefore, the importance of blue agave can be assumed as crucial in the everyday life of Mexican fields, so much that the Agave Landscape and Ancient Industrial Facilities of Tequila have been addressed as a cultural World Heritage Site by the UNESCO. There have also been concerns that loom because of the whole tequila industry depends on monocultivar farms with low germplasm, after waves of different epidemics have reduced the genetic diversity of the tequila agave. The responsibility that comes after being considered a World Heritage Landmark along with the mentioned critic state of the blue agave genetics has put this cultivar in the spotlight of Mexican scientific community overall, but also from different parts of the world, as the use of the plant should now imply a more efficient management of the tilled land.

The contribution of the present work lies in the knowhow of the Biorefinery Processes Group from the University of the Basque Country UPV/EHU, with particular focus in two aspects. One is the eco-friendly pulping processes of which organosolv constitutes perhaps the most studied in the Group. Second is the development of final-use applications. To enhance, or more simply, to change the surface properties of cellulose we decided to use an organosilane-based surface modification. Alcoxysilanes have been studied for many years and have been applied to a diversity of products, the present work takes the lead of such researches and goes on dealing with some application issues that have been addressed before, but the silanization of cellulose nanofibers represents, as far as we are concerned, a suitable, economic and (almost) eco-friendly option to furnish cellulose nanoparticles either for the well-known and delicate polymer-matrix reinforcement or for more technical applications.

This work follows four main steps, to extract native cellulose from sidestreams obtained from the tequila industry, to reduce the size of such native cellulose fibers which can be assumed as isolating smaller particles already present in the original cell-wall without dissolving or precipitating any kind of compound but only by chemical isolation or mechanical defibrillation of the so-called cellulose nanocrystals (or nanocrystalline cellulose, cellulose nanowhiskers, cellulose whiskers, etc) and cellulose nanofibers (or cellulose microfibers, microfibrillated cellulose, etc.); the third one consists in the cellulose nanoparticles modification for which we used two products one was an organic silane: 3-aminopropyl triethoxysilane and the other was a fatty acid: dodecanoyl chloride (or lauroyl choride); the final part consists in final applications of the extracted nanoparticles, either neat or modified. The presented applications are not related between each other, and the

purpose of this is to show how diverse they can be for these obtained nanoparticles. There is neither a logic nor optimized sequence between the studied extraction-modification-application processes, as each of them depended on availability of material, feasibility of the process and time at which such process should have been completed, we hope this can be understood by the reader, as the frequency of the ideas in human mind sometimes is not in synchrony with the pace at which the body (and the perks of the laboratory) can reach.

In the appendix the reader will find a guide for the characterizations performed, the equipments used and the different chemicals along with their corresponding supplier, there is also a table of abbreviations that can be of great use through the text. With these tools and the above advises the reader can continue, as for us, it only remains to wait and to expect that the following pages are both literary and scientifically satisfying for the reader.

With best regards,

Eduardo ROBLES

Jalel LABIDI

Content

I) Introduction

The agaves in Mexican culture

Figure I-1 Wild agave specimen in the Sierra del Tigre, Jalisco.

The word agave comes from the Greek *Αγαυή* who was a maenad, daughter of Cadmo king of Thebes and is interpreted as „admirable"[1]. The first botanist to describe the genus *Agave* was Carl Nilsson Linnæus, who in 1753 called it „Espèce Agave *Americana*"[2]. Although nowadays agave plants are common worldwide, they are native to the arid regions of Mexico and Southern United States (which once was also Mexico) and have been part of Mexican culture for over 10 000 years. The ways native people refers to these plants are different, and depending on the region it can be called *metl* (Nahuatl), *uadá* (Otomi), *doba* (Zapotec) or *akamba* (Purepecha) and since the arrival of Spanish people, the Caribbean voice *maguey* was first introduced and adopted as the most common word to call such plants around the world.

The term mescal or mezcal (from the nahuatl *mexcalli* 'cooked maguey' from *metl* 'maguey' and *ixcalli* 'cooked') has nowadays three interpretations: the common name given to certain agave species (this particularly in northern Mexico) originally, which consisted in the prepared meal obtained after cooking the stem and the leaf basis from different types of agaves; and the most used is to name the distilled beverage obtained from their fermented juices. The addition of the distillation process came with the Spanish and Portuguese settlers, who had just learned it from the Arabs and the alembics (from the arab *al-anbīḳ* and then from Greek *ἄμβιξ*, 'ambix') became common in the New Spain. This history, which is rich in life lessons achieved by the local communities which have been living from agaves since the beginning of the American population, entails a wide traditional know-how about the handling of these plants, therefore, the final product is the result of the used specie, the weather under which the plant was grown , the fermentation process, the distillation technique and the recipient in which it was aged, so that in each bottle are contained both the history of the land that observed its maturing and the knowhow of each farmer. The

interaction man-plant includes from the recollection and the exploitation of wild specimens to the farming of domesticated plants.

From a total of 210 agave species, Mexico owns 161, which compose about 3/4 of the total species, and moreover 119 are endemic to México. For mescal production there are at least 28 species used, 14 of which are used in commercial terms, eight are used locally and six more are used occasionally. The growing of agave plants for mescal production is done in many States; the final distilled product may come from one or several species. These species are distributed mainly through the Western, Central and Southern regions of Mexico, throughout the Western Mother Mountains, the Trans-Mexican Volcanic Belt. The Mexican States with most agave varieties are Oaxaca with 52 varieties, Durango and Puebla with 43, Sonora and Jalisco with 40, Coahuila with 35, Chihuahua with 34, San Luis with 33 and Nuevo Leon and Zacatecas with 29. *Agave vivipara* L is the most used among the agave species, and its distribution encompasses from the northern state of Sonora to Central America, the importance of *agave vivipara* is such, that it has more than 30 common names and 44 heterotypic synonyms including invalid and illegitimate botanical synonyms. For some authors, it was from this species that tequila (*agave tequilana*) and henequen (*agave fourcuoydes*) were domesticated.

The diversity of mescals in Mexico is a reflection of the biological diversity of the genus; such wealth of biodiversity, which is unique, should be protected in its importance as part of the biologic and cultural inheritance of the region.

There are three main beverages protected by origin designation: those are Bacanora in the northern State of Sonora, Mescal (or Mezcal) in Durango, Guerrero, Guanajuato, Michoacán, Oaxaca, Puebla, San Luis Potosí, Tamaulipas and Zacatecas; and Tequila, in the whole State of Jalisco and some regions of Michoacan, Guanajuato and Tamaulipas States, The approximate extension of each origin designations can be seen in Figure I-2.
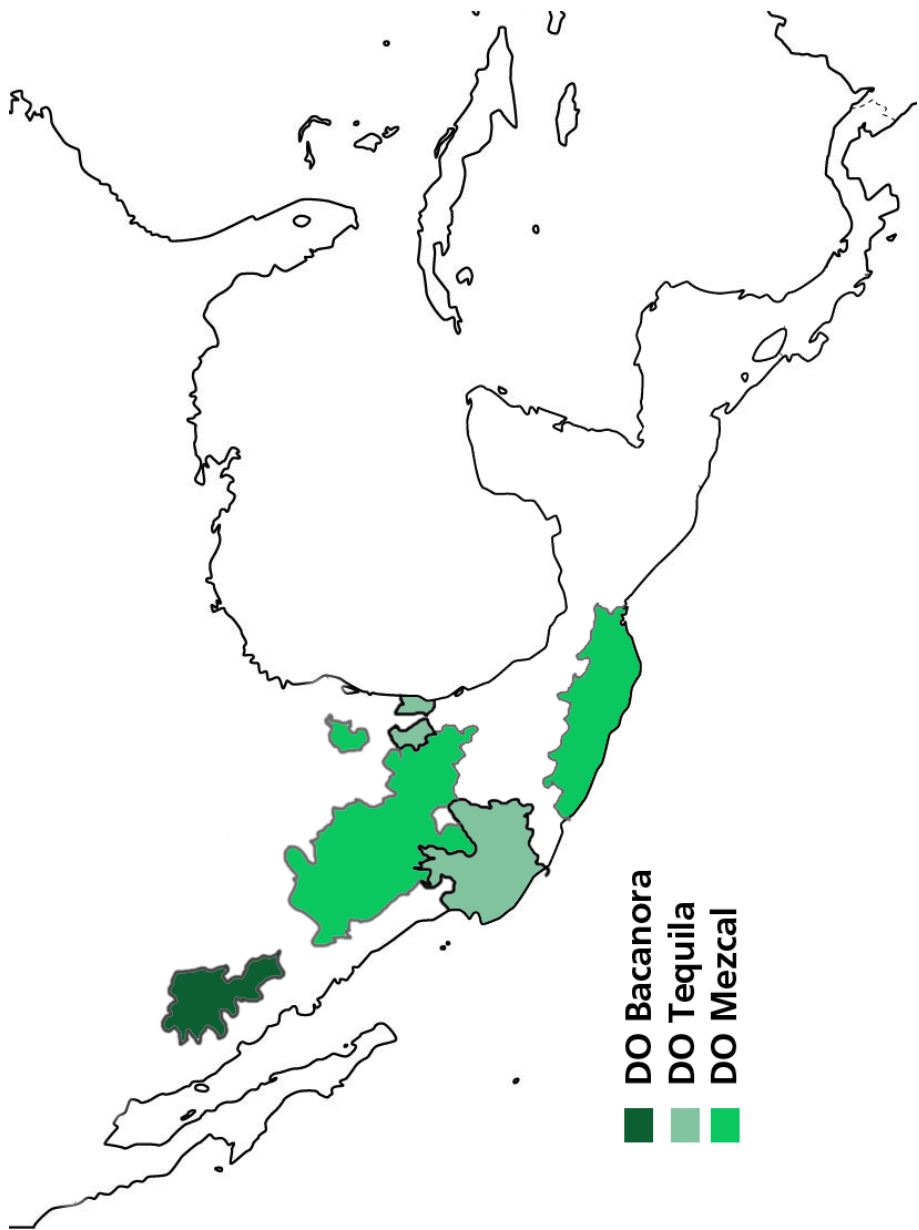
Figure I-2 Map showing the regions in which bacanora, tequila and mescal are under protected designation of origin (DO).

The blue agave

Maybe the most known agave worldwide, *Agave tequilana* Weber, was named after German-born French biologist Frédéric Albert Constantin Weber, who first described it in 1902[3], the description made by Weber has little changed until nowadays, with the main change corresponding to the family classification (stated as *Asparagaceae*) and the inclusion of a sub-family (*Agavoideae*), formerly the term *Agavaceae* was considered as a family by its own until the publication of the Angiosperm Phylogeny Group plant classification APG III in 2009[4].

Figure I-3 Blue agave fields with the Tequila volcano in the back, on the right side, La Rojeña facilities, now house to Casa Cuervo tequila factory.

Blue agave or tequila agave was made popular because of the location in which the first large-scale distilleries were set up in continental America: the town of Tequila. The first records that confirm the harvesting of blue mescal as well as its commerce in the city of Guadalajara date back to 1621. In 1695, Pedro Sánchez de Tagle y Pérez Bustamante, 2nd Marquis of Altamira introduced the farming of blue agave to the valley of Tequila, in which traditionally wild species were harvested from the rift, it is not known if the specie used by the Marquis of Altamira was native to the rift or if it was introduced from a different region, but since the end of the XVII century the distillation of agave juices started to extend through the region of Amatitán and Tequila along with sugarcane and fruit trees. The first registered taverns in which mescal wine from Tequila was sold were those of Pedro Sánchez de Tagle and Nicolás Rojas from La Rojeña (Figure I-3) it was during this century that the agave crops were translated from the rifts to the valleys and the tequila started to be sold in the taverns. During the XVII and XVIII centuries the Spaniards leaded the production of mescal wine from Tequila in the haciendas and ranchos, during the period in which agave-based haciendas constituted a well established model of hacienda. In 1795 José Cuervo was granted with the first license to produce „*mescal wine from Tequila"* by King Charles IV of Spain, which was later called „*mescal from Tequila"* and then simply tequila. These kind of distilled beverages, and tequila in particular, defined the hybrid character of nowadays

Mexico, by taking the juices from *metl,* identified with the goddess Mayahuel, who was also linked with the most traditional mother-earth worldview of native Mesoamericans, and mixing it with the costumes and technologies imported by the Spaniards to the western continent. Such beverages from mixed origin became a reason of pride for *criollo* and *mestizo* communities who no longer identified themselves with the native or immigrant people but were to compose the main Mexican identity which found in the mescal wine an important point of cohesion. The importance of agave haciendas in Mexico was such, that when Alexander von Humboldt and Aimé Bonpland visited Mexico they were impressed about how life revolved around agave plantations in the central-western Viceroyalty of New Spain and wrote in their report „*Voyage aux regions équinoxiales du Nouveau Continent*":

> „A very intoxicating brandy is formed from the pulque, which is called *mexical,* or *aguardiente de maguey.* I have been assured that the plant cultivated for distillation differs essentially from the common maguey, or maguey de pulque. It appeared to me smaller, and to have the leaves not so glaucous, but not having seen it in flower I cannot judge of the difference between the two species. The sugar-cane has also a particular variety, with a violet stalk, which came from the coast of Africa (*caña de Guinea*), and which is preferred in the province of Caracas for the fabrication of rum to the sugar-cane of Otaheite. The Spanish government, and particularly the real hacienda, has been long very severe against the *mexical*, which is strictly prohibited, because the use of it is prejudicial to the Spanish brandy trade. An enormous quantity, however, of this maguey brandy is manufactured in the intendancies of Valladolid, Mexico, and Durango, especially in the new kingdom of Leon. We may judge of the value of this illicit traffic by considering the disproportion between the population of Mexico and the annual importation of European brandy into Vera Cruz. The whole importation only amounts to 32,000 barrels! In several parts of the kingdom, for example in the *provincias internas* and the district of Tuxpan, belonging to the intendancy of Guadalaxara, for some time past the *mexical* has been publicly sold on payment of a small duty. This measure, which ought to be general, has been both profitable to the revenue, and has put an end to the complaints of the inhabitants."[5].

After the independence and the consecutive civil wars, the agave haciendas in Central Mexico were targeted by different armies, as source of food and money to continue the fight or as symbol of the regime they were fighting against: the Spaniard *hacendado* for the second half of the XIX century and the Mexican *latifundista* during the wars of the first loaf of the XX century. In western Mexico the cleverness of some local producers who were shrewd to choose the forces they supported, allowed them to survive throw the different civil wars of the XIX century. The situation of agave plantations was further deteriorated with the popularity gained by beer, taken to Mexico by German and Bohemian immigrants to the detriment of the then popular *pulque*, as well as the popularity gained by other spirits

that were „more sophisticated" to the detriment of *mescal*, which was considered a „low class beverage". It was until the post-war years of the XX century that mescal was rescued from oblivion and gained a renewed interest, with the intention to find a new identity which enclosed the whole Mexican population mescal, and tequila in particular, fitted perfectly the demand for a national beverage. This war further enhanced with the prohibition in the United States of America, which signified the end of the bourbon imports and gave an extra impulse to tequila production. Because of this new boom, producers from Tequila, Amatitán, Atotonilco and Arandas made several efforts to promote the consumption of tequila, with special mention of Francisco Javier Sauza, whose efforts resulted in the protection of their geographical indication gained in 1974 (both in Mexico and United States)[6] and in 1978 the Regulatory Council of Tequila Industry gained the certificate in the registry of 'tequila' in the *Registre International des appelations D'origine* from the World Intellectual Property Organization[7].
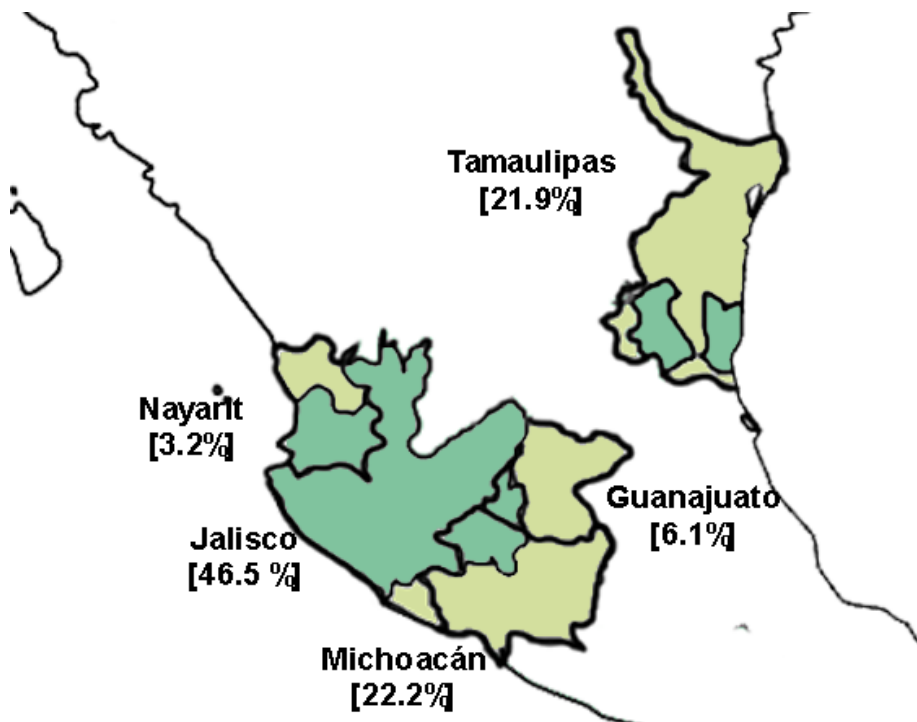
Figure I-4 Map showing the regions (dark blue) in which blue agave plants are farmed in their corresponding state (light green) within Mexico (white).

Following this, two main standards have been published by the Mexican official standard (*NOM, Norma Oficial Mexicana* in Spanish) to regulate the elaboration and commercialization process of tequila (NOM-006-SCFI) first published in 1993, updated in 1994, revised in 2005 and 2012 and currently under new revision (as of end of 2016)[8]. The second is related

to mescal in general (NOM-070-SCFI) first published in 1994, revised in 1997, 2004 and 2014 and currently under new revision (as of end of 2016)[9]. According to the current version of the NOM-006-SCFI, tequila is defined as „regional alcoholic beverage obtained by distillation and rectification of musts, prepared directly and originally from the obtained material, inside the factory location derived from the milling of the mature agave cores, previous or formerly hydrolyzed or cooked, and subjected to alcoholic fermentation with yeasts, cooked or not, being susceptible of being enriched by other sugars up to a share not beyond 49%, with the consideration that cold mixes are not allowed. Tequila is a liquid, which according to its type, it is colorless when bottled with no aging or yellowish when matured in oaken receptacles". This standard considers as tequila both tequila 100%, which is made from blue agave sugars exclusively, and the derivative beverage which contains no less than 51 % blue agave sugars. On the other hand, this beverage is produced exclusively in the Mexican state of Jalisco, as well as some municipalities of the states of Michoacan, Guanajuato, Nayarit and Tamapulipas. The full territory in which tequila is produced is marked in Figure I-4, along with the surface of blue agave cropped as fraction of the total blue agave surface in percent.

Blue agave taxonomy

Blue agave, and agaves in general, have suffered some changes in their taxonomic classification, current taxonomic rank for blue agave (2016) is as shown in Figure I-5.
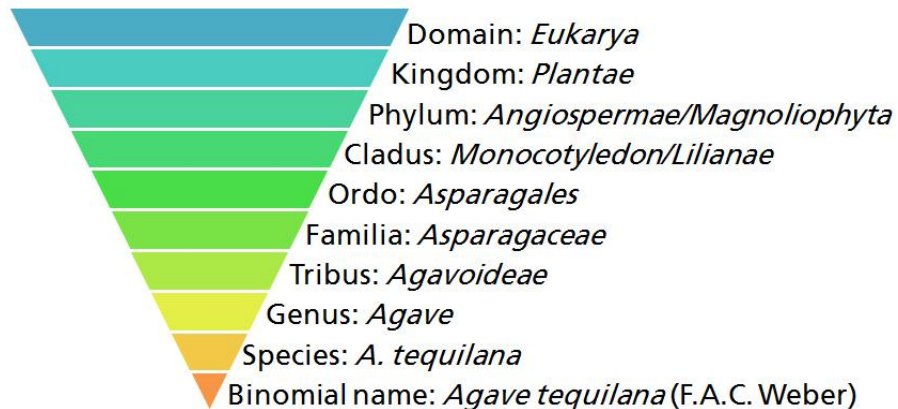
Figure I-5 Taxonomy rank of the blue agave as of 2017.

Besides the official binomial name, blue agave has several accepted synonyms which include the homotypic synonym (even with the *vivipara-angustifolia* controversy): *Agave angustifolia* subsp. *tequilana* F.A.C. Weber[10] and several heterotypic synonyms mainly those compiled by the Belgian botanist Rafaël Govaerts for the Royal Botanical Gardens and listed in the World Checklist of Selected Plant Families (WCSP), these accepted synonyms belong all to descriptions made by American botanist William Trelease, and include: *Agave palmeris* Trel.[11,12], *Agave pedrosana* Trel.[11], *Agave pes-mulae* Trel.[11] and *Agave pseudotequilana* Trel. (WCSP)[11].

Blue agave morphology

It is a succulent plant that grows radically between 120 and 180 cm high, stalks are short and thick with height ranging between 30 and 50 cm when mature, while leaves can reach lengths between 90 and 120 cm. Leaves are in general glaucous or grayish green and have lanceolate shape tapering to a point at the end which consists of a 1-2 cm needle, leaves fibers are steady almost always rigidly stretched, concaves, from 0 to 90 degrees. Leaves have their wider part at half its length while at the base they are generally narrow and thick, apices are acuminated, thin and curved, generally straight but also can be curved. The leaf margin ranges from straight to sinuous with almost homogeneously scattered teeth (3-6 mm) which are brown as it is the needle, limbs are wide, dark brown and are in general decurrent. Average weight varies considerably depending on the soil, the age and the climatic conditions during the growth of the plant, but within the registered plants, average weight is between 18 and 35 kg (Figure I-6).

Core: Used for tequila production

Leaves: Used poorly
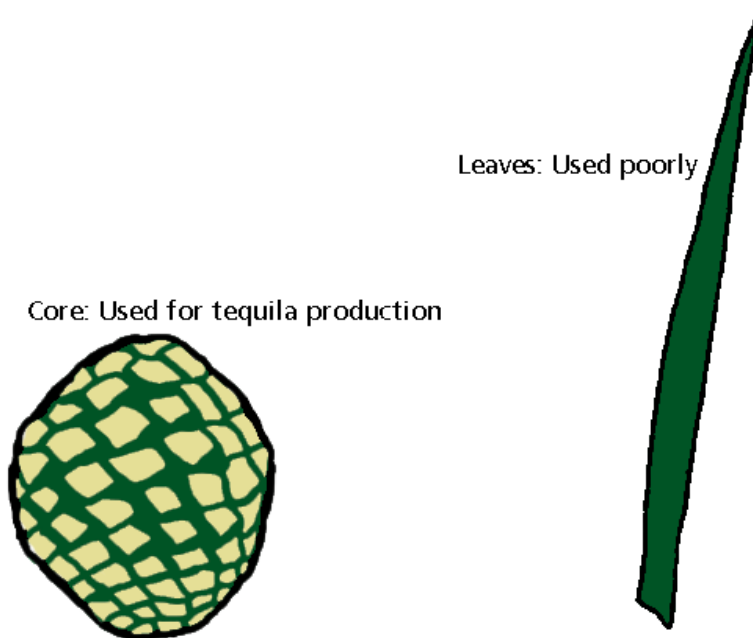
Figure I-6 Diagram of the two main parts of the blue agave plant.

Blue agave is one of the most abundant agricultural products in western Mexico, in which tequila is produced from this plant. Cores represent up to 54% (on wet weight basis) of the blue agave plant while leaves can be up to 36%; after extracting sugars from the core, bagasse is then left after being cooked, shredded and milled thus being an undervalued product[13]. The sugars used during the tequila production process are mainly extracted from their hemicelluloses content, remaining a waste with high amount of cellulose and lignin.

Blue agave inventory and current research

As far as 2011, the National Regulator Council for Tequila Industry (CRT) had registered 235 033 239 plants on Mexican soil. While plant consumption in the last years has been 880.6 thousands of tones in 2012, 756.9 in 2013 788.2 in 2014, 788.9 in 2015 and 701.8 in 2016 (as of September), the full consumption since 1995, the first year after NOM-006 and the refunding of the CRT, is displayed in Figure I-7, it can be seen a considerable decrease between 1999 and 2004, with a further high peak between 2007 and 2008, and with a market being considerably stable since 2013[14]. In this sense, the utilization of these agricultural down-streams has currently been considered for the production of other products, concretely, novel works have been based on the obtaining of value-added products from its sugars, which resulted rich in inulin, a type of sugar that is harder to break in the digestives system.
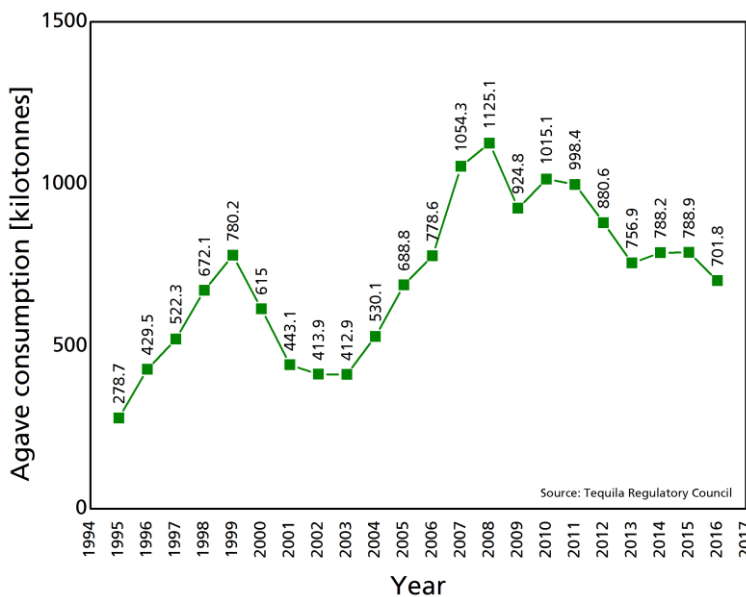
Figure I-7 Tones of agave used for tequila production (tequila and tequila 100%).

Figure I-8 shows a chart with the scientific publications in which blue agave is involved, it shows an increase on the interest from the scientific community to consider this plant for their researches, however, as it can be seen in Figure I-9, most of research is focused on agricultural and biological aspects of the blue agave, with a very low diversity of the current germoplasm (every blue agave nowadays descents from small quantity of plants that survived a terrible plague) the resistance of the plant is vital for the sustaining of the industry, but paradoxically, engineering and materials science has been left apart, as they represent less than 10% of the publications.
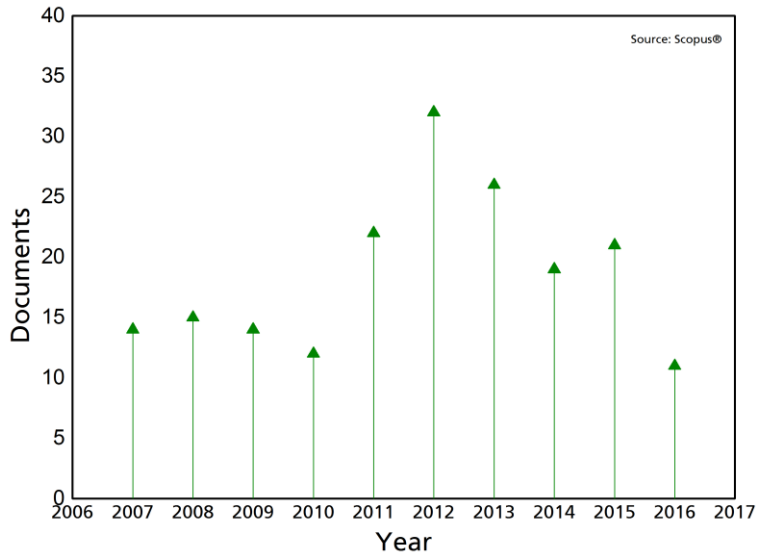
Figure I-8 Scientific publications by number of documents per year.

The diversification of the products obtained from a plant, as well as the cascading of the processes through which they are obtained play a crucial role in the sustainability of agroindustry, and especially if the main product obtained does not constitute a primary commodity, as it can be a distilled beverage, and with a large amount of families depending from monocultivar farming, the development of such value-added products should be in the interest of both authorities and farmers. On the other hand, the availability of agroindustrial by-products which are already generated releases the pressure for new cultivars for biorefinery processes, as the biomass cost is low. This can boost the competitiveness of the bio-based materials, as the biorefining still represents a strong investment.
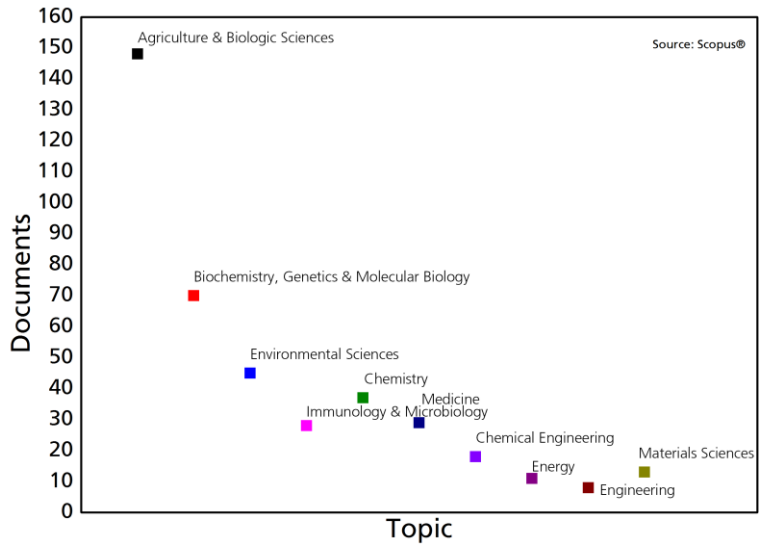
Figure I-9 Scientific publications by topic and number of documents corresponding to the last 10 years.

Biomass

Lignocellulosic materials

Lignocellulosic biomass refers to the three-dimensional polymeric composite material that composes the plant dry matter. It consists mainly of carbohydrate polymers (cellulose, hemicelluloses) and an aromatic polymer (lignin), together they constitute the structural components of plants and along with non-structural compounds form the plant cell wall[15]. The proportion of these compounds in the different lignocellulosic materials depends primarily on the species, the plant tissue and the growth conditions. The cell walls of herbaceous dicots, woody dicots, monocot grasses, and woody gymnosperms, plant groups that include most species being targeted as candidate biomass feedstocks for sustainable biofuel production, have clearly distinguishable compositions, as demonstrated by chemical analyses[16,17]. For instance, the walls of commelinoid monocots (e.g. the grasses), in comparison with those of dicots, non-commelinoid monocots, and gymnosperms, mainly differ in the relative abundances of non-cellulosic polysaccharides and their associations/linkages[17–19]. Primary walls in grasses are characterized by the significant abundance of the hemicellulosic polysaccharides, glucuronoarabinoxylans and mixed-linkage glucans, with relatively minor proportions of xyloglucans, pectic polysaccharides, and structural proteins such as arabinogalactan proteins. In contrast, dicot and gymnosperm primary walls, in general, are characterized by a greater abundance of xyloglucans in the former, and mannans and glucomannans in the latter as the predominant hemicelluloses, and relatively higher abundances of pectic polysaccharides and structural proteins[17]. Secondary walls vary considerably in structure and composition from primary walls, typically containing a higher proportion of cellulose and less pectic polysaccharides, with the predominant non-cellulosic components in secondary cell walls of grasses and woody dicots being xylans and lignin, with glucomannans also present to a small extent in woody dicots[17]. Lignin and hemicelluloses are also the major non-cellulosic components of secondary walls in woody gymnosperms; however, galactomannan and glucomannan are more prominent hemicelluloses in these walls in addition to xylan[16,20,21]. Lignin compositions, in general, also vary among plant families[22]. Woody dicot and monocot grass lignins contain predominantly guaiacyl (G) and syringyl (S) units with traces of hydroxyphenyl (H) units; the grasses typically contain higher levels of H units. In contrast, woody gymnosperm lignins are primarily composed of G units with lower amounts of H units[23].

Plant cell wall

Nägeli described the plant cell wall as composed of ultra-microscopic particles to which he gave the name 'micelles', and which were regarded as discrete units, more or less like the bricks in a masonry wall. In order to explain the shrinkage of wood it was assumed that water entered or left the intermicellar spaces, pushing the micelles farther apart or allowing them to come nearer together, and the elongated shape of the micelles was held to account

for the difference between longitudinal and transverse shrinkage; the optical anisotropy of the cell wall was referred to the optical properties of the micelles themselves[24]. Some revision of the statement of Nägeli was however found necessary, and a large body of workers rejected the conception completely, postulating instead a system of continuous or connected cellulose threads or layers. As neither conception was completely satisfactory, further researchers tried to propose a compromise between both from the point of view of physicists, chemists and botanists, with particular mention of Frey-Wyssling and Clarke[25–28].

As conclusion of many years of research and discussion, in which the gaps between the information available by ultraviolet and visible light wavelengths (which allow to identify larger particles) and X-ray (smaller particles) had to be filled with inferences and conjectures, cellulose was recognized as the structure, the framework substance of plant cell-wall. This because of its capacity to form long threads or chain-like molecules arranged in a form that is parallel to the cell axis with indeterminate lengths because of their molecular weight and the associated chain-molecules length which does not conform a unitarian 'cellulose molecule' as the evidence has proven the uncontinuous character of the above mentioned cellulose-chains. On the other hand, cellulose has since many years showed a paracrystalline character, as it has been stated by X-ray diffraction in several works in which a definite crystal structure has been observed, but it has never been confirmed a definite crystalline form. Furthermore, cellulose is insoluble in all the usual chemical solvents.

Plant fibers may be completely delignified without disintegration, so that the cellulose apparently forms a continuous system throughout the cell-wall. It is also possible to remove the cellulose from the cell walls of some tissues, leaving behind what is presumed to be a continuous skeleton of lignin. In consequence, the cell wall is regarded as having continuous and interpenetrating systems of cellulose and lignin. The structure has been likened to reinforced concrete, in which the iron strands represent the cellulose framework and the concrete the lignin and other substances.

From x-ray powder diffraction patterns, the impression is that the cellulose chain molecules occur in discrete aggregates of about 50 Å in diameter and more than 1000 Å in length which are known as fibrils. This impression is given by both dry and water-saturated material, and it would therefore appear that water penetrates between the aggregates without disturbing their internal crystalline structure. In consequence, they have been regarded as corresponding to micelles, and they are so named, albeit with a somewhat different meaning from that of Nägeli. The cellulose system is therefore visualized as continuous, and yet able to give the impression of being composed of discrete micelles under XRD examinations.

Intermicellar system is mostly occupied by lignin, hemicelluloses and other minor components, which are non-crystalline and have little or no influence on the tensile strength of the cell-wall, nevertheless they form a continuous system within the cell-wall; however, they do have influence under compression stress and increase the rigidity. These intermicellar spaces vary widely in size, and can reach over twice the diameter of the micelles, which on their own have also varying sizes, as they form aggregates called 'microfibrils'.
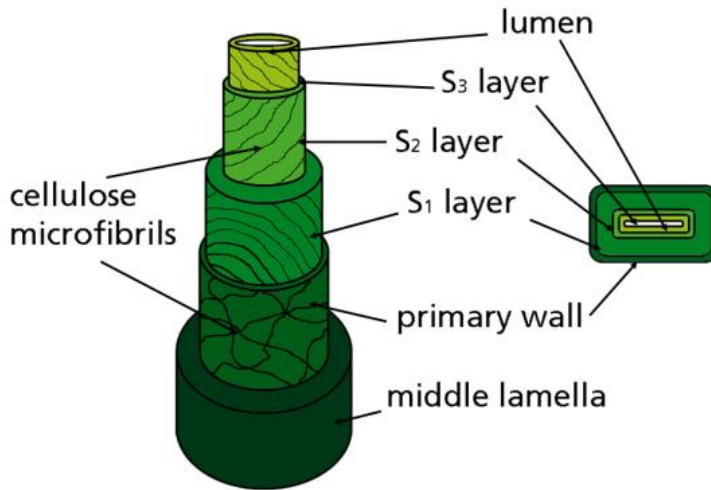
Figure I-10 Three-dimensional structure of the plant cell wall.

Cell-wall is composed of three main regions, namely the middle lamella, secondary wall and primary wall. The middle lamella, or intercellular substance, is an amorphous, isotropic material formed from the cell plate at cell division, and is shared by adjacent cells; is very thin, completely isotropic and composed largely if not entirely, of polyuronides. The primary wall is developed from the cambial wall; it is anisotropic, and is composed of cellulose, with large proportions of hemicelluloses, pectin substances and lignin. It is laid down during the period in which extension growth takes place, and this is reflected in the structure of the cellulose framework, it is capable of growth and extension and has the capacity for under-going reversible changes in thickness. The secondary wall is composed of cellulose, or of varying mixtures of cellulose, hemicelluloses, lignin, pentosans, etc. it is added by apposition during growth and it has usually three different layers. Cells having secondary walls lose their potentiality for growth and enlargement[29]. The layers of the secondary cell wall are usually tree: an outer layer (S1) which is 0.1-0.3 µm, a middle layer (S2) and has 1-5 µm and the least frequent inner layer (S3) which is the thinner having only 0.1 µm. The cellulose fibrillar units in these layers are arranged at a particular angle to the

cell axis on account of differences in the refractive index of cellulose, therefore, in the S1 layer cellulose strands are arranged in a crossed fibrillar structure, in the middle layer they are approximately parallel to the cell axis and in the S3 layer cellulose units have a flat spiral orientation[28]. A simplified picture of the organization of a typical softwood tracheid or hardwood fiber is seen in Figure I-10.

Carbohydrate polymers (Polysaccharides)

As a cell is growing, the primary cell wall layer, composed of cellulose fibers in a matrix of hemicelluloses and pectin, is first secreted; hemicelluloses bind to the surface of the cellulose microfibrils, while pectin cross-links the hemicelluloses molecules of adjacent microfibrils. Glycoproteins, a minor constituent of the cell wall, are also thought to be involved in the cross-linking. During cell growth, enzymes reduce the yield strength of the primary cell walls, allowing significant deformation under the pressure within the cell. Once growth is complete, the stiffness and strength of the cell wall increases, and adjacent cells are bound together by the middle lamella, which is initially high in pectin.

After cell growth is complete, a number of additional processes may occur[30,31]. In some plant materials, such as wood and palms, additional secondary layers, with cellulose fibers in a matrix of lignin and hemicelluloses, are deposited. Lignification of the secondary cell wall layers increases their stiffness and strength compared with unlignified primary layers. In some mature plant cells, such as in wood, the protoplast itself may die, but the remaining cell walls continue to provide mechanical support, while the lumen allows transport of water and other nutrients. With age, both the middle lamella and the primary cell wall may become lignified and less distinct, so that the middle lamella and its two neighboring primary cell walls are collectively known as the compound middle lamella[30].

Cellulose

Cellulose is one of the most abundant and renewable organic polymers from biomass in the biosphere[32–35]. It is a polysaccharide composed exclusively of celobiose units, which are formed by two glucose molecules. The properties of cellulose including good mechanical properties, low density and biodegradability have contributed to a rising interest in this material[36]. Cellulose is the structural material of the fibrous cells with high levels of strength and stiffness per unit weight[37–40], and has a straight carbohydrate polymer chain consisting of β-1-4 linked D-glucose units and a degree of polymerization (DP) of about 10,000[41]. Hydroxyl (–OH) groups in cellulose structures play a major role in governing the reactivity and physical property of cellulose Microcrystalline cellulose bundles of crystallites with different particles have attracted attention as a starting material for nanocomposites[42]. Microcrystalline cellulose has been used as a reinforcing filler and binder for the extrusion/spheronization process. The origin of the raw materials and the manufacturing process decisively influence the characteristics of the extracted microcrystalline cellulose[43,44].
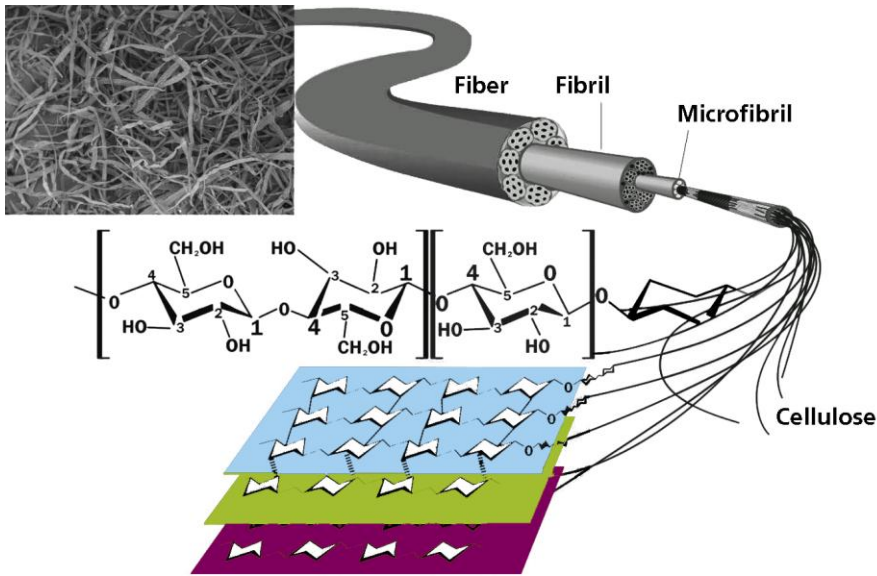
Figure I-11 Cellulose fiber structure.

In addition, molecules of cellulose are long chained and tend to form crystalline regions separated by paracrystalline regions. Although glucose is the monomeric unit within the cellulose molecule. Cellobiose is the repeating disaccharide, since molecules of glucose within the chain are alternately rotated 180°. Thermodynamic theory indicates that cellulose can take on two different polymeric configurations, though only one is assumed by native cellulose within cell walls. One of these, the extended-chain configuration, is that of native cellulose, while the folded-chain configuration occurs when cellulose is chemically extracted from cell walls and when polymerization and crystallization do not occur simultaneously[31].

In its native crystalline state, cellulose exists as an extended-chain polymer; the unit cell within the crystal lattice consists of antiparallel chains that are stabilized by interchain hydrogen bonding (Figure I-11). Cellulose is totally insoluble in water. It is polydisperse linear homopolymer[45], The unit cell has been measured and has the dimensions of 0.835 X 1.03 x 0.79 nm. This polymeric configuration is lost when cellulose is extracted and recrystallized. Under these conditions the cellulose molecule takes on the folded-chain configuration, which is substantially less strong when placed in tension. The differences in the material properties of the extended-chain and folded-chain configurations of cellulose and the failure to appreciate which of these two configurations is represented by native cellulose led early workers to erroneous conclusions concerning the physical biology of plant cell walls.

Hemicelluloses

Hemicelluloses are amorphous low-molecular weight polysaccharides and make up around 25 wt% of the biomass. These carbohydrate polymers are of lower molecular weight than cellulose, with a degree of polymerization around 100–200[46]. Hemicelluloses are composed of both hexose and pentose sugars; the C6 sugars are mainly glucose, mannose, galactose and the C5 sugars xylose and arabinose. Hemicelluloses are usually considered to be structural polysaccharides and are associated in plant tissues with cellulose, where they act as a linkage between cellulose and lignin. Hemicelluloses are thought to bind non-covalently to the surface of cellulose fibrils. They act as an amorphous matrix material, holding the stiff cellulose fibrils in place. It has been suggested that the substitution with hydrophobic groups such as acetyl and methyl groups enhances the affinity of hemicellulose to lignin and thus aids the cohesion between the three major lignocellulosic polymers[47]. The chemistry of wood hemicelluloses has been discussed in several reviews[48,49], as have methods used in hemicellulose research[46,50].

Hemicellulose polymers can be branched and may be garnished with functionalities such as acetyl and methyl groups, cinnamic, glucuronic and galacturonic acids. The content of all those components differ considerably depending on the source of the feedstock[51]. It is convenient to include among them a few other plant polymers, such as the arabinogalactans, which obviously have other functions Hemicelluloses from vascular land plants are built up from relatively few sugar residues, the most common of which are D-xylose, D-mannose, D-galactose, D-glucose, L-arabinose, 4-0-methyl-D-glucuronic acid, D-galacturonic acid, and D-glucuronic acid. Among the more rare constituents are L-rhamnose, L-fucose, and various methylated, neutral sugars[46]. The main chain of galactoglucomannan, a branched hemicellulose found in softwood, is built from (1→4)-linked β-D-glucopyranosyl and (1→4)-linked β-D-mannopyranosyl units. The mannosyl units are also substituted to some extent by both acetyl groups in the C-2 and C-3 position and by a (1→6)-linked α-D-galactopyranosyl units[52].

The most common hemicellulose sugar in grasses and hardwood is xylose. In softwood, annual plants and cereals mannose is the major hemicellulose sugar. Due to its non-crystalline nature, hemicellulose is more susceptible to depolymerization than cellulose (especially in acidic conditions), an aspect of its behavior that is exploited by many deconstruction strategies[53]. They can be removed from the original or delignified tissue by extraction with aqueous alkali or, less frequently, with water.

Pectin

Pectin or pectic substances are collective names for a group of closely associated polysaccharides; it is one of the major plant cell wall components and probably the most complex macromolecule in nature, as it can be composed out of as many as 17 different monosaccharides containing more than 20 different linkages. In a plant, pectin is present in

the middle lamella, primary cell and secondary walls and is deposited in the early stages of growth during cell expansion[54]. Its functionality is quite divers. First, pectin plays an important role in the formation of higher plant cell walls[55], which lend strength and support to a plant and yet are very dynamic structures[54]. Second, pectin influences various cell wall properties such as porosity of the walls which has relevance in the control of the permeability of the walls for enzymes; surface charge, pH, and ion balance and therefore is of importance to the ion transport in the cell wall due to their anionic nature[56]. Furthermore, pectin oligosaccharides are known to activate plant defense responses: they elicit the accumulation of phytoalexin which has a wide spectrum of anti-microbial activity[57–59]. Finally, pectin oligosaccharides induce lignification[60] and accumulation of protease inhibitors[61] in plant tissues. They also contribute to complex physiological processes like cell growth and differentiation; therefore they determine the integrity and rigidity of plant tissue. Pectin plays an important role in the defense mechanisms against plant pathogens and healing properties. As constituents of plant cell wall pectins also determine the water holding capacity[62].

Lignin

The term lignin is derived from the Latin word *lignum* which means wood[63]. Lignin is among the most abundant biopolymers on earth, constituting approximately 30 wt% of the dry weight of softwoods and 20 wt% of hardwood. Most of the lignin is located in the middle lamella, where it serves the purpose of cementing the fibers together strengthening plant cell walls. The remaining part occurs throughout the secondary wall, where it interpenetrates and encrusts the cellulose microfibrils and the hemicelluloses providing resistance against microbial attack, and playing a crucial part in water transport by reducing cell wall permeability[64]. Cellulose, hemicelluloses, and lignin can be classified from a morphological point of view as framework, matrix, and entrusting substances, respectively[65].

Lignin is an amorphous, three-dimensional, complex biopolymer comprised of three phenylpropanoid units (monolignols), namely syrapyl alcohol (S), coniferyl alcohol (G), and *p*-coumaryl alcohol (H). The initial dehydrogenation reaction of the monolignols (H, G or S) is promoted by peroxidases and laccases, and consists in the removal of the phenolic hydrogen atom from the precursors leading to phenyl radicals, which by non-enzymatic and random radical-radical coupling produce a three dimensional amorphous polymer which forms a randomized structure inside the cell walls[66].

Despite of having a randomized structure, there are some common linkages that are repeated throughout the lignin structure: β-O-4 aryl ether bonds, β-5-phenylcourmaran, 5-5´biphenyl, 4-O-5-diarylether, β-1(1,2-diarylpropane), α-O-4-aryl ether and β-β´-resinol linkages. Depending on its source lignin structure presents different concentrations of phenylpronanoid units. In softwood lignin, usually referred as guaiacyl lignin, the structural elements are derived principally from coniferyl alcohol (G) and traces of *p*-coumaryl alcohol

(H). On the other hand, hardwood lignin, known as guaiacyl-syringyl lignin, is comprised of derived units of coniferyl and sinapyl alcohol (S) with different ratios. Grass lignins are also classified as guaiacyl-syringyl lignins, but they additionally contain significant amounts of structural elements derived from *p*-coumaryl alcohol[67]. The proportion of the linkages also varies among lignin of different sources.

Extractives

They derive their name as these compounds are easily extracted by different organic solvents without any kind of chemical reaction[68]. Extractives are formed by a very wide heterogeneity of chemicals mainly consisting in low molecular weight carbohydrates, terpens, tanins, steroids, waxes, aliphatic acids, aromatic compounds, phenols[68]. The extractives protect the plant against fungi attack and also have antioxidant properties being excellent free radical scavengers[69].

Proteins

In plant cell wall there is a little amount of proteins inherent to the biological origin. They have different physico-chemical properties, they may interact with other cell wall components and their relative abundance is variable[70]. In plant cell walls proteins compose 5-10 % of the dry weight of the primary cell wall while the rest 90-95 % is composed of polysaccharides. At the end of growth, specialized cells may synthesize a lignified secondary wall composed of ~65 % polysaccharides and ~35 % lignin[71]. The proteins are essential in controlling cell wall extensibility and structure modification, cell wall metabolism, cell enlargement, signaling, responses to abiotic and biotic stresses, and many other physiological processes[72,73], they also contribute to signaling by interacting with plasma membrane receptors or by releasing signal molecules such as peptides or oligosaccharides[74].

Inorganic compounds

Plants absorb the inorganic compounds that can be found in the soils and fix them in their cell wall. These inorganic minerals are low molecular weight and simple compounds like, silicates, carbonates, phosphates, nitrates, sulfates, sulfites, calcium, potassium[75]. The quantity of inorganic matter in lignocellulosic biomass varies not only among different species but also within different parts of the plant. Usually, it is higher in foliage than in the bark tissues and has the lowest value in the wood tissues[76].

Biorefinery processes

Definition

The term biorefinery has not a widespread definition, and several attempts to englobe all the aspects related to this concept have been made not without debate, but the overall goal of the biorefinery production approach is the generation of a variety of goods from different biomass feedstocks, within particular facilities, through a combination of technologies. Ideally, a biorefinery should integrate biomass conversion processes to produce a range of fuels, power, materials, and chemicals from biomass[77]. Biorefinery was defined in the year 1997 as follows: green biorefineries represent complex (to fully integrated) systems of sustainable, environment and resource friendly technologies for the comprehensive utilization and the exploitation of biological raw materials in the form of green and residue biomass from a targeted sustainable regional land utilization[78]. The term used originally in Germany "complex construction and systems" was substituted by "fully integrated systems". The United States Department of Energy, in its Energy, environmental, and economics (E3) handbook, uses the following definition: a biorefinery is an overall concept of a processing plant where biomass feedstocks are converted and extracted into a spectrum of valuable products, based on the petrochemical refinery[79].
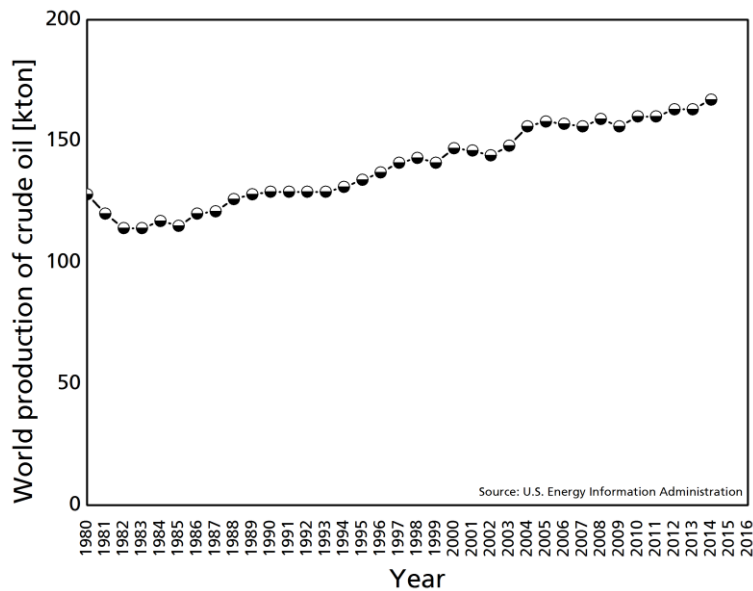

Figure I-12 World production of crude oil since 1980.

Traditionally, the proposal to use biorefineries has had a boost from the crude oil crisis at the beginning of the XXI century (Figure I-12), but the development of new technologies and the finding of new oil fields has brought the crude oil production to high levels and

predictions say that the trend is for it to continue increasing. Therefore, to make biorefineries competitive the fear to oil exhaustion is no longer a valid argument to promote the biorefineries to get fuels chemicals and materials, in this sense, the term 'fully integrated systems' results attractive, as the optimization of the agroforestry exploitation is an undeveloped issue that can represent an attractive investment, not only economically, but also technologically, as the challenge to design such integrated systems represents a new research field for agricultural, chemical and materials engineering, with the possibility to develop multidisciplinary combined processes. Technically feasible separation, which would allow the separate use or subsequent processing basic compounds, has existed until now only in the form of initial attempts. The resulting products of these 'biotechnological products' can then be called 'biorefinery product' term that includes both 'biobased products' and 'bioenergy'[80]. Many of the currently used, industrially made 'biobased products' are the result of a direct physical or chemical treatment and processing of biomass, such as cellulose, starch, oil, protein, lignin and terpene. By 'biotechnological processes' and methods, feedstock chemicals are produced, such as ethanol, butanol, acetone, lactic acid and itaconic acid, and amino acids, e.g. glutaminic acid, lysine and tryptophan[80].

Biorefinery phases

Depending on the applied technology biorefineries can treat different feedstock and can be classified in three different types known as phase I, II, and III have been described by Brigitte and Michael Kamm as well as by Donald Van Dyne[80,81]:

Phase I biorefinery

This type of biorefinery is a dry-milling biofuel plant. It uses grain as a feedstock, has a fixed processing capability and produces a fixed amount of ethanol, feed co-products and carbon dioxide. Both commercial and industrial biofuels have been produced from first generation feedstock. It has almost no flexibility in processing. Therefore, this type can only be used for comparable purposes.

Phase II biorefinery

This type of biorefinery is a wet-milling technology that uses grain feedstocks, yet has the capability of producing various end-products, depending on product demand. Such products include starch, high fructose corn syrup, ethanol, corn oil and corn gluten feed and meal. This type opens numerous possibilities to connect industrial product lines with existing agricultural production units. Thus, the integrated production of biodegradable plastics, such as poly-3-hydroxybutyrate, sugar and ethanol in a conventional sugar plant is an example of a phase II biorefinery[82].

Phase III biorefinery

This type of biorefinery is not only able to produce a variety of chemicals, fuels and intermediates or end products, but can also use various types of feedstocks and processing methods to produce products for the industrial market. The flexibility of its feedstock use is the factor of first priority for adaptability towards changes in demand and supply for feed, food and industrial commodities.

Each biorefinery refines and converts its corresponding biological raw materials into a multitude of valuable products. The product palette of a biorefinery includes not only the products produced in a petroleum refinery, but also in particular products that are not accessible in petroleum refineries. Therefore, it have been developed new biorefinery basic technologies, such as: (1) the lignocellulosic feedstock biorefinery including pre-treatment and effective separation into lignin, cellulose and hemicellulose, (2) development of thermal, chemical and mechanical processes, such as extractive methods, gasification (syngas) and liquefaction of biomass, (3) development of biological processes (biosynthesis, bacteria for the degradation of starch and cellulose, etc.), (4) combinations of substantial conversions, such as biotechnological and chemical processes, (5) corn biorefinery concepts, (6) green biorefinery concepts and (7) the promotion of research and development into phase III biorefinery[83].

Feedstock processing systems

Biobased products are prepared for a useable economical use by a meaningful combination of different methods and processes (physical, chemical, biological, and thermal). Therefore, a profound interdisciplinary cooperation of the various compartment disciplines in research and development known as Biorefinery design has surged to bring together scientific and technologic basics to develop biorefineries, which until 2004 were included in three biorefinery complex systems: the whole-crop biorefinery, the green biorefinery, and the lignocellulose feedstock biorefinery. As of 2007, a fourth system was included, the two-platform concept[79].

The Lignocellulosic Feedstock Biorefinery (LCF)

This system employs nature-dry raw material as lignocellulosic biomass and wastes. Lignocellulosic materials consist of three primary chemical fractions or precursors: (a) hemicellulose/polyoses, sugar polymer of predominantly pentoses, (b) cellulose, a glucose polymer and (c) lignin, a phenolic polymer. Raw material situation is optimal because of availability (straw, reed, grass, wood, paper-waste, etc.) and, on the other hand, conversion products have a good position within both the traditional petrochemical and the future biobased product markets.

The Whole-Crop Biorefinery (WCB)

Whole-crop biorefineries use cereals, such as rye, wheat, triticale, and maize. The first step is mechanical separation into grain and straw, which are obtained in almost the same amount. There is the possibility of separation into cellulose, hemicellulose and lignin and their further conversion within the separate product lines shown in the LCF biorefinery.

The Green Biorefineries (GBR)

Green biorefineries are multi-product systems which handle their refinery cuts, fractions and products in accordance with the physiology of the corresponding plant material, i.e. the maintenance and utilization of the diversity of syntheses achieved by nature. The technology used at these factories is a first stage biorefinery with nature-wet biomasses such as grass from the cultivation of permanent grassland, closure fields, nature preserves and green crops, such as lucerne, clover and immature cereals from extensive land cultivation. Thus, green plants represent a natural chemical factory and food plant[84].

The Two-Platform Concept (2PC)

This system includes the sugar platform, based on biochemical conversion processes and focused on the fermentation of sugars; and the syngas platform, based on thermochemical conversion processes and focused on the gasification of biomass feedstocks and byproducts from conversion processes[79].

Potential

The most determinant and commonly referred factors affecting the biotechnical valorization potential of a given lignocellulosic material can be divided in the following groups:

> Biological and physico-chemical factors: biological nature, physical properties (density, hardness, etc.) and macromolecular and chemical composition.

> Economical factors: seasonality (which is related to availability and storage problems), economic value and market dependency.

> Technological factors: currently applied technology; destination and state-of-the-art of applicable technologies.

> Geographical factors: available quantities, geographical concentration and political-legal constrains[85].

Among the different types of biorefineries the lignocellulosic feedstock biorefinery is by now the most important due to the type of raw material that employs and the products that are obtained. In this type of biorefinery the non-food materials (agricultural and forest residues, energy crops) are transformed into products/energy. The feedstock is mainly

integrated by the residues generated from agricultural-forestry activities (straw, shrubs, pruning, and trimmings) and thereof derived industries. This feedstock is widely available and otherwise the conversion products obtained have a very good position in both, current petrochemical and future biobased product market[79].
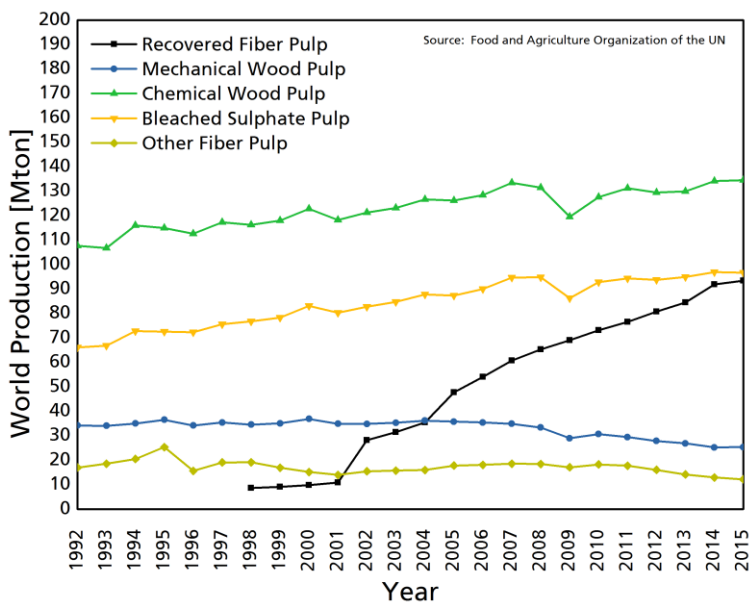
Pulping

Background considerations

Figure I-13 World pulp production from 1992 to 2015

Removal of lignin from lignocellulosic fibers is the first step in the obtention of cellulose for diverse applications. Industrially, bleached cellulose pulp is obtained using two stages: pulping and bleaching. The objective of pulping is to remove the lignin and to release cellulose fibers, thereby separating cellulose from the other components. This process can be either mechanical or chemical. The most widely used pulping process in the world is the Kraft process[41,86] a chemical process based on the cooking in which a white liquor, composed mainly by sodium hydroxide and sodium sulfide is used to remove lignin. Kraft process presents high yield of pulp but as a result of the chemical reactions, sulfide derivatives could be linked to cellulose or can represent an environmental problem during disposal. In this sense, other environmental friendly pulping processes have recently emerged, such as soda (E) and organosolv (O) pulping methods, which are sulfur-free. Soda process is performed as the usual alkaline pulping. On the other hand, organosolv method is based on the extraction of lignin by its dissolution in an organic solvent at high temperature and pressure. The low viscosity of the organosolv white liquors favors the penetration into the chips allowing that a high lignin fraction can be dissolved. Moreover, after the pulping stage, the solvent could be recovered by distillation. Figure I-13 displays the trends in wood pulp production for the last 23 years, the recovery of fibers has supposed a milestone for the pulp and paper industry, but the use of alternative fiber sources has been stagnant and even decreased since 2009, in that year, all the pulp industry

suffered the effects of an economical crisis, but whereas chemical and mechanical wood pulp recovered eventually, the alternative fiber market has not yet recovered.

Types of pulping

There are two technological principles to produce paper pulp from wood, namely mechanical processes or chemical processes. Whereas in chemical pulping the yields are only about 45–55%, mechanical pulping is able to use ~80–95% of the original fiber*s*. Mechanical pulping provides a good yield from the pulpwood because it uses the whole of the log except for the bark, but the energy requirement for refining is high and can only be partly compensated by using the bark as fuel. Whilst this represents a source for the economic potential of mechanical pulps, the higher yield results in certain unfavorable properties compared to chemical pulp. Mechanical pulp gives the paper a yellowish/grey tone with high opacity and a very smooth surface. Thus, from the same portion of wood, a double quantity of mechanical pulp is produced compared to chemical pulp. The increasing demand for paper and board has led to a permanent increase in mechanical pulp production, currently among the total amount of paper pulp produced, mechanical pulp accounts for about 20%. A chemical pulp or paper is called wood free, although in practice a small percentage of mechanical fiber is usually accepted. Paper containing a high level of mechanical pulp and a smaller level of chemical pulp is called 'wood containing paper'. At present, more than 90% of the pulp (virgin pulp fiber) produced worldwide is wood pulp. The first species of trees to be used in great quantities for papermaking were pine and spruce from the temperate coniferous forests located in the cool northern climates of Europe and North America. In Table I-1 the pulp production from 213 to 1015 and the projections for 2016 to 2018 are presented as reported by the FAO in the pulp, paper and paperboard capacity survey. As it can be seen, the use of chemical pulp holds its preponderance and is the only with growing projections, while mechanical pulp and pulps from non-wood sources are not expected to grow. Among the chemical pulps, sulfate pulp continues to be the most important while the projections for sulfite pulp are similar to those of mechanical pulp and pulp from non-wood sources. Softwood-based industries are by far the dominant in pulp production, pine and spruce provide the strongest pulp (for example coniferous sulfate pulp), while non-coniferous sulfate pulp is produced from birch, eucalyptus, aspen, acacia and many other mixed tropical species. Fast growing species of tree, such as planted eucalyptus and acacia, are the most rapidly emerging pulp raw material. Today the main species comprise birch, beech, aspen and maple, in the United States and Central and Western Europe, pine in Chile, New Zealand and United States, eucalyptus in Brazil, Spain, Portugal, Chile and South Africa.

Table I-1 FAO Pulp, Paper and Paperboard Capacity Survey 2013-2018

Total Reported Capacity [kton year^{-1}]						
	2013	2014	2015	2016	2017	2018
Wood pulp for paper and paperboard	**152838**	**153750**	**155733**	**157825**	**159757**	**160449**
Mechanical pulp	**12191**	**11821**	**11649**	**11607**	**11550**	**11543**
Mechanical non-coniferous pulp	40	40	40	40	40	40
Mechanical coniferous pulp	2098	2094	2046	2048	2050	2052
Thermo-mechanical pulp	**12914**	**12662**	**12744**	**12895**	**12964**	**12989**
Thermo-mechanical non-coniferous pulp	12	12	12	12	12	12
Thermo-mechanical coniferous pulp	3007	3007	3007	2773	2787	2787
Semi-chemical pulp	**5345**	**5310**	**5400**	**5555**	**5715**	**5745**
Semi-chemical non-coniferous pulp	604	604	644	704	704	704
Chemical pulp total	**119422**	**121113**	**123041**	**124868**	**126628**	**127271**
Unbleached sulfite pulp	1100	1140	1140	1140	1120	1120
Unbleached coniferous sulfite pulp	810	850	850	850	830	830
Bleached sulfite pulp	**1196**	**1136**	**1136**	**1136**	**1136**	**1136**
Bleached non-coniferous sulfite pulp	115	115	115	115	115	115
Bleached coniferous sulfite pulp	651	591	591	591	591	591
Unbleached sulfate pulp	**34241**	**34521**	**34906**	**35095**	**35170**	**35175**
Unbleached non-coniferous sulfate pulp	1110	1110	1110	1110	1110	1110
Unbleached coniferous sulfate pulp	4305	4138	4163	4168	4173	4178
Bleached sulfate + soda pulp	**70983**	**72376**	**73792**	**75411**	**76982**	**77619**
Bleached non-coniferous sulfate + soda pulp	46630	48008	49359	50895	52436	52883
Bleached coniferous sulfate + soda pulp	26624	26598	26623	26646	26696	26696
Pulp of other fiber for paper and board	**1071**	**1084**	**1094**	**1097**	**1078**	**1064**
Pulp of straw	30	30	30	30	30	30
Pulp of bagasse	596	607	614	614	594	586
Pulp of bamboo	127	127	127	127	127	127
Pulp of other fibers	310	312	315	318	319	313

Chemical pulping

The first chemical pulping process was the soda process, so-named because it uses caustic soda as the cooking agent. This process was developed in 1851 by Hugh Burgess and Charles Watt in England, who secured an American patent in 1854. Because this process consumed relatively large quantities of soda, papermakers devised methods for recovering soda from the spent cooking liquor through evaporation and combustion of the waste liquor and recausticizing the sodium carbonate formed. Since the preparation of sodium carbonate from sodium sulfate was rather expensive by using the Leblanc process, Carl Dahl in Danzig tried to introduce sodium sulfate directly in place of soda ash in a soda pulping recovery system. This substitution produced a type of liquor which contained sodium sulfide along with caustic soda. The pulp so produced was stronger than soda pulp and because of that it was called '*kraft*' pulp, after the Swedish word for 'strong'. The process, which was patented in 1884 by Dahl, has also been termed the 'sulfate process' because of the use of sodium sulfate. In 1857, shortly after the discovery of the soda pulping process, Benjamin Tilghman, a US chemist, invented acid sulfite pulping, who got an US patent 10 years later for the acid sulfite cooking process, using solutions of sulfur dioxide and hydrogen sulfite ions at elevated temperature and pressure[87].

For chemical pulp, logs are first chopped into wood chips which are then cooked with chemicals under high pressure. Cooking removes lignin and separates the wood into cellulose fibers. The resulting slurry contains loose but intact fibers which maintain their strength. During the process, approximately half of the wood dissolves into what is called black liquor. The cooked pulp is then washed and screened to achieve a more uniform quality. The black liquor is separated out from the pulp before the bleaching process. Using chemical pulp to produce paper is more expensive than using mechanical pulp or recovered paper, but it has better strength and brightness properties.

Chemical pulping types[88]

Soda pulping (NP): nonwood pulps belong to the group of chemical pulps, and are predominantly produced according to the soda cooking

Sulfate pulping (SaP/KP): Most chemical pulp is made by the sulfate process, and today the Kraft pulps account for 89% of the chemical pulps and for over 62% of all virgin fiber material. During sulfate pulping caustic soda and sodium sulfate are used to cook wood chips in pressure vessels. In the unbleached stage, a dark brown but very strong pulp results and this can be bleached to a high brightness if required. Sulfite pulp is mainly used for graphic papers, tissue and carton board, wrappings, sack and bag papers, envelopes and other specialty papers. Kraft pulping has developed as the dominating cooking process and its development was further extended since the introduction of modified cooking technology in the early 1980s. Nowadays there are three generations of modified Kraft

pulping processes with their own subcategories, the first two are continuous cooking and batch cooking technology:

Batch cooking

Cold-blow (CB): Cold blow technology can be designated as the forerunner of the modified kraft batch cooking processes. It is characterized by one or two cooking stages and cold displacement. Another key characteristic of this technology is that there is no warm impregnation stage.

Rapid Displacement Heating (RDH): in the rapid displacement heating process, the digester is steam-packed with chips using a shuttle conveyor. Next, weak black liquor from the atmospheric accumulator is used to increase chip compaction density in the digester. Air is displaced from the digesters and the discharge valves are closed. Impregnation is carried out with warm black liquor; therefore, the ratio of hydrosulfide to hydroxide ions reaches values above 3, which ensures that cellulose is not exposed to the hydrolytic effects of high hydroxide ion concentrations as compared to a conventional cooking pattern

The Superbatch Process (SBP): The Superbatch process is characterized by a rather low impregnation temperature of 80–90 °C, which is approximately 40–50 °C less compared to the RDH process. The low temperature is chosen to avoid chemical reactions occurring on the surface of the chips during the impregnation phase in order to strictly separate the physical impregnation and chemical delignification reactions.

Continuous Batch Cooking (CBC): Continuous Batch Cooking represents the latest development of modified cooking procedures, and fully considers the rules of extended delignification and allows an even alkali profile throughout the impregnation and cooking stages. The CBC process is characterized by the prior preparation of all process-related liquors (e.g., impregnation and cooking liquors) in the tank farm, using different tank-to-tank circulation loops. During circulation, the required reaction conditions are adjusted by the continuous addition of cooking chemicals and steam. The content of dissolved solids can be reduced by continuously replacing part of the recycled cooking liquor by washing filtrate.

Continuous cooking

Modified Continuous cooking (MCC): The concept of Modified Continuous Cooking (MCC) implies the process during which the main part of the cooking is performed with a low alkali concentration, while simultaneously allowing the concentration of dissolved lignin to be low.

Extended Modified Continuous Cooking and IsoThermal Cooking (EMCC/ITC): These cooking methods mark the consequent prolongation of the MCC related to the equalizing

of alkali profiles and co-utilization of washing zone volume for cooking and washing. From a process perspective, EMCC and ITC are widely similar; the main difference is that EMCC requires only one wash circulation, whereas ITC uses two sets of wash circulation loops with individual heaters.

The third generation includes black liquor impregnation, partial liquor exchange, increased and profiled hydroxide ion concentration and low cooking temperature (elements of Compact Cooking), as well as the controlled adjustment of all relevant cooking conditions in that all process-related liquors are prepared outside the digester in the tank farm (as realized in CBC).

Prehydrolysis-kraft process (PHK): This process was developed during World War II in Germany, with the first mill operating in Königsberg (Kaliningrad). In the prehydrolysis step, the wood chips are treated either at temperatures between 160 and 180 °C for between 30 min and 3 h with direct steaming, or in dilute mineral acid (0.3–0.5% H2SO4) at temperatures between 120 and 140 °C. This pretreatment liberates organic acids (e.g., acetic, formic) from the wood, and these hydrolyze the hemicelluloses selectively to produce water-soluble carbohydrates.

Sulfite pulping (SiP): The sulfite pulping process is an alternative method best suited for specialty pulp which can be easily bleached, generally with hydrogen peroxide. These pulps fulfill the demand for 'chlorine-free' products in the hygiene paper sector and also in printing and writing papers. Sulfite pulp is produced by cooking pre-cut wood chips in a pressure vessel in the presence of bisulfite liquor. The pulp may be either bleached or unbleached.. Sulfite process is the dominant process for the production of dissolving pulps, and accounted for 60–63% of the total production, while 22–25% originated from PHK process in 2003. The remaining 12–16% was produced from cotton linters which, for purification and viscosity control. Applications for sulfite pulp rang from newsprint, printing and writing papers, to tissue and sanitary papers.

The yield in both chemical processes is much lower than in the manufacture of mechanical pulp, as the lignin is completely dissolved and separated from the fibers. However, the lignin from the sulfate and some sulfite processes can be burnt as a fuel oil substitute. In modern mills, recovery boiler operations and the controlled burning of bark and other residues makes the chemical pulp mill a net energy producer which can often supply power to the grid, or steam to local domestic heating plants.

Organosolv pulping (OP): Organosolv pulping is the process of using organic solvents to aid in the removal of lignin from wood – has been suggested as an alternative pulping route. The pioneering studies on organosolv pulping began with the discovery in 1931 by Kleinert and Tayenthal that wood can be delignified using a mixture of water and ethanol at elevated temperature and pressure. During the following years, a rather wide variety of organic

solvents have been found to be suitable for pulp production[89]. The intrinsic advantage of organosolv over kraft pulping processes seems to be the straightforward concept of recovering the solvents by using simple distillation. Furthermore, organosolv processes are predicated on the biorefining principle – that is, the production of high amounts of valuable byproducts. The advantage of small and efficient recovery units which could fulfill the demand for profitable smaller production units is, however, limited to very simple solvent systems such as ethanol-water derived from the Kleinert process. For example, the use of acid-catalyzed organosolv pulping processes such as the Formacell (formic acid-catalyzed media) and Milox (sulfur-free peroxyformic acid) processes clearly complicates an efficient recovery of the solvents, and this in turn diminishes the advantage over existing pulping technologies[90]. The reason for this is the nature of the solvent system. The spent pulping liquor contains water, formic acid, and acetic acid which form a ternary azeotrope. The complexity of efficient solvent recovery, together with the limitation to hardwood species as a raw material and, moreover, the clearly inferior strength properties of organosolv pulps compared to kraft pulps, indicates that organosolv pulping processes are not ready to compete with the kraft process at this stage of development. The challenge of organosolv pulping for the future is to identify solvents with better selectivity towards lignin compared to those available today which simultaneously allow simple, but efficient, recovery.

Mechanical pulping[91]

Although mechanical pulping is a thermomechanical process, chemical processes may also play a certain role. The mechanical defibrillation of wood is carried out in two different ways: a grinding process or a refining process. For the production of grinded pulp, wood is ground against a water lubricated rotating stone. The heat generated by grinding softens the lignin binding the fibers and the mechanic shear forces separate the fibers to form groundwood. During the second half of the XX century, newer mechanical techniques were developed with the addition of 'refiners'. In a refiner, woodchips are subjected to intensive shearing forces between a rotating steel disc and a fixed plate. After grinding, the pulp is sorted by screening to suitable grades. It can then be bleached with peroxide for use in higher value-added products. Figure I-14 displays a tree with the main mechanical pulping procedures and the way they are related between each other.

Mechanical pulping types[92]

Stone Groundwood pulp (SGW): in this process wood is mechanically grinded into relatively short fibers. The resulting pulp is used mainly in newsprint and wood-containing papers, such as lightweight coated (LWC) and super-calendered papers.

Pressure Grinding (PGW): Groundwood production has been carried out under atmospheric pressure; until investigations into temperature relationships in grinding have led to the introduction of higher pressures in grinding processes high water content lowers

the softening temperature of lignin and hemicelluloses. With high pressures of 100–300 kPa (1–3 bar), the boiling temperature of water increases; from the vapor–pressure relationship, the boiling temperature is seen to be 120 °C at a pressure of 100 kPa (1 bar). Pressurized grinding prevents the water from boiling in the grinding zone.

Refined mechanical pulp (RMP): This kind of pulp is manufactured by the mechanical defibrillation of wood chips in a disc refiner with no further pretreatment.

Thermomechanical pulp (TMP): the wood particles are softened by steam before entering a pressurized refiner. Grinding is a thermomechanical process that is divided into two parts, each of which overlaps one another: (a) Softening and breakdown of the fiber structure by heat; and (b) peeling of the softened fibers from the wood matrix in the grinding zone. The resulting pulp is light-colored and has longer fibers. TMP has mainly the same end-uses as Stone Groundwood pulp.

Chemi-ThermoMechanical pulp (CTMP): A further development of the thermo-mechanical pulping which involves a gentle chemical treatment stage combined this can be done with mechanical defibrillation such as disc refining. in which the wood chips are impregnated with a chemicals treatment with sodium sulfite before the grinding. The end result is an even lighter-colored pulp with better strength characteristics.
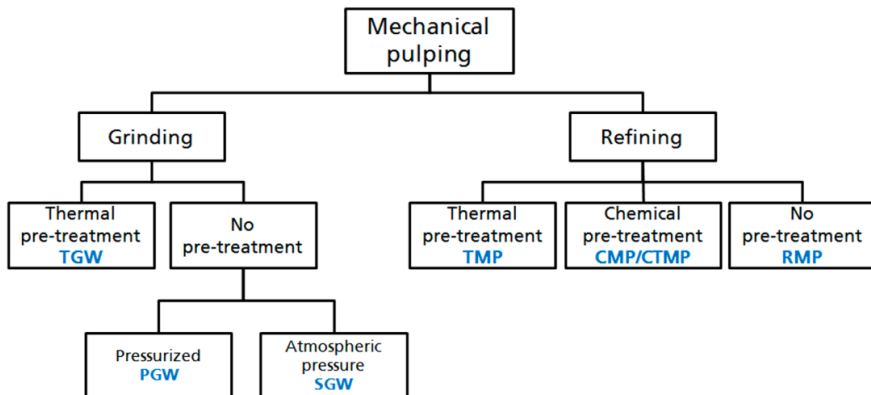

Figure I-14 Basic mechanical pulping procedures.

Bleaching

Although most lignin is removed during cooking, some residual lignin remains and is usually removed in oxidative bleaching reactions. Bleaching is performed as a chemical treatment in stages and under different operating conditions, some of which are summarized in Table I-2. The main chemical reagents used are elemental chlorine (Cl_2), chlorine dioxide (ClO_2) and hydrogen peroxide (H_2O_2) which are known as C, D and P stages respectively. For many years, the main reactions followed to achieve pulp bleaching have involved chlorinated reagents (Cl_2, ClO_2, and NaOCl), but nowadays the inclusion of other reagents has gained attention as they constitute environmentally friendly alternative bleaching sequences[93–95]. The introduction of new regulations has boosted the chlorine free bleaching, as it can be seen in Figure I-15, with elemental chlorine free bleaching becoming the predominant bleaching system since 1996, while total chlorine free systems have been the same since 1995 until 2012. During the last quarter of the XX century, many of the developments in chemical pulp production of both sulfite and Kraft processes were driven by severe environmental concerns, especially in Central Europe and Scandinavia. Increasing pulp production resulted in increasing effluent loads. The need to reduce the amount of organic material originating mainly from bleach plant effluents was most pronounced in highly populated countries, where filtered river water was used as a source of drinking water. The biodegradability of the bleach plant effluents, particularly from the chlorination (C) and extraction stages (E), turned out to be very poor due to the toxicity of halogenated compounds. Finally, the detection of polychlorinated dioxins and furans in chlorination effluents and even in final paper products during the 1980s caused a rapid development of alternative, environmentally benign bleaching processes[96,97], therefore chlorine was eliminated from industrial bleaching of most pulp[94,98].

The initial intention was the complete replacement of all chlorine-containing compounds, resulting in Totally Chlorine Free (TCF) bleaching sequences. This could be easily accomplished with sulfite pulps due to their good bleachability. Kraft pulp mills have been converted dominantly to Elemental Chlorine Free (ECF) bleaching rather than to TCF bleaching, because the latter, by using ozone or peracids to yield high brightness, deteriorates pulp quality. ECF bleaching, comprising chlorine dioxide (D) -containing bleaching sequences, such as DEOpDEpD, is acknowledged as a core component of the best Available Technology (BAT), since numerous field studies have shown that ECF bleaching is virtually free of dioxin and persistent bioaccumulative toxic substances[99]. ECF pulp, bleached with chlorine dioxide, continues to dominate the world bleached chemical pulp market. In 2002, ECF production reached more than 64 million tones[99]. Market data show that ECF production grew by 17% in 2001, whereas TCF pulp production remained constant, maintaining a small niche market at just over 5% of world bleached chemical pulp production. The transition to ECF is essentially complete in Europe, the United States and

Canada, with ECF production now representing more than 96% of the whole bleached chemical pulp production[88].
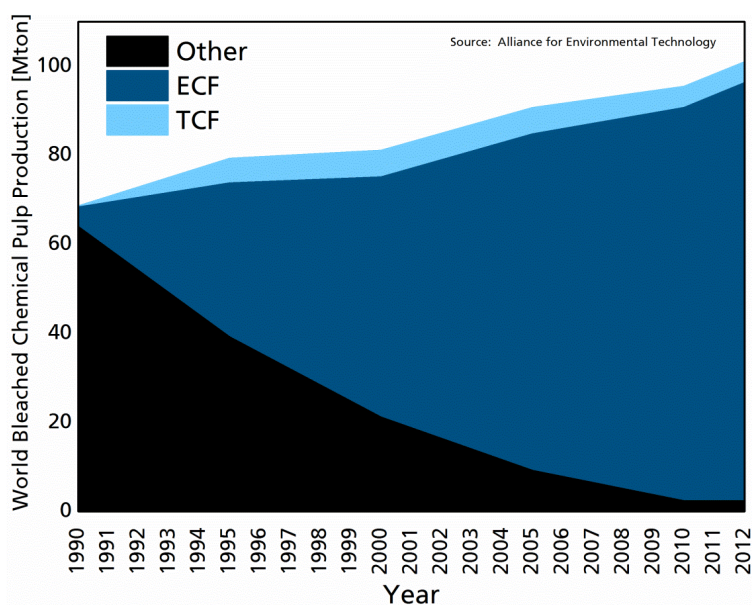

Figure I-15 World bleached chemical pulp production 1990-2012.

Current ECF bleaching sequences are dominant, as chlorine dioxide has proved to be the most efficient reagent to remove phenolic chromophores originated from precipitated lignin, On the other hand, the presence of certain chromophores (carbonyl structures) in the residual lignin or even produced from the reaction between chlorine dioxide and lignin[100–102], are easily cleaved with alkaline peroxide oxidation of chromophores in lignin through the cleavage of side chains[103], for which hydrogen peroxide is the most efficient reagent on the chromophores that are still present at the end of any ECF bleaching sequence (mainly quinine type)[100,104]. Since the first approach to TCF bleaching processes, an interest from both industry and governments has developed around this method to refine cellulose for further applications, which avoids releasing chlorine derivates into the waste streams or atmosphere. However, most TCF chemical reagents, such as hydrogen peroxide and oxygen, are less efficient than chlorine reagents in attaining high and stable pulp brightness degrees. Delignification with hydrogen peroxide is to a large extent the action of the radicals produced during single electron transfers between hydrogen peroxide and catalysts or as a result of thermal cleavage of the oxygen-oxygen bond[103,105,106] at moderate temperature under buffered conditions and in the absence of transition metals, the delignification effect of hydrogen peroxide is limited. This is due to their lower delignification power that not only results in lower brightness but also in higher color reversion, owing to their higher residual lignin content. Therefore, hydrogen peroxide

treatment is dominantly used at final stages of ECF bleaching after D stage. The degradation of condensed lignin, which can be the result of high intensity pulping conditions, with hydrogen peroxide is limited. The perhydroxyl anion, being a nucleophile, is not able to attack the electron rich aromatic rings of the residual lignin. For hydrogen peroxide bleaching, a pH range of 10.2-10.7 is considered optimum, as lower pH values can lead to decreasing solubility of sodium silicate stabilizer as well as lower whiteness due to less activation of the peroxide.

Table I-2 Most common stages for elemental chlorine free and total chlorine free bleaching sequences.

Process	Letter designation	ECF	TCF
Chlorine	C		
Sodium hypochlorite	H		
Chlorine dioxide	D	✓	
Extraction with sodium hydroxide	E	✓	✓
Oxygen	O	✓	✓
Alkaline hydrogen peroxide	P	✓	✓
Ozone	Z		✓
Chelation (metal removing)	Q		
Enzymes (xylanase)	X		
Peracids (peroxy acids)	Paa		✓
Sodium dithionite (sodium hydrosulfite)	Y		

Since hydrogen peroxide is typically applied in ECF bleaching after first D stage, the metal profile normally is already low enough and no specific measures are required. For this reason, when doing a TCF bleaching, the removal of the metals becomes more important, because hydrogen peroxide is applied early in the sequence at higher charges. The elimination of the metals is improved with the addition of a chelating agent In the bleaching stage with hydrogen peroxide or ozone, those metals promote the formation of hydroxyl radical (OH-) which destroys the cellulose fiber and decompose the bleaching agents. Ethylenediaminetetracetic acid (EDTA) and diethyleneaminepentacetic acid (DTPA) compounds are the best chelating agents for double charged metal ions. The addition of a small amount of DTPA can chelate higher charged metal ions, which are present in the pulp and are very likely bound to lignin or cellulose. Alkali earth metals are also chelated by DTPA or EDTA[107]. However, the use of either DTPA or EDTA in Green pulping and bleaching is currently discouraged as none of these agents are biodegradable, nor are they easily treated as normal water treatment plants are not capable to remove these components from water, therefore they represent a considerable harm to the ecosystems in which those streams are deployed. For this reason, it is recommended to use another metal chelating

agent instead, among them 2,6-Pyridinedicarboxylic acid (PDA) has been proved to be an effective chelating agent with similar results to those of EDTA[108].

Non-wood fibers as source of lignocellulosic materials

Concerns on sustainability have let to the industrial use of crop fibers or agricultural residues as a complement or even a substitute for traditional pulping wood. Traditionally, the use of nonwood fibers has been a practice in countries with limited access to wood supply and was used as last resource as the quality of the obtained fibers was not as good as that of wood[109]. But as the environmental concerns have increased in developed countries and the disposal of agricultural byproducts has become an issue of greater interest among producers, recent researches have focused in enhancing properties of crop fibers to make them more competitive with wood pulp[110].

Advantages from nonwood pulp and paper industry include: little strain in ecological balance as they are based on fast growing renewable raw materials that are abundant, this also ensures the availability of the fiber, either crop fibers or agricultural residues. The sales of agricultural residues also provide to the farmers extra revenue that increases the value of the crop. And at last, the localization of mills near the agricultural exploitations can reduce the cost of raw material transport thus making the pulp economically competitive[111].

Fiber dedicated crops are grown mostly for fabrics or paper manufacturing, Plant fibers may include hairs such as cotton (*Gossipum hirsutum*); fiber-sheafs or dicotylic plants or vessel sheafs or monocotylic plants such as bast fibers such as kenaf (*Hibiscus cannabinus*), flax (*Linum usitatissimum*), hemp (*Cannabis sativa*), ramie (*Boehmeria nivea*) and there are also hard fibers as sisal (*Agave sisalana*), henequen (*Agave fourcroydes*) among others[112], Kenaf is one of the most promising fiber crops, for many years it has been used as fiber source for ropes and sacks, but recently it has been considered as reinforcing agent for composites, therefore it has reached the target of many governments from Southeast Asian countries, as Malaysia to develop new applications. Also hemp and sisal have proved their performance as pulping raw materials, sisal is a leave plant native to Mexico, although the main producers are Brazil and Tanzania, sisal as henequen or blue agave are slow growing plants, and usually 4-6 years are needed before the first harvesting[113].
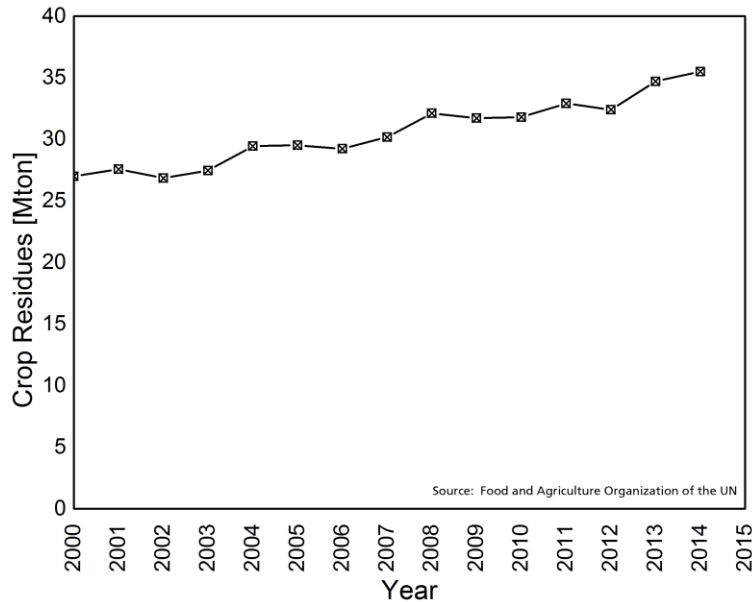
Figure I-16 World crop residues for the last 15 years.

Agricultural residues, which are also called harvesting residues or agricultural by-products[114], are either materials left in an agricultural exploitation after the crop has been harvested as the case of sugarcane (*Saccarum officianarum*) and blue agave (*Agave tequilana*) bagasse; or waste left after agricultural products have been processed into a usable product as coconut (*Cocos nucifera*) husk or almond (*Prunus dulcis*) shells. This kind of products are characterized for their low price, as the growing cost is already absorbed by the main purpose industry, the relatively cheap harvesting costs, especially in the case of industrial residues, as they already are in factories and the medium-high quality of the obtained pulp[115]. Besides, the use of harvesting residues in the elaboration of pulp and paper products averts the need of disposal from these products in the large European and American exploitations which currently represent an environmental issue as pollution and fires are a constant risk when disposing of this kind of materials, Figure I-16 shows the amount of crop residues of the last 15 years, the continuous increase of such residues and therefore, the potential they have as source of lignocellulosic biomass[116]. Sugarcane bagasse is one of the most promising agricultural fibers used for pulping, as it is easily accessible and available in several locations, especially in regions where lack of wood represents a challenge for pulping industry, after the cane processing through roller mills to extract sugar juice, bagasse is usually burnt in sugar-mill boilers[117]. Coir or coconut husk is characterized for its toughness and durability due to high lignin content, huge quantities of coconut palm residues are burnt , but recent works have focused in finding a further use for its less used components, such as coir or other fibrous parts[118].

Table I-3 shows some of the most used raw materials as analyzed in recent publications for cellulose obtention with their respective composition[112,118–127].

Table I-3 Composition of the different raw materials

Type of fiber	Cellulose [%]	Lignin [%]	Hemicelluloses [%]	Ash [%]
Aspen	52.1	21.4	20.6	0.4
Acacia	46.5	27.1	24.4	0.22
Birch	45	18	33	0.3
Slash pine	46	27	18	0.2
Spruce	45.5	28.3	25.7	-
Kenaf	58	17.5	22	2.4
Flax	64.1	2.0	16.7	-
Sisal	65.8	9.9	12	-
Hemp	60.09	12.36	23.83	3.16
Ramie	68.6	0.6	13.1	-
Cotton	82.7	-	5.7	-
Sugarcane bagasse	54.3	24.3	16.8	1.1
Blue agave bagasse	64.8	15.9	5.1	2
Coconut husk	44.2	32.8	12.1	2.2

Nanocellulose

The term 'nanocellulose' generally refers to cellulosic materials having at least one dimension in the nanometer range. Nanocellulose can be produced by different methods from various lignocellulosic sources[128]. Recently, active research on the isolation of cellulose nanoparticles from plant cell wall has been a trending topic in materials science, chemical engineering, nanomaterials, biotechnology, wood industry and environmental sciences among many others. This boom reported by nanocellulose responds to its versatility to be modified, availability of raw materials and the biocompatibility that is characteristic to polysaccharides and cellulose in particular. This has potentiated its use as reinforcing material in nanocomposites[129–131], as its presence in such field provides a new direction for the development of value-added novel composites. These cellulose nanoparticles have been extracted from cell walls by chemical[132,133] or mechanical treatments[134–136]), as well as diverse combinations of them[137].

Background

The earliest report on the preparation of fibrillated cellulose fibers from lignocellulosic biomass as well as the dynamics of such defibrillation with an Electronic Force Microscope was presented in 1946 by Wuhrmann, Heuberger and Mühlethaler from ETH Zurich and EMPA St. Gallen[138]. The authors disintegrated ramie, hemp and cotton fibers "treating the fibers in strong ultrasonic fields a very fine and gentle fragmentation occurs, the original texture of the cleaved fiber parts remain intact" thus being the first to use high intensity ultrasound into their respective elementary fibrils reaching diameters as small as 6 nm, their results are shown in Figure I-17.
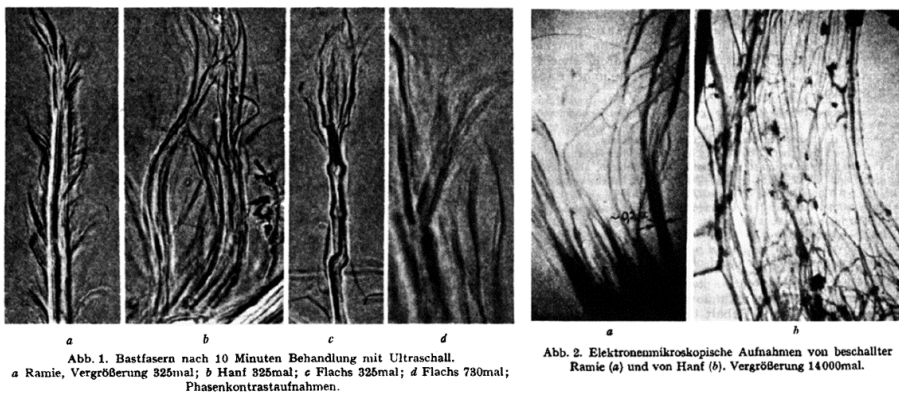

Abb. 1. Bastfasern nach 10 Minuten Behandlung mit Ultraschall.
a Ramie, Vergrößerung 325mal; *b* Hanf 325mal; *c* Flachs 325mal; *d* Flachs 730mal;
Phasenkontrastaufnahmen.

Abb. 2. Elektronenmikroskopische Aufnahmen von beschallter Ramie (*a*) und von Hanf (*b*). Vergrößerung 14000mal.

Figure I-17 First published image of defibrilated cellulose fibers.(Wuhrmann[138])

"wir haben gefunden, dass bei Behandlung der Fasern in starken Ultraschallfeldern eine sehr feine und schonende Zerteilung eintritt, wobei die ursprüngliche Textur der abgespaltenen Faserteile vollständig erhalten bleibt. Es ist ferner leicht, den Übergang von mikroskopisch sichtbaren Spaltstücken zu den elektronenmikroskopisch abgebildeten Molekülsträngen darzustellen, so dass die Interpretation der übermikroskopischen Bilder sichergestellt wird."
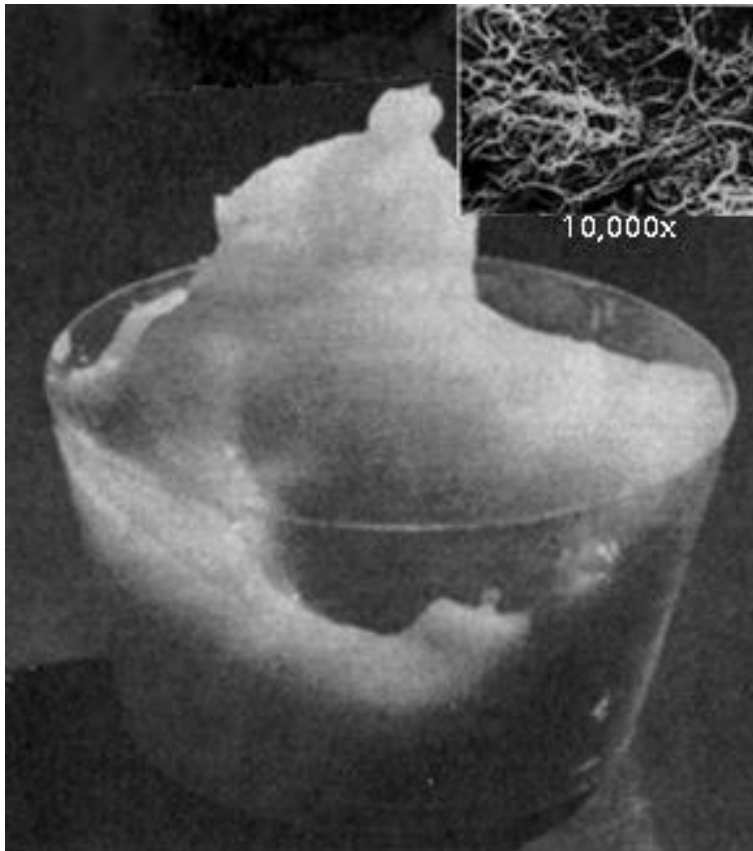

Figure I-18 First published image of Nanocellulose „gel" by Turbak[139].

In 1977 a research manager at the ITT Rayonier Eastern Research Division (ERD) Lab in Whippany, N.J., USA, who had used a Gaulin-type Milk Homogenizer to make edible breakfast sausage casings from cowhides, decided to run 3% slurry of chopped pulp fibers through a high-pressure Manton Gaulin Milk Homogenizer. As the slurry reached 80°C at 8,000 psi, the fibers started to undergo a total phase change and turned into a translucent, firm "gel" that they called microfibrillated cellulose (MFC). Evidently, at the high temperature the high forces (pressure/cavitation/shear/impact) of the homogenizer acting in tandem or sequentially had broken down the cell walls of the microfibers and liberated the desired nanofibrils.

Many years had to pass to retrieve the first public mentions of nano-scaled cellulose fibrils or microfibrillated cellulose (MFC), which were done in 1983 during a ITT Rayonier Inc. meeting. At that meeting, Franklin W. Herrick from the ITT Rayonier Eastern Research Division (ERD) Lab in Whippany, N.J., USA presented a method to obtain dry cellulose powder[140], in a later conference, Albin F. Turbak, from the same Rayonier laboratory, presented a method to elaborate microfibrillated cellulose at low concentrations for applications in the food industry with a Gaulin-type milk homogenizer[141], the resulting gel can be seen in Figure I-18.

Definitive studies subsequently established that this stiff gel Rayonier was calling microfibrillated cellulose was, indeed, the long sort-after nanocellulose, and it had been isolated by a simple method with little degree of polymerization loss (10% - 15%). In 1982 – 1983, world economics forced ITT to shutdown both Rayonier labs and curtail further efforts in this area, but by then 11 patents had issued covering the preparation and uses of MFC.

While Rayonier gave free license to all of these patents to its pulp customers, there can be little doubt that the Rayonier MFC discovery was the birth of a totally new branch of cellulose technology, i.e. nanotechnology. For the next 30 years, all nanotechnology starting gels and developments that involved using the MFC high-pressure homogenizer procedure at some stage benefited from this discovery. Acid hydrolysis of nanocellulose produces nanocrystalline cellulose (NCC) rods that are capable of making products with unique properties and are currently under close scrutiny.

Many companies became active in the field and the three patents and the two papers published by the Rayonier group in 1983 grew to 825 by 2007 and is much larger in current days. Various organizations used oxidized, derivatized, hydrolyzed, pre-swollen, enzyme-treated, and otherwise modified pulps as feed stocks with specially designed 2000-3000 bar homogenizers to lower energy requirements and vary nanoparticle-size distributions, which has simultaneously morphed MFC into NFC. These efforts have reportedly resulted in commercial MFC based scale-ups by Innventia (Sweden), Daicel (Japan), UPM Kymmene and VTT (Finland), Borregaard (Norway), and Rettenmaier (Germany), and should be applauded.

Nanocellulose and its different modifications are currently being developed or commercially used, Figure I-19 shows the increasing trend in the study of nanocellulose to elaborate new materials, among the uses of nanocellulose in both industrial and academic researches it can be highlighted:

- Making lighter auto components, thus improving gas mileage
- Making low calorie bread and baked goods with extended shelf life

- Making healthier, low calorie desserts, gravies, and salad dressings
- Making high quality cosmetics to minimize or prevent skin wrinkles
- Improving diaper, non-woven, and catamenial fluid retention
- Stabilizing foams of all types, edible and non edible
- Making strong, translucent films
- Making non-settling sand, coal, and other pumpable solids suspensions
- Relieving arthritis joint pain
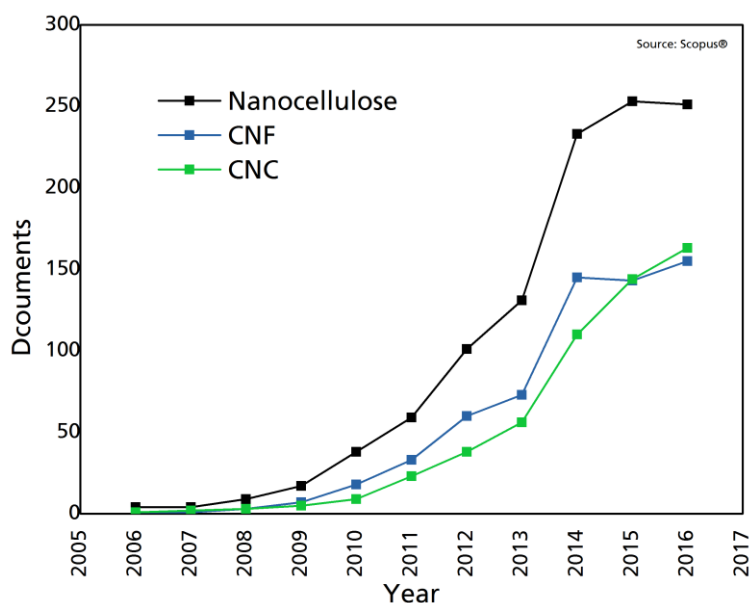- Making artificial body parts
-

Figure I-19 Number of publications related to nanocellulose, CNF and CNC in the last 10 years.

Nanocellulose types

Nanocellulose can be classified in three main categories depending on their dimensions functions and preparation methods, as well as the origin and processing conditions. The first two correspond to top-down extraction methods and are known as cellulose nanofibers (CNF) and cellulose nanocrystals (CNC). The third one corresponds to a bottom-up method and is synthetized from glucose units through bacterial agents and is called bacterial cellulose (BC)[142].

Cellulose Nanofibers

Cellulose nanofibers also known as microfibrillated cellulose, cellulose nanofibrils[143] or nanofibrillar cellulose[144], are the smallest structural unit of plant fiber consists of a bundle of stretched cellulose chain molecules with long, flexible and entangled cellulose nanofibers

hey consist of alternating crystalline and amorphous domains[145] which diameters are below 100 nm but their length reaches from 800 nm to several microns. They have been obtained by refining and homogenizing action. When isolated by mechanical treatment with acid hydrolysis as pretreatment results in even finer cellulose nanofibrillated structures with diameters below 50 nm.

CNF are manufactured by repeated treatments of cellulose fiber/water slurries using a high-pressure homogenizer, and is strongly swollen in water. NFC tends to have high aspect ratio and is more flexible and prone to formation of physical entanglements. Also, wood-based NFC can be prepared in a cost-effective way by enzymatic pretreatment of wood pulp[146] and has the potential for large-scale industrial use.

The defibrillation of NFC needs intensive mechanical treatment. However, according to degree of processing and raw material, chemical pretreatments are performed before mechanical fibrillation to promote the accessibility of hydroxyl groups, increase the inner surface, alter crystallinity, and break cellulose hydrogen bonds and therefore, boost the reactivity of the fibers. Mechanical approaches to diminish cellulosic fibers into nanofibers can be divided into refining and homogenizing, microfluidization, grinding, cryocrushing and high intensity ultrasonication[128].

High pressure homogenization (HPH): These processes consist on passing cellulose slurry at high pressure into a vessel through very small nozzle. High velocity and pressure as well as impact and shear forces on fluid generate shear rates in the stream and decrease the size of fibers to nanoscale[147]. HPH can be considered as an efficient method for refining of cellulosic fibers, because of high its efficiency, simplicity and no need for organic solvents. Figure I-20 shows defibrillation of cellulose fibers at different passes through homogenizer a) 10 passes, b) 15 passes and c) 20 passes.

Figure I-20. Different fibrillation grades as view with O.M. with 200x.

Mechanical Grinding (MG): In grinding equipment, there is static and rotating grind stone and pulp slurry passes between these two stones. The mechanism of fibrillation in grinder is to break down of hydrogen bond and cell wall structure by shear forces and individualization of pulp to nanoscale fibers[148]. The heat produced by friction in fibrillation process leaded to evaporate water and solid consistency raised from 2 to 3.2% after 11 h

which caused to boost up specific fibrillation energy. They mentioned two main structures, first highly kinked and untwisted fibrils, and second entangled and twisted nanofibers. They found that extended fibrillation could form nanowhiskers with high crystallinity from the untwisted nanofibers[149].

Cryocrushing (CC): Cryocrushing is another method for mechanical fibrillation of cellulose. In this process, water swollen cellulosic fibers immerse in liquid nitrogen and subsequently crush by mortar and pestle[147]. Application of high impact forces to the frozen cellulosic fibers leads to rupture of cell wall due to exert pressure by ice crystals and thus, liberating nanofibers[148].

High intensity ultrasonication (HIUS): is a mechanical process in which oscillating power is used to isolate cellulose fibrils by hydrodynamic forces of ultrasound[150]. During the process, cavitation leads to a powerful mechanical oscillating power and therefore, high intensive waves, which consists of formation, expansion, and implosion of microscopic gas bubbles when molecules absorb ultrasonic energy[151]. Better fibrillation can be achieved by higher power and temperature; on the other hand, longer fibers usually have lower fibrillation. However, concentration and larger distance from probe to beaker also influence the level of fibrillation.

All these mechanical methods involve high consumption of energy, which can cause dramatic decrease in both the yield and fibril length. Thus, current research has been focused on finding environmental conservation, high efficiency and low costs methods to isolate nanocellulose. Pretreatment of cellulose or combination of two or more methods have brought some positive results in this regards.

Cellulose Nanocrystals

Cellulose nanocrystals, also known as cellulose whiskers, cellulose nanorods or nanocrystalline cellulose; have been obtained through more aggressive acid hydrolysis. CNC are renewable materials which possess high availability, light weight and high mechanical properties. They consist of slender parallelepiped rods and, depending on their origin, the lateral dimensions range from about 2–50 nm in diameter for length than can reach several tens of micrometers[152,153]. During acid hydrolysis, the amorphous sections of native cellulose are hydrolyzed and after careful timing the crystalline sections can be retrieved from the acid solution by centrifugation and washing. Cellulose nanowhiskers are rod-like highly crystalline particles (relative crystallinity index above 75%) with a rectangular cross section. They present a needle-like structure of the cellulose crystallite, have been mainly studied for their liquid crystalline behavior in concentrated aqueous suspensions[154,155] and for their reinforcing effect when added to a polymeric matrix giving rise to very strong and tough percolating networks of hydrogen bonded whiskers[156,157].

The most used method to obtain CNC consists in exposing cellulose to hydrochloric acid (HCl) or sulfuric acid (H_2SO_4) at different conditions (temperature, concentration, stirring, time). The hydrolysis process consists basically in removing the amorphous regions present in the cellulose fibrils leaving the crystalline regions intact; therefore, the dimensions of the cellulose whiskers obtained after hydrolysis are mainly dependent on the percentage of amorphous regions that varies for each organism. Traditionally the yields of cellulose whiskers by acid hydrolysis have been quite low (2–3%); however, in a recent study the process was optimized to reach yields up 30% and suspensions of nanocrystals with a length between 200 and 400 nm and a width less than 10 nm. Their dimensions depend on the native cellulose source material, acid employed as well as its concentration and hydrolysis conditions as time and temperature.

Bacterial cellulose

Bacterial cellulose (BC) was first described by Brown[158], who based in previous works from Pasteur with the *Mycoderma aceti* in his in his '*'Mémoire sur la Fermentation Acétique'*, along with the Fractional method of Kleb and the Dilution method of Nägeli. Brown discovered that the fermentation of *Mycoderma aceti* (now the preferred term is *Acetobacter aceti*) produced, when cultivated in a medium containing fructose, extremely strong 'pellicles'. He reported: „A pure cultivation of the 'vinegar plant' when commencing to grow in a liquid favorable to its free development, is usually first noticed as a jelly-like translucent mass on the surface of the culture fluid; this growth rapidly increases until the whole surface of the liquid is covered with a gelatinous membrane, which, under very favorable circumstances, may attain a thickness of 25 mm". The gelatinous membrane that he observed during the cultivation was shown to be chemically identical to cotton pure cellulose by the Müller method and after acidification formed a similar precipitate thant hat o cotton-wool. This cellulose is now known as bacterial or microbial cellulose. The dynamics throw which these bacteria produce cellulose is still an open question and current trends support three main hypotheses: 1) to maintain close proximity to the surface of the culture medium where the oxygen concentration is highest, 2) to protect against ultraviolet light and 3) to protect against heavy metal ions and improve nutrient transport by diffusion[159].

There are several works that use both microfibrils of cellulose and cellulose whiskers to compare the reinforcement properties for these two types of cellulose[160]. Results from different studies have found that tensile strength and tensile modulus increased when the cellulosic fibers were added; however, the highest values were found for the microfibrillated cellulose (CNF) are used, but not with CNC. Other factor that is highlighted is the entanglement of CNF, as it can decrease the elongation at break for the material. For the CNC reinforced material, the elongation at break increased as a function of acid hydrolysis strength. All of this is an indication of the significance of entanglement in the overall macroscopic physical properties of the cellulosic reinforced composites. The hydrogen bonding that takes place between the nanocellulosic materials is well known but the study

mentioned above demonstrates how important entanglements are for the microfibrillated cellulosic materials.

The dimensions and characteristics of CNC or NFC depend not only on the biological origin but also on the disintegration procedure. NFC forms network structures with very interesting mechanical behavior such as substantial plastic deformation and high strength[143].

Cellulose functionalization

The most serious issues that requires to solve is incompatible nature and difficult dispersion of cellulose in polymer matrix[161,162] as well as poor interfacial adhesion[163] between cellulosic fibers as polar materials with non-polar medium like polymeric materials. One approach to overcome these problems is surface modification of fibers or modification of matrix[164]. Identification of optimum surface modification is very important for NFC quality and can be done by the following ways[162]:

A. Verifying the treatment regime which should not damage cellulose structure.

B. Optimizing qualities such as impact resistance, modulus of elasticity and strength to breakage by controlling the bonding degree of structural elements and matrix in composite.

One of the reasons why nanocellulose has found reticence to its wider use is their difficulty to disperse in most of the non-polar solvents because of the hydrophilic nature of the hydroxyl groups. Consequently, the modification of nanofibers prior to their further use is of high interest, in order to limit this phenomenon and open new applications, within this research field, several reports have emerged focused on the surface modification of nanocellulose with quite pleasant results. The surface of cellulose nanoparticles can be modified by various methods, on the one hand by the use of chemical methods for covalent bonds between cellulosic substrates and the grafting agent, and partly by physical interaction or adsorption of molecules or macromolecules surface,

The modification of the surface of cellulose microfibrils to make them compatible with non-polar polymers has been attempted. Cellulose nanocrystals are currently modified via the reaction between the hydroxyl groups located at their surface and a functional group from the organo-modifying agent. Interaction of cellulose with surfactants has been another way to stabilize cellulose suspensions into nonpolar systems. The use of organosilanes to achieve surface modification with silanes has been studied for many years and has proved to be a good method to render nanocrystalline surface hydrophobicity, giving stability to the nanocrystals[165]. Silane chains can improve matrix-filler interactions either as suspension in organic solvents or added as bulk into the polymeric matrix[166,167] by serving as a coupling agent between the cellulosic filler and the polymeric matrix.

Silane based surface modification is a popular way to change the surface of fibers from hydrophilic to hydrophobic. In the absence of water, even at elevated temperature, no reaction happens between Si–OR and OH groups of cellulose, whereas Si–OR reacts with lignin's phenolic OH. Addition of moisture initiates a reaction between silanol groups and OH groups of cellulose at high temperature[162]. Surface silylation of NFC from bleached softwood pulp using chlorodimethyl isopropylsilane was investigated by Andresen et al. [154]. They noted that the degree of surface substitution was around 0.6–1 which indicated that silylated NFC could be dispersed in a polar solvent. They found that derivatization became negligible because of the competitive hydrolysis of silane agent when the molar ratio of

silane agent of repeating glucose unit turned into lower than 3:1. Goussé, Chanzy, Cerrada, and Fleury[165] in 2004; studied the rheological properties of mild silylation of NFC by isopropyl dimethylchlorosilane. Schematic reaction between these two materials is seen in Fig. 9. The morphology of these nanofibers was similar to un-derivatized ones and produced stable suspensions without fluctuation. The suspension showed shear thinning influences and thickening characteristics, but had no noticeable yield stress point. They noted that NFC obtained inherent flexibility and their suspensions rheological behavior was like a polymer solutions by silylation process.

On the other hand, esteric stabilization of cellulose nanocrystals with different fatty acids has shown good properties forming continuous composites with polymer matrices, as they show high degree of substitution when the esterification is performed both at the fiber surface and in the inner layers; resulting in a heterogeneous esterification, causing de-crystallization of cellulose which enhances hydrophobicity and bonds between the matrix and the cellulose fiber, in expense of thermal stability of the cellulose[168].

Composites

Nanocellulose as reinforcement

Cellulose since the origins of human-made technology has been present in the use of composites, being part of either structural composites of natural origin (wood-based) or as fibrous organic materials added as a reinforcement to form new composites(adobe bricks, paper, etc.). With the arrival of nano-scale technology in the second half of the twentieth century, new materials have been developed to fulfill the emerging necessities that are presented to mankind, as the potential of nanocomposites in various sectors of research and application has been proved as promising and thus is attracting an increasing number of investors. In the nanocomposite industry, a reinforcing particle is usually considered as a nanoparticle when at least one of its linear dimensions is smaller than 100 nm (width or lenth). Native cellulose fibers are built up by smaller and mechanically stronger long thin filaments, the microfibrils consisting of alternating crystalline and noncrystalline domains, such hierarchical structure and the semicrystalline nature of cellulose, allows nanoparticles to be extracted from this naturally occurring polymer. Multiple mechanical shearing actions can be used to fibrillate native cellulose to release more or less individually such microfibrils. This material is usually called microfibrillated cellulose (MFC) or cellulose nanofibers (NFC; CNF). On the oher hand, more crystalline cellulose obtained through acid hydrolysis is called nanocrystalline cellulose (NCC) or cellulose nanocrystals. Such nanoparticles have been extracted from diverse sources ranging from trees, plants or agricultural wastes[146,169–171].

Natural fiber composites are prepared using various composites manufacturing methods such as compression molding, injection molding, resin transfer molding (RTM), and vacuum bagging. The preforms are mostly fibers, fabrics, or nonwovens. Pre-impregnated fibers (prepregs) are also widely used to prepare composites[172]. Recent studies have found a broad range of applications of nanocellulose in different types of industries, and still a high number of unknown applications are to be found, as several publications show its potential even if most of the studies focus on their mechanical properties as reinforcing phase and their liquid crystal self-ordering properties. However, as for any nanoparticle, the main challenge of cellulose nanoparticles is related to their homogeneous dispersion within a polymeric matrix as usually nanocellulose dispersions tend to behave as anisotropic materials[173]. Some of the main applications of cellulose nanoparticles as reinforcing fillers are in, paper industry, polymer composites and cement-based composites.

Nanocellulose as reinforce in paper

By far, the predominant use of the fiber material is the manufacture of paper, where it is re-assembled as a structured network from an aqueous solution. Paper is one of the most traditional applications of cellulose based materials, with a history in human life that can be

tracked back 5000 years when Egyptians invented papyrus parchments because of the adhesion in cellulose-based fiber materials[174]. The ease of adhesion that occurs between cellulose fibers has contributed to a globally important industry that is among the largest in the world. Cellulose fiber bonding in paper and related products occurs over a practical length scale ranging from the nanoscale to millimeters, and this topic has received considerable attention over the past century[175,176]. The bonding of cellulose fibers in paper relies primarily on hydrogen bonding between the fibers that occurs as the wetted fibers dry in contact with each other, and the bond strength can vary greatly depending on the methods used to prepare the fibers, which include: pulping, bleaching and refining processes. Hydrogen bonding between fibers requires close proximity between adjacent hydroxyl groups. The partial solubility of cellulose in water and the diffusion theory of adhesion have also been reported since refined fibers have a fibrillar structure on the near-molecular size scale that contributes to adhesion[175]. Mechanical interlocking has not been shown to be important in the bonding of cellulose fibers in paper except for paper in the bone-dry condition[160]. The adsorption of hydrophobic materials on cellulose fibers during papermaking greatly decreases fiber-to-fiber bonding and is related to the weak boundary layer theory of adhesion[177].

Nanocellulose-reinforced plastic composites

Polymer-based composites with the addition of cellulose nanoparticles are perhaps one of the most studied materials manufactured with nanocellulose. Several studies have focused in the addition of cellulose nanofibers or cellulose nanocrystals to polymeric matrices, these matrices can be traditional plastics obtained from oil refineries or either way can be bio-based polymers. The natural origin of cellulose and the high content of organic matter in bio-based plastics (over 80%) has made these the most valued for their end-of-life disposition, and are in trends in recent years to convert in the most studied applications for cellulose, either as biocompatible materials for medical uses or as food-contact packaging. The main criteria for the selection of the appropriate process technology for natural-fiber composite manufacture include the desired product geometry, the performance needed, and the cost and the ease of manufacture. The fabrication methods for natural fiber composites are similar to those used for glass fibers. The most commonly used manufacturing processes are introduced in the following. Although many variants on these techniques exist, this overview gives a good indication of the production possibilities.

The main processing methods for composites with cellulose fibers at any size have been synthesized by Kalia, and collaborators in 2011[178], all of them present advantages and drawbacks that should be considered depending on the application and the characteristics that are expected from such composites.

Hand Laminating: The fibers are placed in a mould and the resin is later applied by rollers. Cheap and flexible design; long production time and intensive work (automation difficult).

Resin Transfer Molding (RTM): The fibers are placed inside a mould consisting of two solid parts, called close mould technique. A tube connects the mould with a supply of liquid resin, which is injected at low pressure through the mould, impregnating the fibers. This process allows the rapid manufacturing of large, complex, and high performance parts

Compression Molding: Semifinished composite sheets widely known as sheet molding compound (SMC) are later molded into the final parts by compression. Fibers are added and then a second film of resin is then applied, the composite is then compressed in a composite sheet that may be stored for few days. This technique allows high volume production, excellent part reproducibility and short cycle times, while its main drawbacks are the maximum pressure before the damage of the fibers and the structure.

Injection Molding: This molding procedure allows forming complex shapes and fine details with excellent surface finish and good dimensional accuracy for high production rate and low labor cost. In the injection molding resin granules and short fibers are mixed into a heated barrel and transported to the mould cavity by a spindle.

Pultrusion: The impregnated fibers are pulled through a die, which is shaped according to the desired cross-section of the product. The resulting profile is shaped until the resin is dry. Advantages of this process are the ability to build thin wall structures, the large variety of cross-sectional shapes, the ability to manufacture composite profiles at any length and the possibility for high degree of automation.

Very few studies have been reported concerning the processing of cellulose nanofibers-reinforced nanocomposites by extrusion methods. The hydrophilic nature of cellulose causes irreversible agglomeration during drying and aggregation in nonpolar matrices because of the formation of additional hydrogen bonds between amorphous parts of the nanoparticles. Therefore, the preparation of cellulose whiskers-reinforced polylactide (PLA) nanocomposites by melt extrusion was carried out by pumping the suspension of nanocrystals into the polymer melt during the extrusion process[179]. An attempt to use polyvinyl alcohol (PVA) as a compatibilizer to promote the dispersion of cellulose whiskers within the PLA matrix was reported[180]. Organic acid chlorides-grafted cellulose whiskers were extruded with low density polyethylene[181]. The homogeneity of the ensuing nanocomposite was found to increase with the length of the grafted chains. Polycaprolactone (PCL) grafted cellulose nanocrystals obtained by ring-opening polymerization (ROP) of the corresponding lactones have been used as 'masterbatches' by melt blending with a PCL matrix[182].

II)   Capítulum prímum

Cellulose extraction

Motivation

The first step to obtain nanocellulose consists in the elimination of non-cellulosic materials from the lignocellulosic fibers; such process is done through solubilization of the different components under selected conditions. For the present work, environmentally friendly processes were used to obtained cellulose pulp from agricultural waste which consisted in blue agave bagasse and leaves fibers, two by-products of the tequila industry. Such process consisted in a sodium-hydroxide based elemental chlorine free pulping/bleaching and a combination of an organosolv pulping with a total chlorine free bleaching sequence; together they represent a green cellulose extraction with the further utilization of a cost-effective source. The resulted pulps were characterized according to standard methods used for cellulose evaluation at the pulp and paper industry.

Experimental Methods

Raw Materials

Blue agave (*agave tequilana*) leaves (AL) and bagasse (AB), the two main components of tequila industry byproducts were provided by Eng. J. R. local distillery owner from Amatitán, Jalisco Mexico and by Eng. D. R. local farmer from Tequila, Jalisco, Mexico. Leaves were cut mature fresh from the plant and then decorticated to scrape off the epidermis and pithy material from the line fiber and then rinsed and dried. Bagasse was collected after core cooking and milling and was also rinsed and dried. Materials were conditioned at the Regional and Urban Planning Faculty of the Autonomous University of Mexico State with the help of M. Eng. Patricia Mireles and shipped to the University of the Basque Country UPV/EHU. Received fibers were milled with a Retsch milling system until an average fiber length of 5 mm was achieved; fibers were measured according to TAPPI standard methods[183] and were kept in a dry environment at 20 °C.

Pretreatments and pulping

Organosolv pulping (O$_P$):

An ethanol-water (70-30) organosolv treatment was carried out in order to extract lignin from the fibers; the method followed has been reported by this group previously[184,185] with slight modifications: temperature was set at 200 °C, agitation at 150 rpm and reaction time was 90 min. Liquid fraction was separated via filtration and the solid fraction was washed several times until remaining dark liquor was eliminated. Fibers were dried and separated for following treatments.

Sodium Hydroxide pulping (E$_P$/E$_1$):

As a second lignin elimination treatment, sodium hydroxide was used with a 1.5 M concentration. Fibers were submerged for 24 h at 20 °C and then heated at 90 °C for 2 h after which they were washed until neutral pH was achieved. Following alkali treatment,

fibers were subjected to a steam treatment at 120 ºC during 2 hours. Fibers were dried and separated for following treatments.

Elemental Chlorine Free Bleaching:

Elemental chlorine free bleaching (ECF) was done in three stages as shown in Figure II-1: 1) an alkali treatment (E_2) in a 1.8 M NaOH solution with a 1:20 w/v ratio at 120 ºC during 90 min, 2) a sodium chloride stage (D) in 0.2 M $NaClO_2$ solution with 1:30 w/v ratio at 75 ºC for 2 h, and 3) a peroxy stage (P_Q) in a 3 M H_2O_2 solution with 1:10 ratio and pH 11 using magnesium sulfate (0.2 wt%) to protect the fibers and pentetic acid (0.5 wt%) as chelant. Bleached pulp was washed several times until neutral and then oven dried at 50 ºC for 24 h[186].
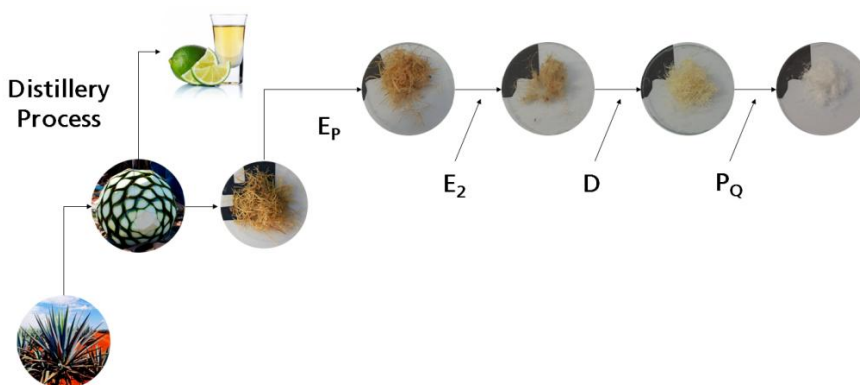
Figure II-1 Flowchart of the processes followed to achieve Elemental Chlorine Free bleached cellulose fibers.

Total Chlorine Free Bleaching:

An industrial type of total chlorine free (TCF) bleaching process was performed on the pretreated fibers as reported by David Ibarra and collaborators[93,187] using a O-O-P_Q-P_O sequence with slight modifications as seen in Figure II-2: (1) Double oxygen stage (O) with water at pH 11 stabilized using NaOH and 0.2 wt% $MgSO_4$ to neutralize remaining metals, this was performed under a 6 bar oxygen atmosphere at 98 ºC during 60 minutes. (2) Peroxide stage (P) with secondary chelating reaction (Q) using 3 M H_2O_2, at pH 11 with 0.3 wt% DTPA as chelant for 120 min at 105 ºC and (3) alkaline peroxide stage (P_O) using a 3 M H2O2 solution at pH 11 and 0.2 wt% $MgSO_4$ at 98 ºC during 150 min with 6 bar O_2 atmosphere. Bleached pulp was washed several times until neutral pH after each stage and then oven dried at 50 ºC for 24 h[188]. All reactions were carried out in a 4 L stainless steel reactor with pc-controlled stirring, pressure and temperature, fiber to liquid ratio was kept 1:15 w/v during all the process.
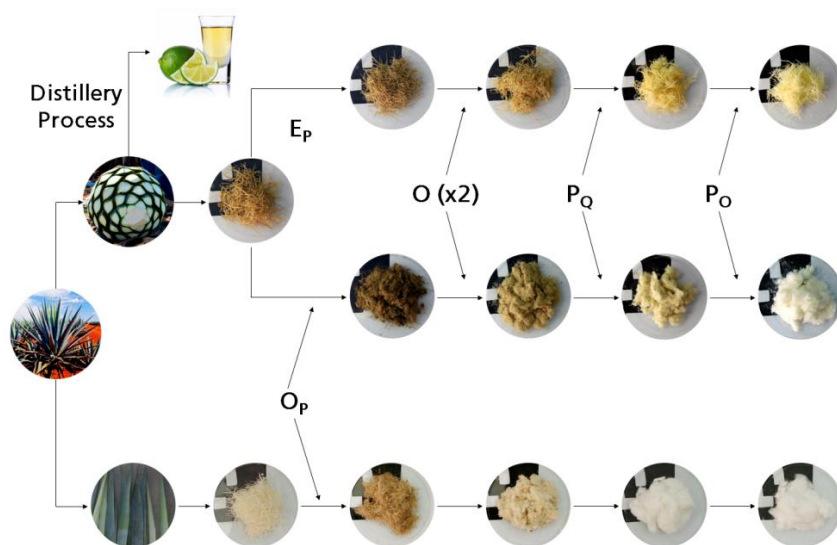
Figure II-2 Flowchart of the processes followed to achieve Total Chlorine Free bleached cellulose fibers.

Cellulose characterization

Raw Material Chemical Composition: Chemical analysis of the agave fibers was performed to determine the amount of cellulose available for further extraction. This characterization was carried out according to standard methods[121,189–194].

Attenuated Total Reflectance (ATR): Infrared spectra were recorded on a PerkinElmer Spectrum Two FT-IR Spectrometer equipped with a Universal Attenuated Total Reflectance accessory with internal reflection diamond crystal lens. The defined range was from 800 to 4000 cm^{-1} and the resolution 4 cm^{-1}. For each sample 20 scans were recorded.

Colorimetry: Color properties of the different composites were measured to determine the influence of the composition of the final layer in the optical properties. This was elaborated with an X-Rite 500 series colorimeter over 10 different regions of each composite, RGB profile was made for the final surface layer of each composite.

Scanning Electron Microscopy (SEM): Scanning electron microscopy images were obtained with a Scanning electron microscope Hitachi S-3400N with field emission cathode, with a lateral resolution of 10-11 Å at 20 kV.

Process parameters

Through the different stages of each of the processes selected, the total water used, as well as the energy and time were considered and are displayed in Table II-1 as the average used after each treatment for 100 g of material used as input. Water considered includes reaction water as well as the water used to clean after the treatment, this is why more aggressive treatments (like soda pulping or soda ECF stages) required higher amount of water, as the fibers were heavily impregnated with sodium hydroxide. On the other hand, treatments that required higher temperature or longer time had higher energy consumption. The recovery of reagents and the cost of stream final disposition are not considered for this table.

Table II-1 Input streams for each process stage.

Treatment	Total water used [mL]	Time elapsed [min]
O_P	5450	90
E_P/E_1	21500	240
O_2	15985	60
P_Q	3880	120
P_O	3985	150
E_2	14500	90
D	8200	120

Results and Discussion

The chemical composition of blue agave bagasse and blue agave leaf fibers is shown in Figure II-3. Cellulose is the main component in both leaves and bagasse, although cellulose and hemicelluloses are lower in content in bagasse fibers because of sugar degradation that occurs during the tequila production process in which blue agave cores are cooked and milled, depolymerizing a considerable part of the sugars for the further alcohol production[195], this also makes these results to differ from other chemical compositions evaluated for blue agave bagasse[13,126,196,197] as the extraction process and the maturity of the plant may not be the same. On the other hand, cellulose contained in the leave fibers is similar to those reported by previous works[197,198], the high cellulose content and low lignin of the blue agave in general, makes it a good cellulose source for bio-pulping and ECF bleaching, as low amount of chemicals would be required, this can be particularly seen in the case of agave leaves, which after P_Q stage were almost as white as bagasse after P_O stage (see Fig. 1).
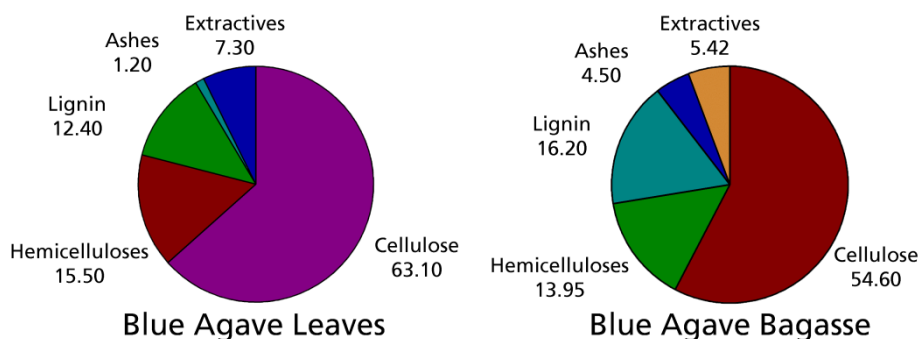
Figure II-3 Chemical composition of the raw material used on this study.

Scanning electron images of the raw material were acquired to analyze the morphology of the fibers (Figure II-4 a and b); the most evident difference is the fiber shape, as leave fibers present a rounded cross-section, while bagasse fibers have rather rectangular sections; this phenomena is caused by the mechanical beating to which bagasse fibers are subjected during juice extraction (ball milling) in which fibers are pressed. However widths are in both cases within the same range, with an average width of 50 µm. Leave fibers are longer (70-100 cm) while bagasse fibers rarely reach more than 20 cm; color also differs as it is analyzed further.

Morphology of the bleached fibers as observed by SEM is presented in Figure II-4 c and d; it can be appreciated a considerable difference between leave fibers and bagasse fibers, as two main factors condition such morphology: first is the function of the fibers inside the structure of the plant and second the cooking and beating of the bagasse fibers during tequila elaboration. Leave fibers are rounded, thinner and longer, and bagasse fibers are

prismatic, wider and shorter, with a special feature which is the presence of vessels along the fibers, these vessels are visible in bagasse fibers after pulping and bleaching, but are not visible in leave fibers nor in the raw material without treatments.
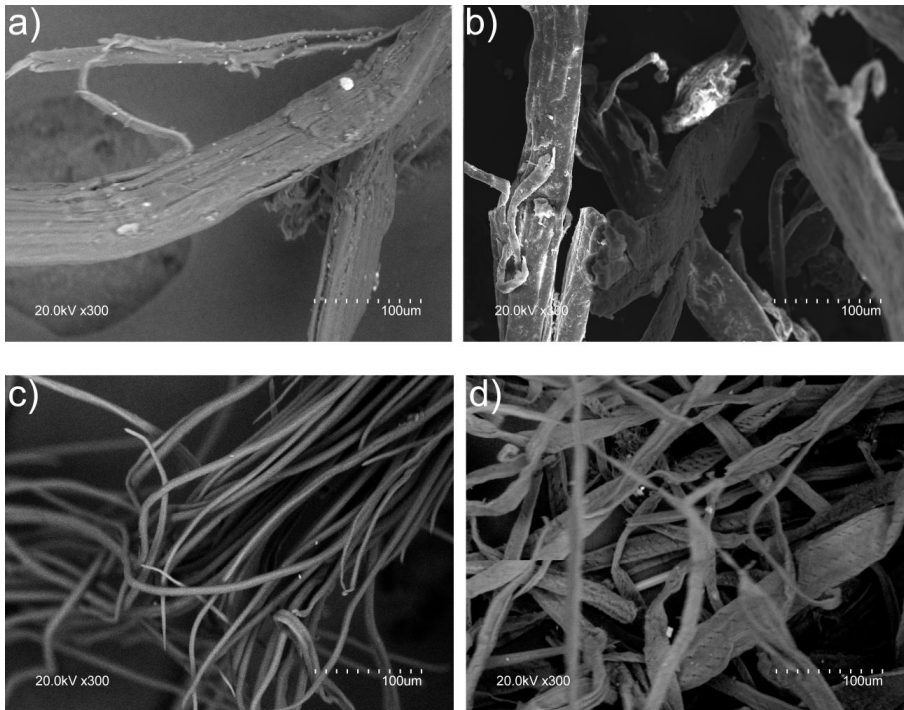
Figure II-4 SEM images of blue agave leave (a), blue agave bagasse (b) fibers before bleaching and blue agave leave (c) and blue agave bagasse (d) after TCF bleaching.

Figure II-5 shows the infrared spectra of the bagasse and the leave fibers either raw or after each treatment. It can be observed the gradual disappear of signals that are characteristic to lignin; the main bands which intensity is lost are ~1585 corresponding to the aromatic ring vibration (C=O stretch), another aromatic ring vibration at ~1500 and the C-C deformation at ~1450. On the other hand, bands that are characteristic of cellulose present a sharper definition, this is evident specially in case of the free ν(OH) band at 3500-3000, the carboxyl groups at ~2900 and ~2860 corresponding to ν(C-H) and ν(CH$_2$) symmetrical stretching of cellulose. In the 1500-500 bands, it can be pointed the higher resolution of bands at ~1335, corresponding to glycosidic ν(C-O-C), ~1280 of δ(CH$_2$) bending of crystalline cellulose ~1165 of C-O-C asymmetrical stretching of cellulose, ν(C-O-C) glycosidic linkage ~1108 and the double band between 1100 and 1000 corresponding to δ(CH$_2$) wagging and ν(C-OH) of 1° and 2° alcohol[199,200].
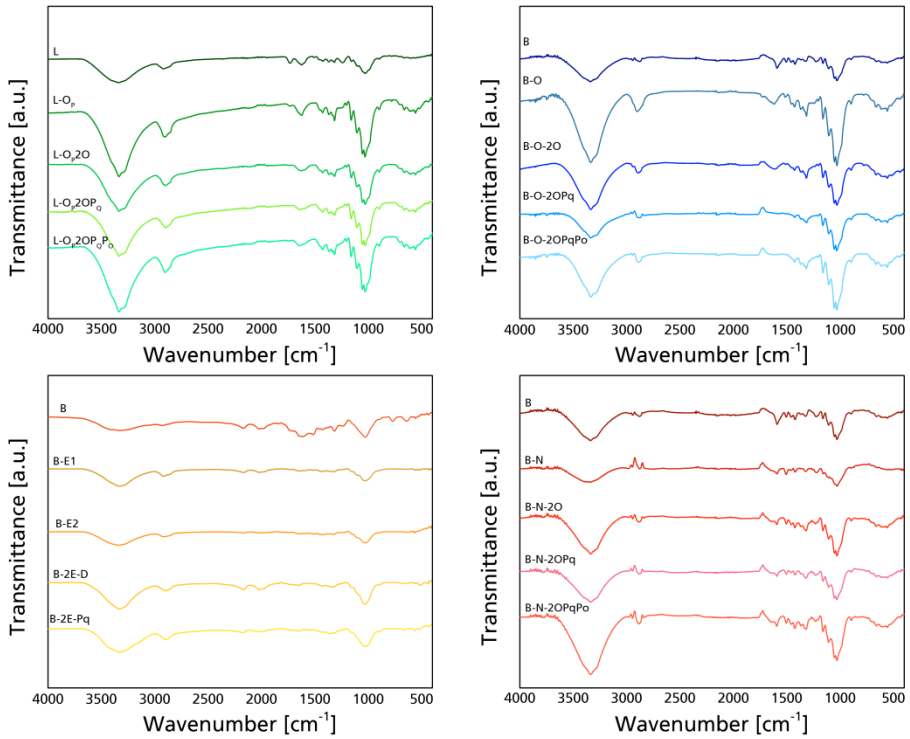
Figure II-5 FT-IR spectra of the fibers after each treatment

Table II-2 shows the average yield after each bleaching treatment, these yields are related to the relative yield, which is the yield of the total bleaching sequence, and the overall yield (Oy) which is the relation between the relative yield and the amount of cellulose present in the raw material according to TAPPI standards which was about 54 $g \times 100g^{-1}$ for bagasse and 63 $g \times 100g^{-1}$ for leaf fibers, from which after organosolv pulping and ECF bleaching 40 $g \times 100g^{-1}$ and 51 $g \times 100g^{-1}$ of cellulose were obtained from bagasse and leaf fibers respectively. This means that O_P and ECF sequences obtained a 72 % yield for bagasse and 81 % for leaf fiber, with mayor cellulose losses occurring during O_P and the double oxygen stage, as high temperatures and the presence of sodium hydroxide may have depolymerized cellulose chains to glucose. Yields at peroxide stages (P_Q and P_O) are above 90 % mainly because the mayor lignin and hemicellulosic fractions have been already solubilized or are left more available after organosolv pulping.

Table II-2 Output of fibers after each treatment.[1]

	Sample	Py [g×100 g⁻¹]	Oy [g×100 g⁻¹]	Ry [g×100 g⁻¹]
	O_P	68	68	
	O_P2O_2	67	67	
	$O_P2O_2P_Q$	90	41	
	$O_P2O_2P_QP_O$	95	39	71
	E_P	45	45	
	E_P2O_2	81	36	
BAB	$E_P2O_2P_Q$	94	34	
	$E_P2O_2P_QP_O$	95	33	60
	E_1	40	40	
	E_1E_2	69	28	
	E_1E_2D	84	24	
	$E_1E_2DP_Q$	98	23	43
	O_P	72	72	
BAL	O_P2O_2	81	58	
	$O_P2O_2P_Q$	92	54	
	$O_P2O_2P_QP_O$	97	52	82

Color measurements allow the checking of the visual changes occurring in the model samples before and after weathering, indicating with the parameters L*, a*, b*, ΔE* and C* which help understanding the colors differences.

Table II-3 shows the color properties of the fibers after their respective pulping and each stage of the bleaching sequence. To achieve bleached cellulose pulp, the most important value is L*, which is an approximate measurement of luminosity, the property according to which each color can be considered as equivalent to a member of the grey scale, between black and white, taking values within the range 0–100. Solid white has values of 100 for L* and 0 for a* and b*. ΔE* resumes the overall color changes throughout the color space, by relating L* a* and b* in absolute values, on the other hand, chroma (C*) is related to the intensity o colors, grayscale colors lack of chroma as they are closer to the L⁻/L⁺ axis of the CIEL*C*h*(a*b*) tridimensional space.

---

[1] Py corresponds to the yield after each process, Oy corresponds to overall yield, the amount of cellulose obtained related to the biomass used and Ry corresponds to relative yield, the obtained cellulose compared to the cellulose content as obtained from TAPPI methods.

Table II-3 CIELab* color space measured after each treatment.

	Sample	L*	a*	b*	C^*_{ab}
	Bagasse	61.55±0.59	8.21±0.16	24.02±0.13	25.38
	O_P	51.80±0.62	6.65±0.07	17.08±0.08	18.33
	O_P2O_2	67.33±0.72	4.48±0.07	15.34±0.37	15.98
	$O_P2O_2P_Q$	82.21±0.37	2.61±0.04	12.75±0.09	13.01
	$O_P2O_2P_QP_O$	93.66±0.17	0.64±0.03	6.88±0.15	6.91
	E_P	61.54±0.07	5.93±0.03	19.44±0.12	20.33
	E_P2O_2	67.76±0.49	6.55±0.12	23.88±0.25	24.77
BAB	$E_P2O_2P_Q$	83.54±0.47	2.61±0.06	24.80±0.35	24.94
	$E_P2O_2P_QP_O$	86.19±0.96	0.11±0.14	22.87±0.53	22.87
	E_1	56.29±0.28	25.60±0.04	42.67±0.84	32.64
	E_1E_2	61.38±0.87	7.36±0.26	26.63±0.92	14.46
	E_1E_2D	92.48±1.12	0.71±0.02	17.20±0.21	8.29
	$E_1E_2DP_Q$	94.33±0.95	0.22±0.05	5.95±0.49	6.10
	Leaves	84.21±0.55	1.98±0.09	18.75±0.07	25.38
	O_P	64.99±1.00	5.36±0.15	15.77±0.19	18.33
BAL	O_P2O_2	75.08±0.16	3.55±0.05	13.76±0.14	15.98
	$O_P2O_2P_Q$	92.94±0.65	0.92±0.04	7.00±0.56	13.01
	$O_P2O_2P_QP_O$	94.61±0.13	0.14±0.00	4.29±4.25	6.91

It is to highlight that the final bleached pulps (AL and AB after $O_P2O_2P_QP_O$) present good luminosity values (L*) which are 93.66 for the bagasse and 94.61 for the leaves, these results are quite satisfactory as the industry requirements usually demand between 93 and 95 L*. Bagasse pulped with alkali treatment and bleached with ECF also presented an acceptable L* value of 94.33 which in fact, is the highest value achieved for bagasse fibers in the present study, on the opposite side, bagasse bleached with a TCF sequence showed a luminosity of 86.19, which is below bleaching standards and therefore will no longer be considered for the present study.

In both fibers after organosolv pulping the color was darkened with respect to the starting material, this feature has been observed in similar works that use organosolv pulping[127,201] and it can be associated to the presence of polyphenolic chromospheres originated from the ring-opening of lignin chains, this phenomenon is not present in alkali pulps, in which L* maintains more or less the same value after pulping regarding the initial material. The most significant achievement in augmenting the L* corresponds to the D stage of ECF bleaching, which explains the preference Industry still has for such procedure, with a significant increase of 50.67 % regarding the previous stage, for TCF bleaching the most outstanding augmentation of L* takes place during the P_Q stage of the TCF bleaching of agave leaves, in which an increase of 23.78 % is achieved.
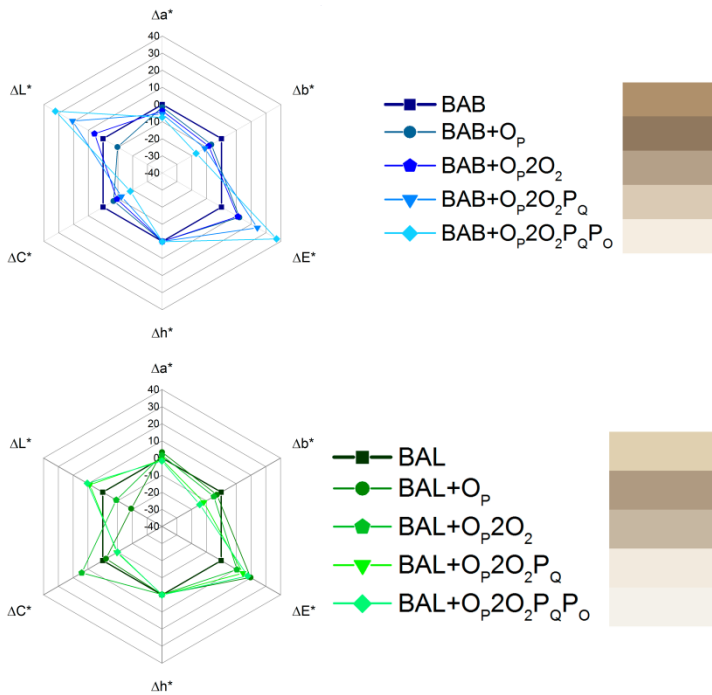
Figure II-6 Color appearance parameters of bagasse and leaves pulped with organosolv pulping, values correspond to Lab* space (ΔL^*, Δa^* and Δb^*) as well as chrominance (ΔC^*), hue (Δh_{ab}) and color difference (ΔE^*). Beside each name the corresponding solid color simulated in the RGB space is represented.

Figure II-6 and II-7 present further information, related to the changes achieved through the bleaching sequence presented as differences in a radial graphic with the initial state as reference. Δa^* is the degree of redness and greenness and it takes positive values for reddish colors and negative values for the greenish ones. Δb^* is the degree of yellowness and blueness and it takes positive values for yellowish colors and negative values for the bluish ones. ΔL^* is, as mentioned before, the degree of lightness. Positive values of Δa^* and Δb^* indicate that the samples are more red and yellow, respectively, than the reference fibers. Negative ΔL^* values indicate that the analyzed fibers reflect less light than the reference surface. Beside each bleaching sequence, the simulated color solid corresponding to the RGB space is represented for a better appreciation of the color changes throughout the whole sequences.
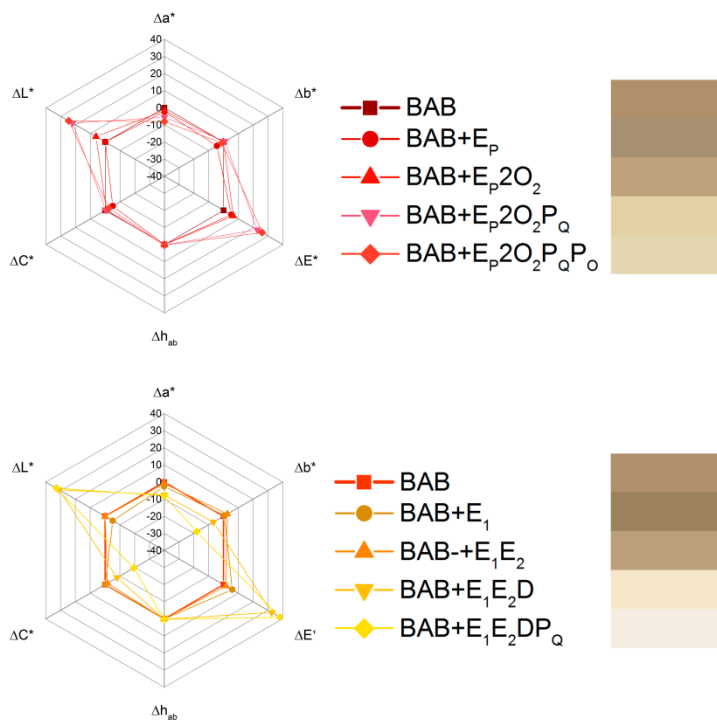
Figure II-7 Color appearance parameters of bagasse pulped with soda pulping and TCF (above) or ECF (below) bleaching sequences, values correspond to Lab* space (ΔL*, Δa* and Δb*) as well as chrominance (ΔC*), hue (Δhab) and color difference (ΔE*). Beside each name the corresponding solid color simulated in the RGB space is represented.

Both bagasse and leave fibers show darkening (-ΔL*) after organosolv pulping, which is less evident in alkali pulping. However this situation is then reverted during bleaching for all the cases. Chroma presents reductions from initial values (25 for AB and 18 for AL) which were further reduced (7 for AB and 4 for AL) after pulping and bleaching, Bleached pulp for bagasse had higher value for both a* and b* than pulp from leave fibers, these numbers (+a* and +b*) are related to red-yellow colors which can be due to residual chromospheres for example carbonyl and carboxyl groups either corresponding to residual lignins or, more likely, because of glucose oxidation in cellulose[202,203].

Conclusions

Different bleaching approaches were used to extract native cellulose from blue agave bagasse and blue agave leaves. Optical and chemical analyses were used to determine the most suitable process. Considering this, the presence of residual lignin in the $BAB+E_P2O_2P_QP_O$, makes it unfit to be considered further, as it has been highlighted before. In the following chapters, to shorten the further reference to the cellulose fibers obtained through the selected pulping and bleaching sequences, blue agave leaves pulped with organosolv pulping and bleached through a TCF sequence ($AB+O_P2O_2P_QP_O$) will be referred as LO; blue agave bagasse pulped with organosolv pulping and bleached through a TCF sequence ($AL+O_P2O_2P_QP_O$) will be referred as BO and blue agave bagasse pulped with alkali pulping and bleached through a ECF sequence ($AB+E_1E_2DP_Q$) will be referred as BE.

III) Capítulum secundum

Nanocellulose production

Motivation

Nanocellulose is produced throw diverse methods that range from enzymatic treatments to mechanical defibrillation, among them the most common are acid hydrolysis (to produce cellulose nanocrystals) and high pressure homogenization (to produce cellulose nanofibers). Acid hydrolysis with sulfuric acid at different concentrations is probably the most common process used in the CNC elaboration, and therefore it was the reagent used in the present work, on the other hand, cellulose nanofibers were obtained by homogenization through high shear dispersion followed by high pressure homogenization, the starting materials were fibers from bagasse bleached ether through ECF bleaching or through TCF bleaching, as well as leave fibers obtained by TCF bleaching and nanocellulose from these three pulps was obtained as CNF and CNC for all of them, resulting in six different cellulose nanoparticles which were then characterized to assess their properties and potential for further composite elaboration.

Experimental methods

Cellulose preparation:

Cellulose fibers obtained from the previous chapter were refined with a rotor cutting Retsch mill using a 1 mm sieve. After milling samples were oven dried for 24 h at 50 ºC and then kept inside a conditioning chamber with no humidity at 25 ºC.

Cellulose nanocrystals (CNC):

Acid hydrolysis was performed to cellulose by using 10.2 M H_2SO_4 (1:15 w/v) solution which corresponds approximately to 63-65 wt%. Two methods were used to produce CNC; the first one corresponds to the most commonly used sulfuric acid hydrolysis[145,196,204] consisting in submerging the fibers in the H_2SO_4 solution (1:20 w/v) during 120 min with mechanical stirring at 45 ºC (Figure III-1a). The second was developed in our laboratory and consisted in submerging the fibers in H_2SO_4 solution (1:15 w/v) at 50 ºC temperature during 60 min inside an Elmasonic Elma S 70 H sonication bath (Figure III-1b) where ultrasonic cavitations were induced at 37 kHz instead of the mechanical stirring, the selected conditions correspond to the best results obtained in a previous work[205]. The use of an integrated physic-chemical treatment reduced significantly the elapsed time with similar temperature with CNC having similar properties after either method.
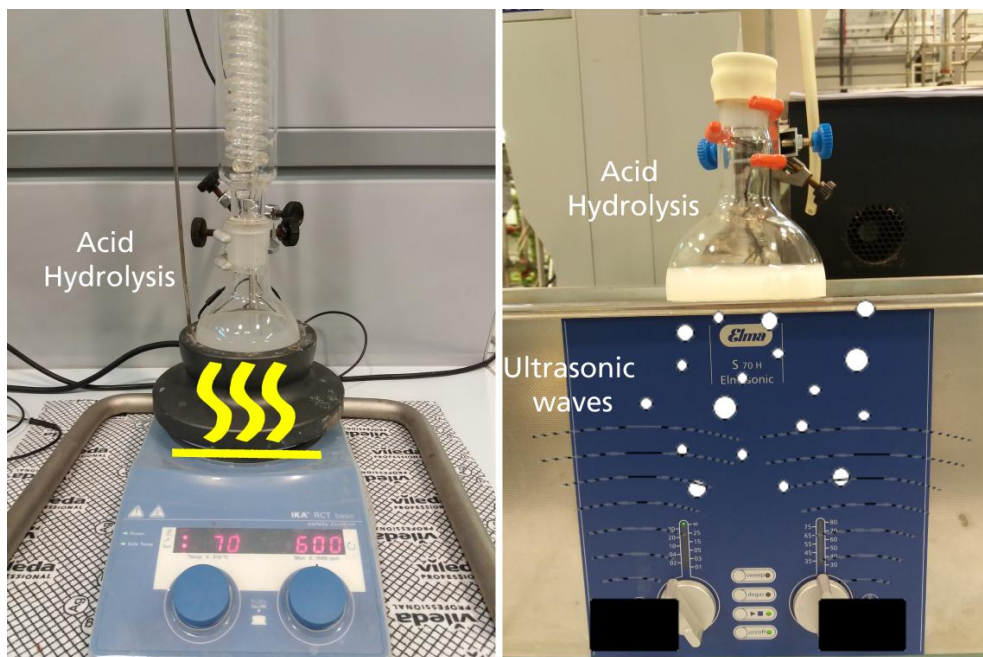
Figure III-1 Images corresponding to the two employed systems of acid hydrolysis.

Reactions were stopped with cold distilled water (1:3 v/v) for any hydrolysis performed. Separation of non-hydrolyzed fraction was done with a glass Buchner funnel (No. 1); the retained fraction was discarded, while the filtrate suspension was centrifuged once at 8000 rpm for 10 min and then dialyzed to distilled water until neutral pH was stabilized. An alternative method to neutralize the CNC suspension consisted in passing the filtrate again through a Buchner funnel using a 0.22 µm Nylon membrane and washing several times with distilled water; this step reduced considerably the neutralizing time as dialysis can take several days, but in the present work no distinction was made for these methods as the physic-chemical properties of the CNC are not directly influenced by the neutralizing methods. To avoid agglomerations and obtain a stable colloidal suspension, CNC suspensions were sonicated for 10 minutes at 20 ºC[206] after either dialysis or washing with a sonication tip at 60 % of the equipment amplitude. Figure III-2 show the separation and concentration adjustment for CNC dispersions after acid hydrolysis.. CNC suspensions were adjusted to 3 wt% and kept at -15 ºC for long term storage and at 3 ºC for short-term storage.
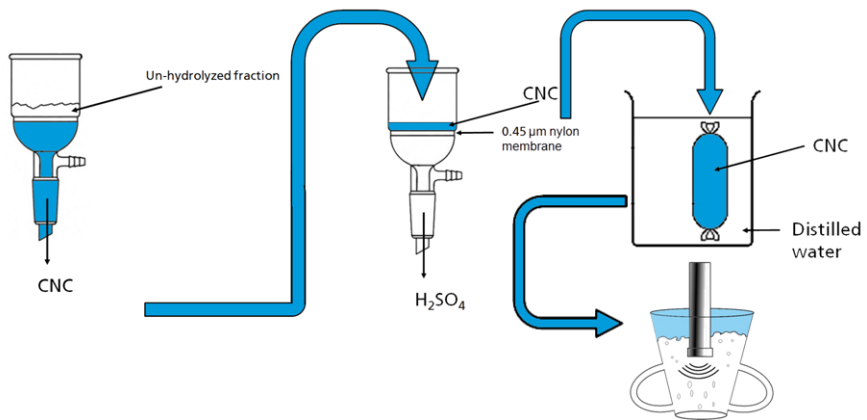
Figure III-2 CNC processing from hydrolysis to storage conditions.

Cellulose Nanofibers (CNF):

To produce CNF, dried refined cellulose was first dispersed in a water solution with a 1:10 w/w ratio and then passed through a Heidolph SilentCrusher M homogenizer during 5 minutes at 23000 rpm. After shear blending cellulose suspension was dispersed in water until 1:100 w/v suspension was obtained and then passed through a Niro-Soavi Panda high pressure homogenizer (Figure III-3). Homogenizing cycles were done under increasing pressure, starting at 300 bar and increasing 100 bar each pass until ~1000 bar were reached at which suspension was passed with constant flow-rate for a total homogenizing time of 90 min[207]. The use of shear blending, the low concentration as well as the gradual increase of homogenizing pressure avoided clogging of the homogenizing chambers, which has been reported as the main drawback of high pressure homogenizing for CNF manufacturing. CNF suspensions were adjusted to 3 wt% and kept at -15 ºC for long term storage and at 3 ºC for short-term storage.
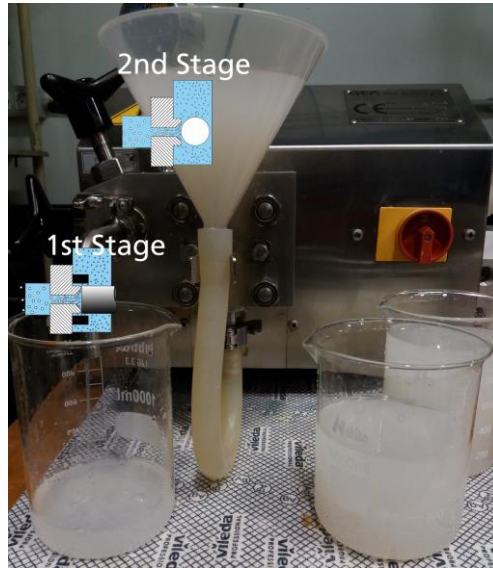
Figure III-3 Image of the high pressure homogenizer with diagrams of its two stages.

Nanocellulose characterization

Gravimetric analysis: Cellulose nanoparticles were dry measured to control the yield of each treatment after hydrolysis by using the following equation:

$$Y = (MC \times MT) (MS \times MO)^{-1}$$

Where MC is the mass of dried cellulose nanoparticles (freeze-dried and then kept inside a desiccator); MT is the mass of the total suspension, MS is the mass of the suspension sample before drying and MO is the cellulose mass before hydrolysis.

Atomic Force Microscopy (AFM): Atomic force microscopy images were obtained operating in tapping mode with a NanoScope IIIa, Multimode TM-AFM from Digital Instruments-Veeco scanning probe microscope equipped with an integrated silicon tip cantilever with a resonance frequency of 300 kHz. To obtain representative results, different regions of the samples were scanned.

Size measurement and zeta potential: Particle size and zeta potential were measured inside Malvern Z nanosizer equipment, refractive index for cellulose was considered at 1.47, measurements were performed at 25 ºC. For size analysis 0.1 g L^{-1} of cellulose suspension were put inside a disposable plastic cuvette performing 13 scans with an incidence angle of 173 ° repeated three times for each sample. For zeta potential nanocrystal suspensions were put inside Malvern folded capillary zeta cell and measured using Smoluchowski approximation for particles in polar media f(ka)=1.5[208]. For each specimen 10 runs were performed and 3 specimens were measured for each sample.

X-ray Diffraction (XRD): X-ray powder diffraction was measured to compare crystallinity. Patterns were collected with a Panalytical Phillips X'Pert PRO multipurpose diffractometer, with samples mounted on a zero background silicon wafer fixed in a generic sample holder, using monochromatic CuKα radiation (λ = 1.5418 Å) in a 2θ range from 5 to 50 with step size of 0.026 and 80 s per step of at room temperature.

Nuclear Magnetic Resonance (NMR): Solid state ^{13}C NMR spectrometry with cross-polarization (CP) and magic-angle spinning (MAS) was performed using a Bruker 500 MHz spectrometer at a frequency of 250 MHz with an acquisition time of 0.011 s, at room temperature. Spectra were recorded over 32 scans for all the nanocelluloses.

Process parameters

Table III-1 resumes the process conditions to produce all the cellulose nanoparticles. For further identification, particles produces by sulfuric acid hydrolysis are identified by capital S, while particles produces by high pressure homogenization are identified by a capital H. on the other hand, as it has been stated in the previous chapter, celluloses depending on their origin and the extraction method are identified as bagasse (B) or leaves (L) and as organosolv (O) or alkali (E). With these considerations, CNC were identified as BOS for bagasse-organosolv-TCF-acid hydrolysis; BES for bagasse-soda-ECF cellulose-acid hydrolysis and LOS for leaves-organosolv-acid hydrolysis. CNF were identified as BOH for bagasse-organosolv-TCF-homogenizer; BEH for bagasse-soda-ECF-homogenizer and LOH for leaves-organosolv-TCF-homogenizer.

Table III-1 Processing conditions for the obtention of the different cellulose nanoparticles.

Sample/ Method	Method[2]	Medium	Concentration [wt%]	Time [min]	Temperature [ºC]
BOS	HL+US	H_2SO_4 (10.2 M)	6.7	60	50
BES	HL+ST	H_2SO_4 (10.2 M)	5	120	45
LOS	HL+US	H_2SO_4 (10.2 M)	6.7	60	50
BOH	HPH	Distilled water	1	90	20
BEH	HPH	Distilled water	1	120	20
LOH	HPH	Distilled water	1	90	20

---

[2] HL is hydrolysis; US is ultrasounds; ST is mechanical stirring and HPH corresponds to high pressure homogenization.

Results and Discussion

Figure III-4 presents the atomic force microscopy of cellulose fibers after mechanical or chemical treatment. The action of sulfuric acid in the cellulose fibers allowed the isolation of cellulose nanocrystals (d, e, f) with an average width of 33±13 nm and length 350±153 nm with a very homogeneous morphology, which is due to the retention of particles with bigger size by the Buchner filter funnel cellulose separation. Bagasse fibers are more susceptible to chemical fraction because of the cooking and beating that takes part during tequila production, therefore CNC obtained from bagasse are significantly smaller than those of leave fibers under the same conditions, while CNC from bagasse prepared from alkali fibers (BOS) are thicker and larger than all. This can be due to the morphology of the fibers after pulping and bleaching, as fibers from alkali pulping end with larger dimensions than those of organosolv pulping and TCF bleaching. The use of hydrogen peroxide has been reported as an influential factor in the determination of fiber morphology after pulping as it weakens the fiber structure by oxidizing low chain carbohydrates[209,210]. While this situation is often counterproductive for pulp and fabrics, it makes TCF fibers desirable for nanocellulose production as the feasibility to obtain smaller fibers under same conditions makes them more competitive. In the case of cellulose nanofibers (a, b, c), the action of the high pressure homogenization allowed to tear microfibrillated cellulose into single nanofibers or groups of 2-3 nanofibers attached; in this case, shape is less constant as fibers are presented sometimes separated in one of their ends but still attached in the other (branching), this occurs because mechanical isolation methods do not eliminate amorphous cellulose that can still be left after the bleaching processes, anyhow the average length was 607±85 nm and the average width 68±22 nm. Mechanical defibrillation of alkali-ECF fibers presents under the same conditions more entanglement and more incidence of branching than organosolv-TCF. Moreover, CNC elaborated from alkali fibers have larger dimensions than their organosolv-TCF counterparts.
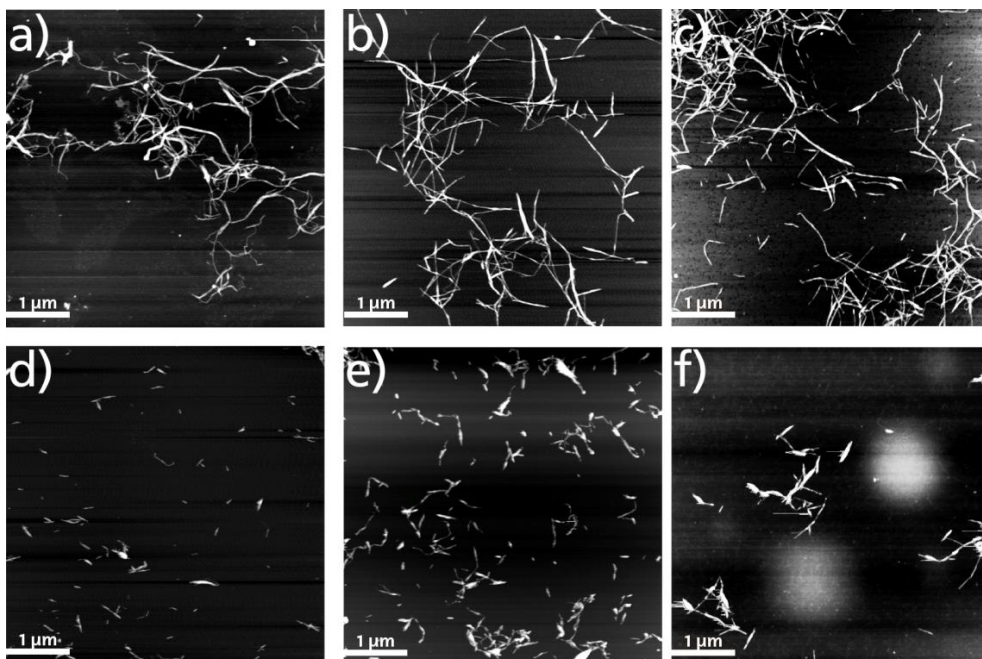
Figure III-4 AFM figures from the obtained cellulose nanoparticles: a) BOH, b) LOH, c) BEH, d) BOS, e) LOS and f) BES.

Further dimensional analysis can be achieved with the size distribution values from Figure III-5. Determining the exact dimensions of cellulose nanoparticles is difficult by the unique constraints of the different analytical methods chosen. Size distribution for cellulose nanoparticles through light scattering (LS) analysis for colloidal suspensions presents the difficulty that it reports results as the equivalent spherical diameter based on collisions of particles from the surrounding solvent molecules from a Brownian movement. In anisotropic particles, such as rod-like CNC or ribbon-like CNF the accuracy is limited and therefore is better to talk about a particle region than a precise dimension, for which AFM analysis results more precise. Nevertheless, while by AFM gives information about a particular sample that is more limited, LS gives a wider statistical approach for the range in which the obtained particles can be located, with equivalent spheres that considers from the sphere of same minimum length up to the sphere of same maximum length. Therefore it can be appreciated from Figure III-4 and Figure III-5 that there is a correlation in the tendencies of size predominance for each obtained cellulose nanoparticles. BOS samples have a predominant size range between 30 and 40 nm, which is also visible in Figure III-4d.
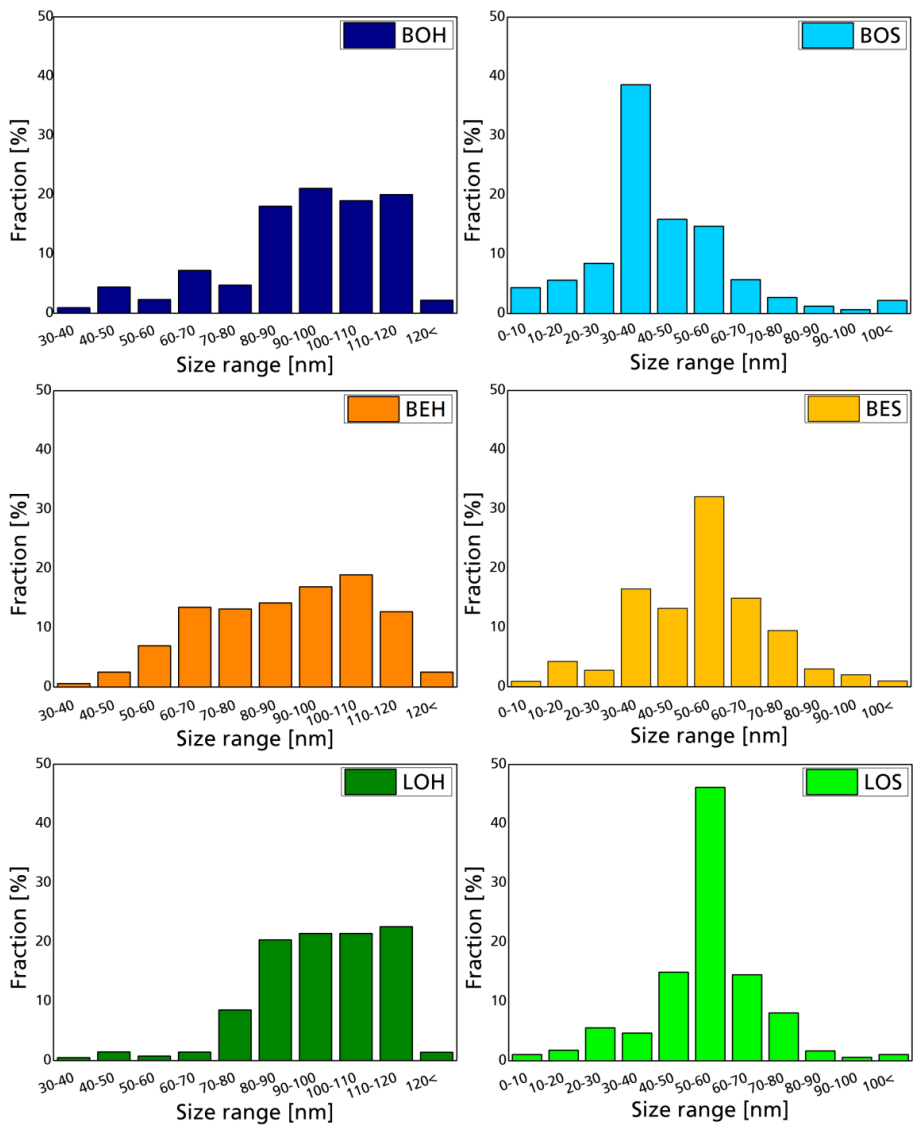
Figure III-5 Size distribution of the different cellulose nanoparticles.

The crystalline structure of cellulose has been studied since its discovery in the 19th century. Cellulose is a polycrystalline material built from ordered crystallite and low ordered non-crystalline (amorphous) phases with considerable contributions from a paracrystalline phase[211,212]. The most used approach to elucidate the crystalline structure of cellulose was done by Leon Segal and collaborators in 1969[213]. In this study, Segal used cotton cellulose in native state and decrystallized with ethylamide to give a relative crystallinity index. To achieve this index, they used the 002 lattice diffraction related to the scatter of the dissolved amorphous cellulose, which showed a 'hump' with its highest intensity around $2\theta = 18°$. Segal equation for relative crystallinity index is given by the following equation:

$$C.I._S = 100 \times (I_{200} - I_{AM}) \times (I_{200})^{-1}$$

Segal method equates peak height with degree of crystallinity, which if may not be wrong it is considerably inaccurate. Nevertheless, the Segal crystallinity index is easily implemented with data from a powder diffractometer, and it is readily understood. Thus, despite the objections is still widely used and constitutes a fast and easy tool to analyze and compare qualitatively different cellulose structures[214]. Even though this can be useful to compare diffraction patterns with the available data, the use of more accurate methods is desirable.

More recent methods to estimate the crystalline content in cellulose by powder X-ray diffraction consist in fitting a simulated curve to the diffraction pattern and decomposing the peaks that correspond to the crystalline contributions, this method has been wrongly called 'deconvolution' method, but the signal resulting from the diffraction scatter does not correspond to a convolution of two continuous signals but to an overlapping of individual peaks, therefore the correct term would be peak decomposition or peak fitting. Another method, which accuracy can be placed between the peak fitting method and the signal method is the amorphous subtraction method, which consists in subtracting the amorphous contribution to the whole diffraction pattern and then dividing the integrated area of the resulting curve by the integrated are of the whole powder diffraction pattern. The use of either these methods is more representative of the fraction of a material that is crystalline than Segal method.

For the curve fitting, a few assumptions have to be made, such as the shape and number of peaks. The most commonly used functions for XRD spectra fitting are Gaussian[215,216], Lorentzian[217] and Voigt[218] functions. Depending on the study, four crystalline peaks (101, 10ī, 002 and 040) have been assumed, but other studies consider even five crystalline peaks with the inclusion of the peak corresponding to the (021) plane[217]. However, the three main crystalline peaks for the Iα one-chain triclinic unit cell have Miller indices of (100), (010) and (110); while the counterparts corresponding to cellulose Iβ monoclyinic unit cell have Miller indices of (1–10) (110) and (200). Cellulose Iα and Iβ have the same conformation of polysaccharide chains, but differ in the hydrogen link pattern; they form the natural form of

cellulose (native cellulose) with the composition of the cellulose fibers depends on the species.

In this work, peak separations of the profiles to determine the position of signals generated by the cellulose crystalline phases individual crystalline peaks were extracted by a curve-fitting process from the diffraction intensity profiles using a non-linear least squares fitting program (PeakFit4.12), assuming pseudo-Voigt functions[219] for each crystalline reflection and a broad peak at around $2\theta = 21.5°$ assigned to the amorphous contribution. Apparent crystallinity index (Cr.I.$_D$) with peak fitting method was determined from the ratio of the separated crystalline peak area to the total reflection area including the amorphous contribution with extracted background[220]. Selected peaks correspond to the 1-10, 110, 200 and 004 Miller indices for cellulose Iβ. Apparent crystallinity was estimated with the following equation:

$$CrI._D = 100 \times (A_{-110} + A_{110} + A_{200} A_{004}) \times (A_{tot})^{-1}$$

In which the sum of the areas correspondent to the diffraction of crystalline planes is assumed to be the area of the crystalline region, while A_{tot} corresponds to the total area[215,221]. Least square iterations were done until coefficient of determination $R^2 \geq 0.997$ was achieved, which corresponds to a 99.7 % accurate fitting.

The Scherrer method[222] is used to obtain X-ray diffraction measurements in powders. Assuming some hypothesis as good crystallinity, distribution of length or particle shape, it can be related to the mean domain size also called crystallite, but not 'crystal size' nor 'particle size'. This method is applicable to crystallites ranging from 10 to 1000 nm in diameter. Therefore, the use of this method is quite inaccurate to determine real size parameters for cellulose, as CNF can reach several microns, and both CNF and CNC present shapes that under no circumstance can be assumed as spherical particles. Moreover, while CNC have higher crystalline order, they still content paracrystalline and yet some residual amorphous patterns. Nevertheless, while in crystallographic analysis the use of Scherrer crystallite size has been considered obsolete[223] and has been surpassed by electronic microscopies or light scattering to gather information about nanocrystalline structures, in the nanocellulose studies the Scherrer crystallite size is still encouraged. Therefore the Scherrer apparent crystallite size is presented in this work, but without risking into giving a deep analyze of this parameter as it cannot be considered objective. Crystallite size was estimated with the Scherrer equation using the peak corresponding to the (200) plane as seen in the following equation:

$$d_{200} = \varkappa \lambda \times (H_{200} \cos\theta)^{-1}$$

With $\varkappa$ being the Scherrer constant most adjusted to the nanocrystal shape (0.86), λ the wavelength (1.5418 Å), H200 corresponds to the breadth (β_{hkl}) or full width at half

maximum intensity (FWHM) for the (002) peak and θ is half the Bragg angle at peak maximum given in radians[222,224,225].

In the present work, powder diffraction patterns are presented in three different formats, the first (Figure III-6) corresponds to the raw powder diffraction patterns obtained using symmetrical transmission mode with normalized intensities, the second (Figure III-7) corresponds to the fitted curves as obtained with PeakFit4.12 software and the third (Figure III-8 and Figure III-9) corresponds to the normalized individual signals attributed to the crystalline diffractions, Miller indices corresponding to cellulose Iα (green) and cellulose Iβ (blue) are marked in the X axis.

Normalized diffraction patterns show similar shapes which are also concurrent with those published elsewhere for cellulose I crystalline allomorphs[226] with two main overlapped signals at 2θ = 14-16° and 2θ = 20-24° and a small signal at 2θ ~34°. Fitted curves show peaks associated with cellulose corresponding to 1-10, 110, 200 and 004 crystalline planes, which are present in all the cases with different intensity and broadening. A general assumption for this analysis is that increased amorphous contribution is the main contributor to peak broadening. However, more than a crystalline disorder (amorphous content), there are other intrinsic factors that influence peak broadening, such as crystallite size and the anisotropy of the shape of the crystallites[227], (not to be confused with an anisotropic distribution) as there have been reported non-uniform strains within the crystal[228]. However, the presence of hidden 'humps' or 'halos' which is more visible in CNF from organosolv pulping, is without any doubt due to amorphous presence. CNC samples have more defined shapes with the peak due to 002 plane being well defined and broad (small crystallites) while homogenized CNF have scatters with more differences between each other. BEH does not present the characteristic halo between 2θ = 10-15°, which corresponds to low-crystalline cellulose as it has been stated in other works, this typical 'hump' starts at 2θ ~ 12° and has its main height at 2θ~ 19.92° which corresponds to typical amorphous contribution of native cellulose[229].
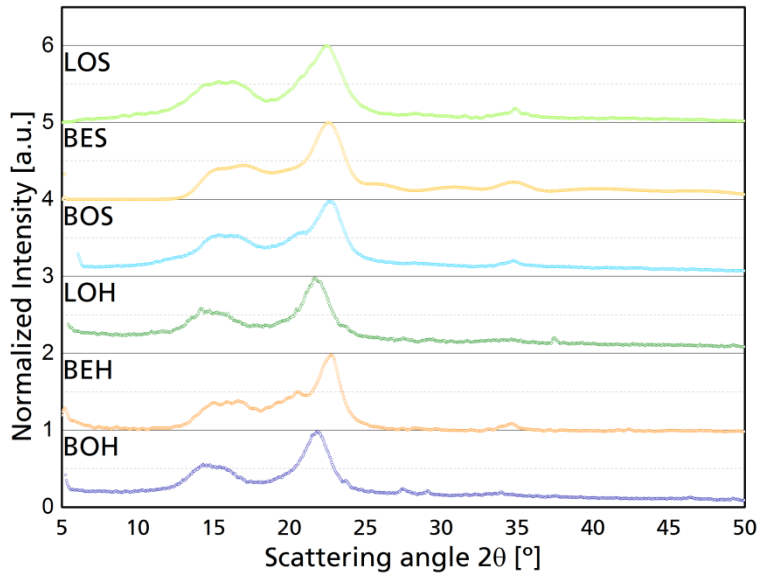
Figure III-6 Raw powder XRD patterns with normalized intensities.
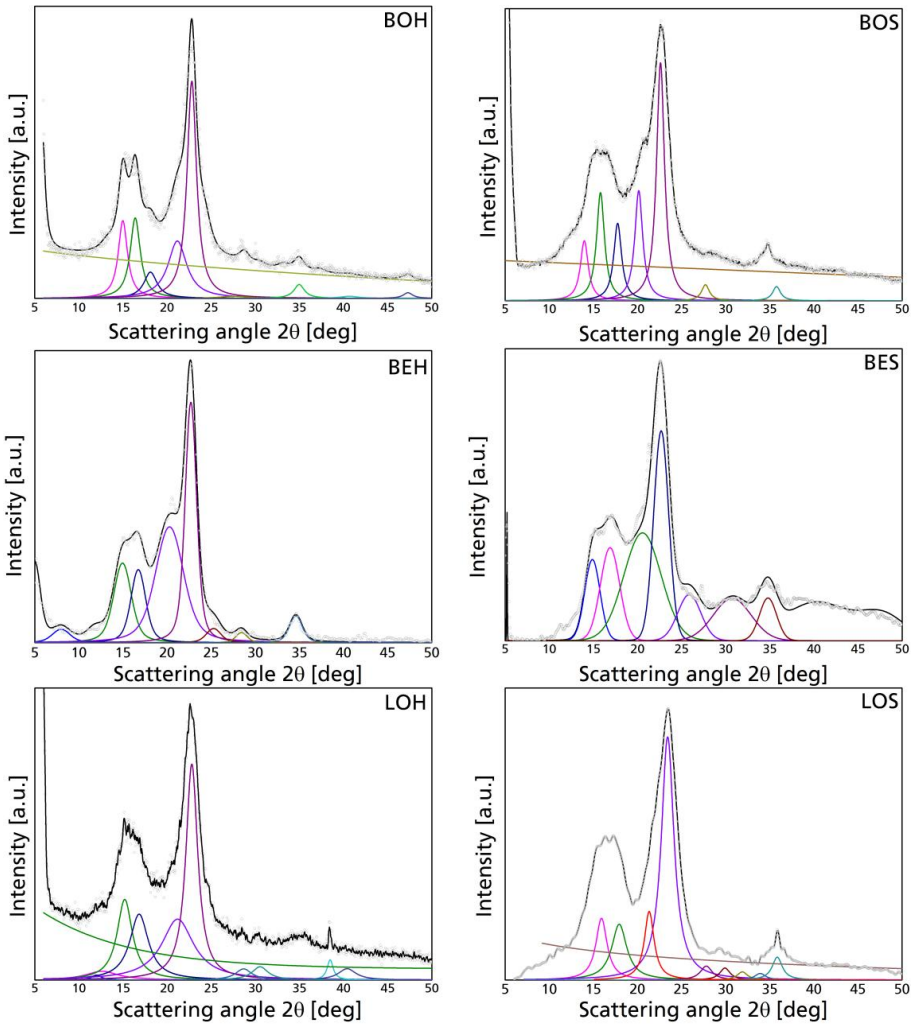
Figure III-7 Fitted curves with individual peaks for the different elaborated nanoparticles.
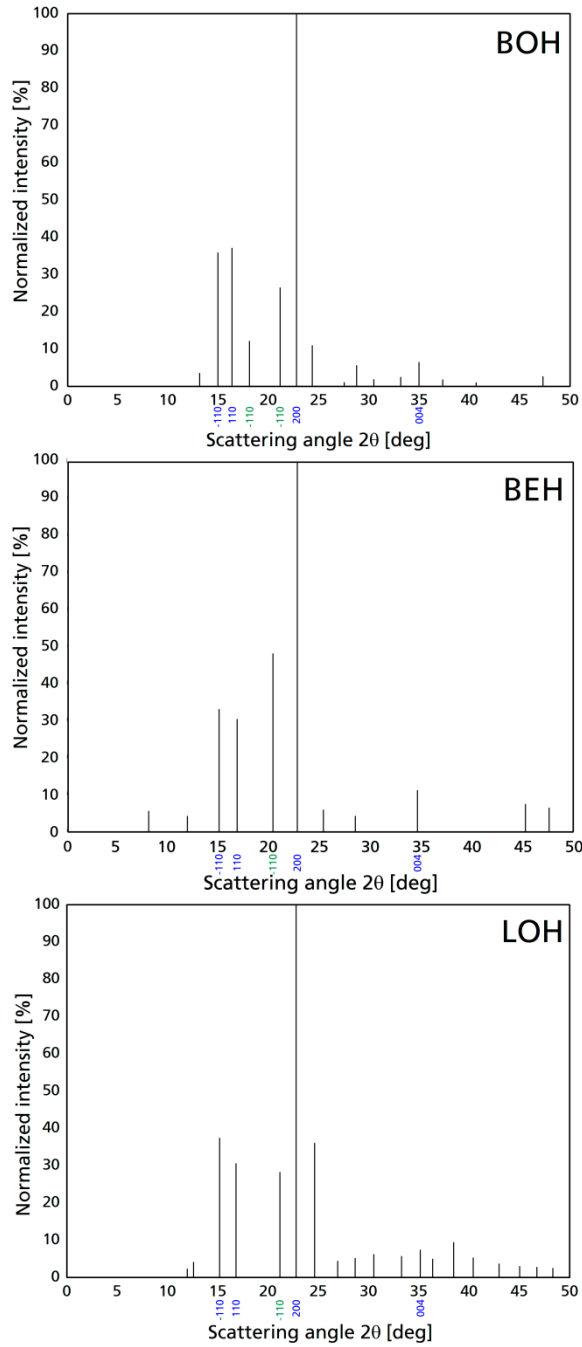
Figure III-8 Normalized stick patterns of the different CNF. Blue numbers correspond to the Miller indices of cellulose Iβ main crystalline planes, while green numbers correspond to cellulose Iα crystalline planes.
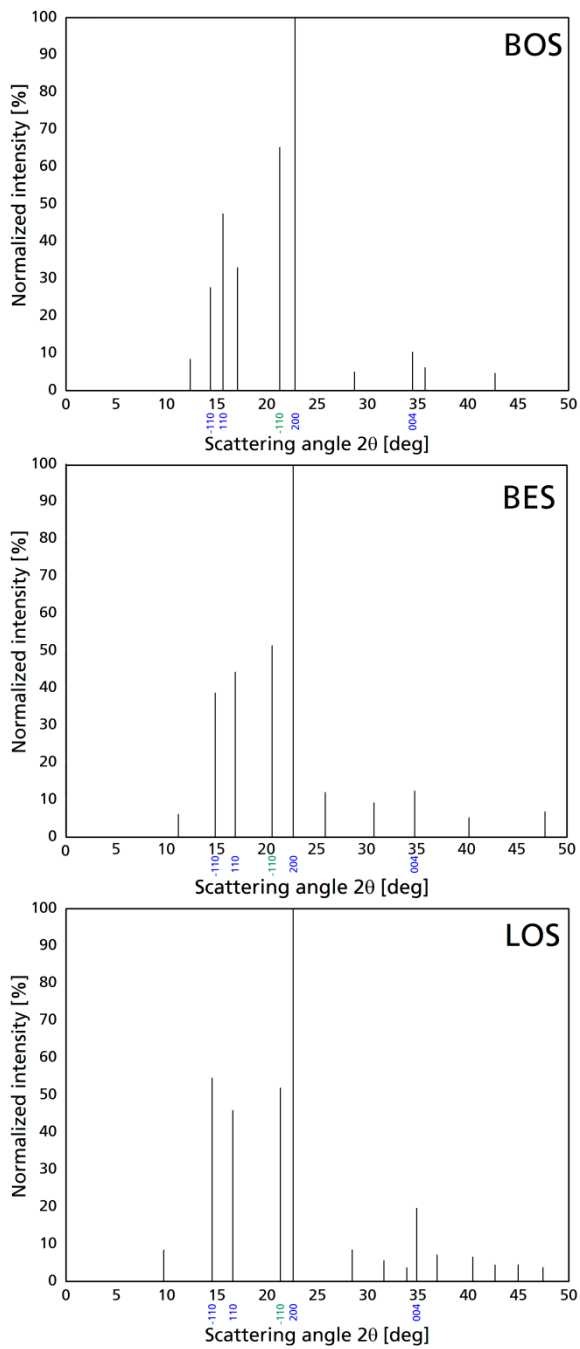
Figure III-9 Normalized stick patterns of the three types of CNC. Blue numbers correspond to the Miller indices of cellulose Iβ main crystalline planes, while green numbers correspond to cellulose Iα crystalline planes.

When obtaining cellulose nanoparticles, two main issues are observed besides the yield, those are the crystallinity and the zeta potential (ζ_{POT}), Table III-2 presents yields (Oy and Ry), medium dimensions (L and D), zeta potential and crystallinity index, it also displays crystallite size as approximated by Scherrer equation. Crystallinity index was calculated using Segal method (Cr.I$_S$) which is the easiest way to qualify crystallinity indexes and therefore the most widely used but, as explained before, with low accuracy and, therefore crystallinity index obtained with the peak fitting or peak decomposition method (Cr.I$_D$) is also presented, which represents a more accurate crystallinity value as it considers the signals generated by all the crystalline planes as well as the errors generated by the equipment. For this work, crystalline indexes show little differences between the two methods, but is concurrent with previous works in which Segal index is lower than that of peak decomposition method, on the other hand, both methods show higher indexes for cellulose nanocrystals obtained by acid hydrolysis than cellulose nanofibers obtained by mechanical methods, which is related to the elimination of paracrystalline cellulose during hydrolysis in which glucose chains of amorphous cellulose are dissolved from the main fibrils. Moreover, soda pulped cellulose has in general higher crystallinity by either method than their organosolv counterparts, which is related to the solubility of non crystalline cellulose in soda under determined circumstances[230].

Zeta potential presented values that are characteristic of cellulose nanocrystals and cellulose nanofibers respectively; with nanocrystals presenting more stability than nanofibers because of residual sulfur particles attached to the –OH groups on the cellulose surface that may remain after hydrolysis[231]. Previous works have also achieved stable cellulose nanoparticles[232,233]. Oy is the yield of cellulose nanoparticles after hydrolysis or homogenization and Ry is the yield of cellulose nanoparticles referred to the original cellulose content, this is important as this value shows the expected cellulose nanoparticles that can be obtained from the initial cellulose after cellulose loses or degradation after each treatment. As acid hydrolysis dissolves non-crystalline regions of the cellulose structures, yields for cellulose nanocrystals are lower than those of cellulose nanofibers, which in contrast present lower crystallinity indexes with both crystallinity evaluation methods. Leave fibers have the highest yields as no previous treatment is performed, with 60.84% and 93.84% for CNF and CNC respectively, while bagasse had 50.23% and 86.24%, bagasse fibers were less resistant to chemical hydrolysis and presented more degradation, as the auto-hydrolysis done during sugar extraction had already influenced the fiber morphology. Crystalline indexes show little differences between the two methods, but is concurrent with previous works in which Segal index is lower than that of Deconvolution method, on the other hand, both methods show higher indexes for cellulose nanocrystals obtained by acid hydrolysis than cellulose nanofibers obtained by mechanical methods, which is related to the elimination of paracrystalline cellulose during hydrolysis in which glucose chains of amorphous cellulose are dissolved from the main fibrils.

Table III-2 Yields and properties of the different nanoparticles[3].

Sample/Method	Oy [g×100 g⁻¹]	Ry [g×100 g⁻¹]	Cr.I$_S$ [%]	Cr.I$_D$ [%]	ζ_{POT} [mV]	L [nm]	D [nm]	δ_{200} [Å]
BOS	50.23	36.17	84.68	78.12	-32.1±2.52	300±13	60±4	~38
BOH	86.24	61.92	75.89	73.75	-20.4±1.59	850±180	91±3	~54
BES	55.41	23.82	57.09	61.52	-30.61±1.17	350±153	80±12	~34
BEH	90.15	38.76	54.93	53.95	-20.54±2.15	607±85	68±22	~39
LOS	60.84	49.28	87.10	82.65	-34.7±2.74	210±15	45±5	~34
LOH	93.84	75.33	72.29	72.16	-24.2±1.89	1140±115	85±3	~53

---

[3] Oy Corresponds to overall yield, the amount of CNC/CNF obtained for each 100 g of cellulose, Ry Corresponds to relative yield, the amount of CNC/CNF obtained related to the cellulose content as calculated by Tappi methods, Cr.I$_S$ corresponds to the crystallinity index calculated with the Segal method, Cr.I$_D$ corresponds to the crystallinity index calculated with the deconvolution method, ζ_{POT} is the zeta potential and δ_{200} is the crystallite size approximated with the Scherrer equation.

Nuclear magnetic resonance chemical shifts corresponding to ^{13}C CP-MAS are presented in Figure III-10. In general, the position of carbon chemical shifts which correspond to cellulose carbons as obtained by NMR are within the same range as those reported by other researches[234], however the shape of the peaks differ between the different nanocelluloses. To identify celluloses by NMR the most important aspect can be found in the C-4 and C-carbons, which have a crystalline and an amorphous contribution that has been identified in several researches in which C-4 region can be found between 95 and 80 ppm divided in a crystalline region (90-85 ppm) and an amorphous region (85-80 ppm) while C-6 region is generally found between 65-55 ppm also with defined with crystalline region (65-60 ppm) and amorphous region (60-55 ppm). In the present work, C-4 crystalline region is similar for all the elaborated nanocelluloses, and most of them have similar peaks at the C-6 crystalline region, but it is in the amorphous region that main differences can be found.
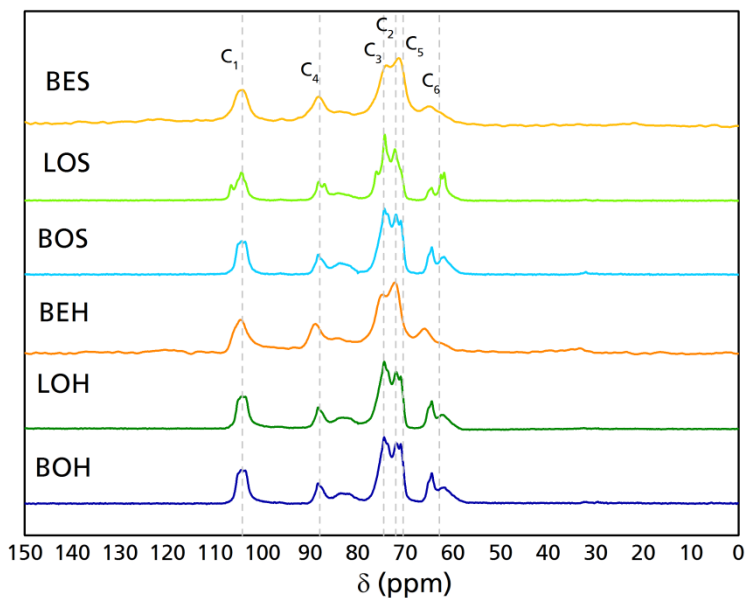
Figure III-10: Chemical shift of the different nanoparticles. With the cellulose I carbons highlighted.

LOS signal has a different shape in the C-4 and C-6 regions, with a less intense signal in the accessible fibril surface region (85-80 ppm) and with the Iα and Iβ peaks more pronounced in the C-4 region, which may imply a reduction in the paracrystalline region (this can be corroborated with the Cr.I in Table III-2). On the other hand, soda nanocelluloses (BES and BEH) have different C-6 regions than organosolv nanocelluloses. These differences are in the paracrystalline region of the C-6 peaks in which hemillellulose overlapping is not present[235], and this effect is seen in previously reported nanocelluloses obtained from soda pulping[236].

Conclusions

Six different nanocelluloses were extracted from the main residues of blue agave plantations for tequila industry. The properties of each type could make them useful for different applications. In general organosolv CNF from either blue agave leaves or bagasse are more competitive as nanofibers than soda pulped CNF. While CNC from soda pulping are more competitive as CNC than organosolv, as they have more properties in common with previously reported CNC.

The selection of the pulping and the morphology of the nanocellulose, either CNC or CNF, should be made taking in to account the final application intended, as CNC and CNF present differences in their morphology and mechanical properties, while organosolv pulped and soda pulped celluloses have chemical and physical differences, therefore, for the further experiments of the present work, BOH, BEH, LOH and BES were used for surface modification and composites elaboration.

IV) Capítulum tertium

Nanocellulose functionalization

Motivation

Surface modification with silanes has been proved to be a good method to render cellulose surface hydrophobicity, giving stability in non polar environments[165]. Silane chains can improve matrix-filler interactions either as suspension in organic solvents or added as bulk into the polymeric matrix[166,167] by serving as a coupling agent between the cellulosic filler and the polymeric matrix. On her behalf, esteric stabilization of cellulose nanocrystals with different fatty acids has shown good properties forming continuous composites with polymer matrices, as they show high degree of substitution when the esterification is performed both at the fiber surface and in the inner layers; resulting in a heterogeneous esterification, causing de-crystallization of cellulose which enhances hydrophobicity and bonds between the matrix and the cellulose fiber, in expense of thermal stability of the cellulose[168]. In this chapter, two modifications were performed in the surface of cellulose nanoparticles as a mean to enhance the inherent properties of cellulose either as a reinforcement in polymeric matrices or as surface layer in biobased composites. The selected reagents were a fatty acid and an organosilane, being the first 3-aminopropyl triethoxysilane and the second dodecanoyl chloride.

Experimental methods

Surface modifications

Esterification

Fatty acid esterification as previously reported method by Freire and collaborators was used with slight modifications[168]. For this, one equivalent of dodecanoyl chloride (DDC) per gram of CNC was put inside a flask alongside 50 mL of toluene and 1 equivalent of pyridine as catalyst, then CNC were added and stirred with 400 rpm for 6 hours at 110 °C using reflux. The slurry was centrifuged and then washed with toluene, acetone, and ethanol before setting it inside a soxhlet where the remains were extracted during 12 hours using ethanol. After this, the modified CNC were oven dried at 50 °C for 24 hours. A resumed scheme with the reaction parameters is displayed on Table IV-1; on the other hand, visual aspect of esterified CNC can be seen in Figure IV-1.

Table IV-1 Sample and treatment conditions of the esterified CNF.

Sample	Solvent	Cellulose sample	DDC ratio	T_R [°C]	T_C [°C]	t [min]
F1	Toluene	BOS/BES	1 eq.	110	105	360

Silanization

Cellulose nanofibers were modified with 3-aminopropyl triethoxysilane (ATS) solution inside a plastic beaker to avoid ATS reactions with glass surface, the use of distilled water is not necessary, but water containing fluoride ions must be avoided, however for this work distilled water was used for the whole process.

Traditionally, silanes are diluted in aqueous alcohol solutions prior to applying, with a conventional ratio of 95 % ethanol and 5 % water, which is further adjusted to a pH of 4.5-5.5 with acetic acid. The recommended silane concentration for silanes is 2 %. For the present work, neat silane relation to cellulose nanofibers was 1:1, 2.5:1 and 5:1 w/w which correspond to approximately 0.5 to 2.0 % silane concentration in de solution. ATS solution was first diluted in ethanol, ethanol-water (50/50) or water; pH was neutralized by dribbling acetic acid with constant stirring. Once pH was stable, CNF were dispersed in ethanol, ethanol-water (50/50) or water at approximately 3 wt% and added to their corresponding silane solution. The mixture was stirred with a Silent crusher homogenizer at 2000 rpm during 5 min and left at room temperature for another 45 min, during which hydrolysis and silanol formation take part. The slurry was vacuum-filtered to stabilize the cellulose content and kept at 3 wt% in the form of gel, which was stored at 3 ºC in plastic containers for further analysis. The completion of silanization requires a curing at 110 ºC during 5-10 minutes, but preserving the nanocellulose-silane solution in wet state allows better dispersion and better processing conditions for composites elaboration.

For solid-state analysis of the silanized nanocelluloses, the gel was oven cured until no solvent was left and rinsed two times with ethanol; then pressed to form films with a hydraulic press at 185 bar and 100 ºC[237]. Table IV-2 presents the reaction conditions for the different silanizations, moreover, the visual aspect of one of the silanized CNF can be seen in Figure IV-1.

Table IV-2 Samples and treatment conditions of the silanized CNF.

Sample	Solvent	Cellulose sample	ATS ratio	T_R [ºC]	T_C [ºC]	t [min]
W1	Water	BOH	1:1	20	105	50
W2	Water	BOH	1:2.5	20	105	50
W5	Water	BOH/BEH	1:5	20	105	50
M1	Ethanol-Water	BOH	1:1	20	105	50
M2	Ethanol-Water	BOH	1:2.5	20	105	50
M5	Ethanol-Water	BOH	1:5	20	105	50

E1	Ethanol	BOH	1:1	20	105	50
E2	Ethanol	BOH	1:2.5	20	105	50
E5	Ethanol	BOH	1:5	20	105	50
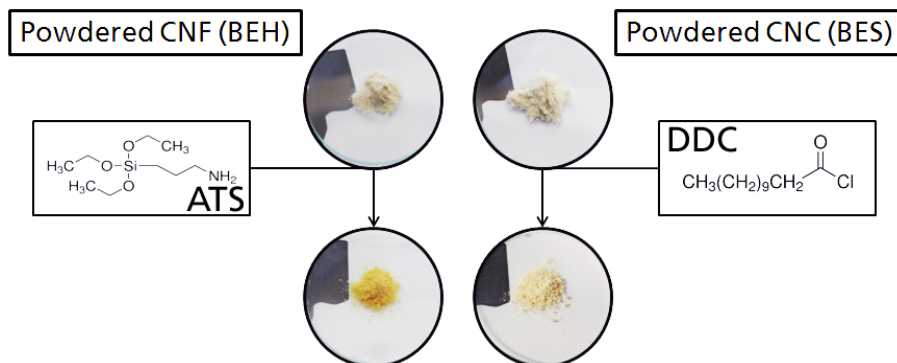
Figure IV-1 Visual aspect of powdered BEH and BES before and after modification with ATS (BEH-W5) and DDC (BES-F).

Characterization methods

Chemical analysis of the fibers was performed to determine the amount of cellulose available for further extraction. This characterization was carried out according to standard methods[191–194,121].

Atomic Force Microscopy (AFM): Atomic force microscopy images were obtained with a NanoScope IIIa, Multimode TM-AFM from Digital Instruments-Veeco scanning probe microscope operating in tapping mode equipped with an integrated silicon tip cantilever with a resonance frequency of 300 kHz. To obtain representative results, different regions of the samples were scanned, for films AFM images are presented in 2D and 3D.

Attenuated Total Reflectance (ATR): Infrared spectra were recorded on a PerkinElmer Spectrum Two FT-IR Spectrometer equipped with a Universal Attenuated Total Reflectance accessory with internal reflection diamond crystal lens. The defined range was from 4000 to 400 cm^{-1} and the resolution 8 cm^{-1}. For each sample 10 scans were recorded.

Thermogravimetric analysis (TGA): TGA essays were carried out in a TGA/SDTA 851 Mettler Toledo instrument according to standard test methods[238], this consisted in putting ~5 mg of sample under 20 mL min^{-1} nitrogen atmosphere from 25 to 800 °C at 10 °C min^{-1}. The thermal decomposition temperature was taken as the onset of significant weight loss, after the initial moisture loss.

X-ray Diffraction (XRD): X-ray powder diffraction was measured to the contribution of amorphous silanes in the structure of nanocrystalline cellulose. Diffraction scatters were collected with a Panalytical Phillips X'Pert PRO multipurpose diffractometer, with samples mounted on a zero background silicon wafer fixed in a generic sample holder, using monochromatic CuKα radiation (λ = 1.5418 Å) in a range from 5 to 50 2θ with step size of 0.026 and time per step of 80 s at room temperature.

Nuclear Magnetic Resonance (NMR): The ^{13}C and ^{29}Si NMR spectrometry were performed using a Bruker 500 MHz spectrometer at 250 MHz of frequency with an acquisition time of 0.011 s, at room temperature. The spectrum was recorded over 32 scans using water as solvent for all the samples.

Surface energy: Contact angle measurements were performed with a DataPhysics video-based measurement contact angle system OCA20 with a software controlled dosing volume using 5 µL drops with water, formamide and diiodomethane to determine surface tension, results correspond to at least 6 measurements. To determine the surface free energy Owens, Wendt, Rabel and Kaelble (OWRK) method was used for the cellulose-silane films[239–241].

Results and discussion

Cellulose esterification

In both cases aspect ratio left a large amount of surface able to modify show silanized nanofibers and esterified nanocrystals respectively, it can be clearly observed the surface modification and the formation of particle aggregates.

Cellulose silanization

Silanes are silicon chemicals that possess a hydrolytically sensitive center that can react with inorganic substrates such as glass to form stable covalent bonds and possess an organic substitution that alters the physical interactions of treated substrates.

Silanization occurs in four steps that will be further described but which basically involve a chemical grafting on the OH groups that are in the surface of cellulose polymorphs (in this case CNF consisting basically in cellulose Iβ), which reacts at temperatures ranging between 80-110 ºC. In this work, prior using or curing, silanized CNF were kept in form of gel, the different types of silane-cellulose couplings are presented in Figure IV-2.

The general formula of an organosilane can be written as follows:

R_n Si X (4-n)
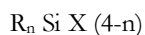
The X functional group is involved in the reaction with the inorganic substrate, which is a hydrolyzable group, typically, alkoxy, acyloxy, amine, or chlorine. The most common alkoxy groups are methoxy and ethoxy, which give methanol and ethanol as byproducts during coupling reactions. R is a nonhydrolyzable organic radical that possesses a functionality which enables the coupling agent to bond with organic polymers. Most of the widely used organosilanes have one organic substituent. In most cases the silane is subjected to hydrolysis prior to the surface reaction.

Following hydrolysis, a reactive silanol group is formed, followed by condensation to oligomers with other silanol groups to form siloxane linkages. The oligomers then hydrogen bond with OH groups of the cellulose, stable condensation products are also formed with other oxides form stable bonds with Si – O –. Water for hydrolysis may come from several sources; it may be added or present on the substrate surface or it may come from the atmosphere. During drying or curing, a covalent linkage is formed with the substrate with concomitant loss of water although described sequentially, these reactions (R_x) can occur simultaneously after the initial hydrolysis step. At the interface, silicon units of the organosilane may bond uniquely by one to the substrate surface (R_1); the two remaining silanol groups are present either bonded to other coupling agent silicon atoms or in free form. Further surface interactions include: two silylether bonds reacted onto cellulose (R_2), aminosilane reacted onto cellulose with three silylether bonds (R_3), aminosilane reacted onto cellulose but also condensed with another aminosilane (R_x-R_n), or aminosilane is

polymerized (R4)[242]. At the interface, there is usually only one bond of the organosilane silicon on the substrate surface. The R group remains available for covalent reaction or physical interaction with other phases. Silane coupling agents with three alkoxy groups are the usual starting point for substrate modification. These materials tend to deposit as polymeric films, effecting total coverage and maximizing the presentation of organic functionality.
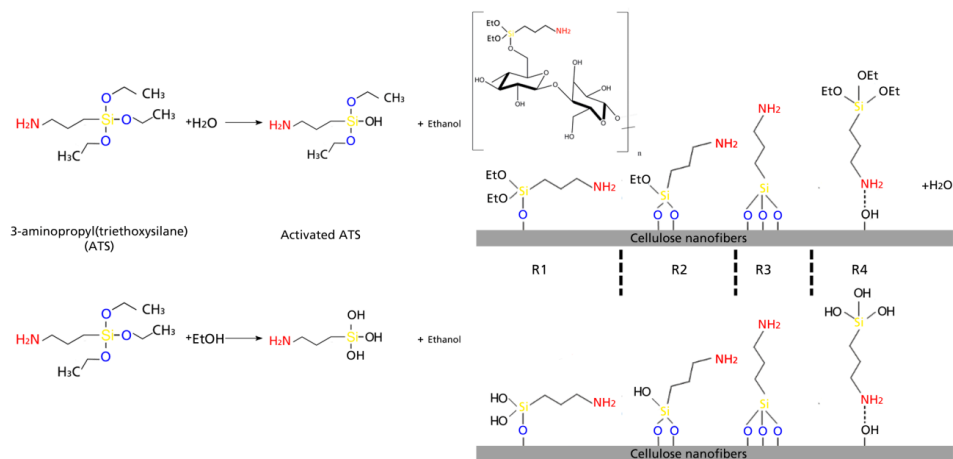
Figure IV-2 Reaction dynamics for the cellulose silanization.

To analyze individual silanized fibers, cured CNF were redispersed in the media in which they were elaborated until a 0.5 wt% concentration was achieved, and then sonicated during 5 minutes to disperse entanglements. Figure IV-3 shows selected redispersed fibers after silanization. The interaction of silanes in water-media (W-series) generates more hydrolyzed silanol units, which makes it more reactive to form covalent bondings with cellulose free hydroxyl groups. Visually, the formation of agglomerations between CNF in Figure IV-3a as well as the halo formed around the fibers, which is not present in the ethanol-media (E-series) modified CNF neither in the mixed media (M-series). Besides this phenomenon, there is no significant difference in the morphology of the silanized CNF.
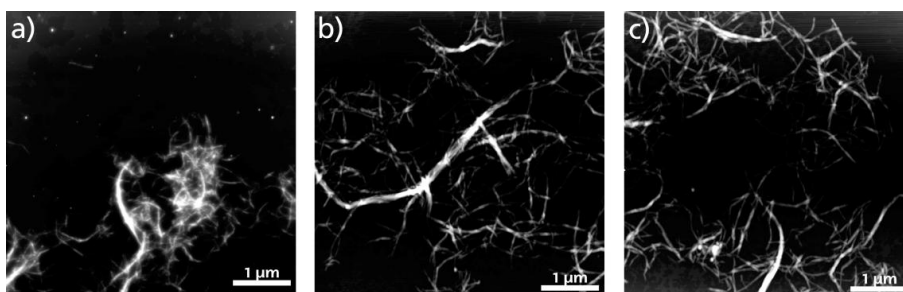
Figure IV-3 AFM images of a) W5, b) M5 and c) E5.

Surface topographies of modified CNF give further information regarding the interactions between fibers after the solvent is evaporated, the assembly is anisotropic, as is common in CNF solvent casted films, with significant differences between the fibers modified in aqueous or ethanol media. Figure IV-4 presents AFM topographies of selected solvent-casted films which correspond to the CNF containing the highest yield of silanes in the solution (W5, M5 and E5), this was done as the higher amount of silane would make it easier to appreciate changes in the CNF topography. There is an unquestionable difference between CNF modified in aqueous media regarding those modified in alcoholic media; with the first presenting a broader and stiffer structure i.e. CNF tend to be straighter and with wider diameters as it can be appreciated in Figure IV-4a and b. On the other hand; when little water is present, the way silanes are attached to the CNF and the way modified CNF interact between each other is significantly changed, individual fibers are narrower and have more visible entanglements. Figure IV-5 shows the visual aspects of casted CNF-silane films before and after pressing.
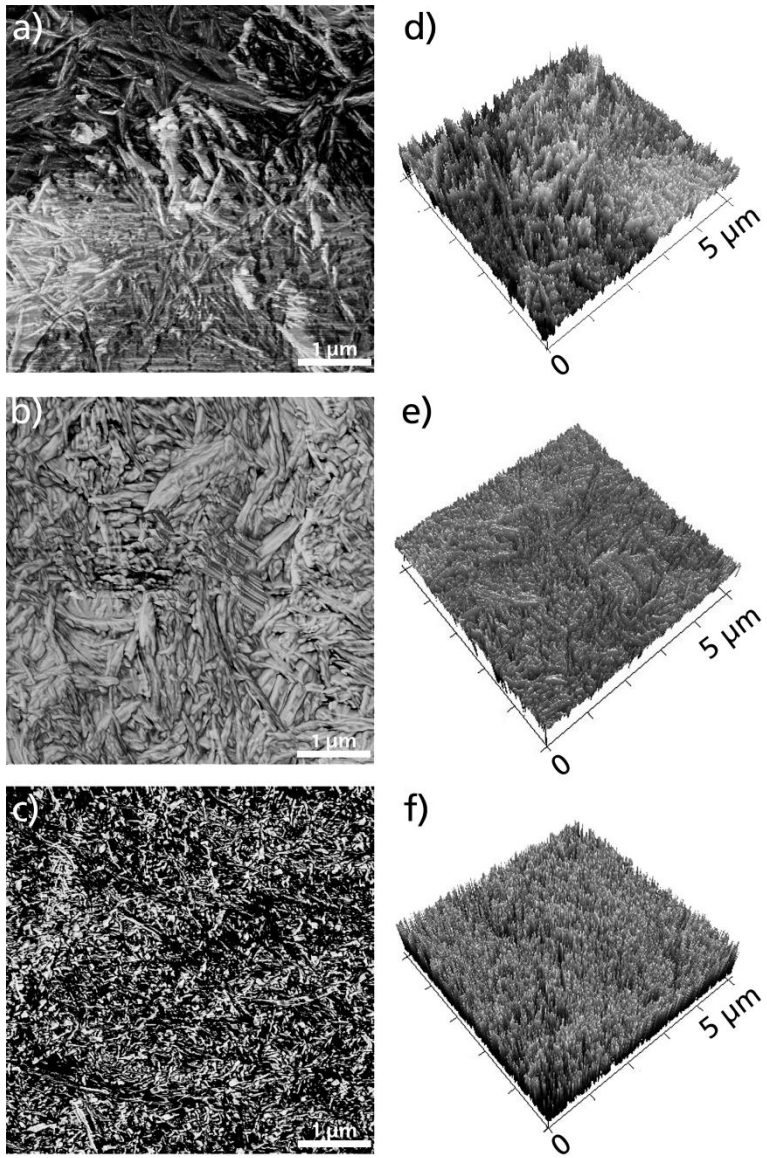
Figure IV-4 AFM topographies of a) W5, b) M5 and c) E5 on 2D; and d) W5, e) M5 and f) E5 on 3D.

Figure IV-5 Visual aspects of the elaborated CNF-ATS films a) before pressing, b) before and after pressing and c) after pressing.

The infrared spectra were analyzed to identify ATS, Figure IV-6 presents the FT-IR spectra of native and silanized CNF; spectra in the left column correspond to the normal spectra as obtained from the equipment, while right column presents the same spectra in tile form separated by y-axis offsets, moreover, tile spectra have shadowed the bands to enhance visual appreciation of the different variations.

In general, silanized nanocelluloses present changes in the behavior of bands between 3600-3000 cm^{-1} because of the modification of the free hydroxyl present in native cellulose, this band tend to reduce its intensity as the hydroxyl groups are less available as they have reacted with the silanol groups. The IR spectrum at 1800–1500 cm^{-1} of the different nanocelluloses was used to estimate the effect on the binding of the aminosilane with the cellulose. The band at 1750 cm^{-1} proved to be characteristic for the vibrations of the carbonyl group $C = O$. The IR spectra contained bands at 1600–1580 cm^{-1}, characteristic of deformation vibrations of N–H coming from the I amine group in the ATS. Moreover, the IR spectra contained bands at 1550 cm^{-1}, characteristic of amino scissoring bending vibration from the amine group in the silane. The presence of these bands in the IR spectra of the modified cellulose also confirmed the stable bonding of the silane preparations with the cellulose. In the 1300-1000 cm^{-1} band, there is an increase in the intensity of the bands because of the chemisorbed ATS related to the Si-O-Si bonding[243].

In the spectra of the modified cellulose with the ATS, there was also a band at 710 cm^{-1}, characteristic of vibrations of Si–C and Si–O groups coming from the ethoxy group in the organosilane. This confirmed that a reaction had occurred between the cellulose and organosilane, as discussed earlier.
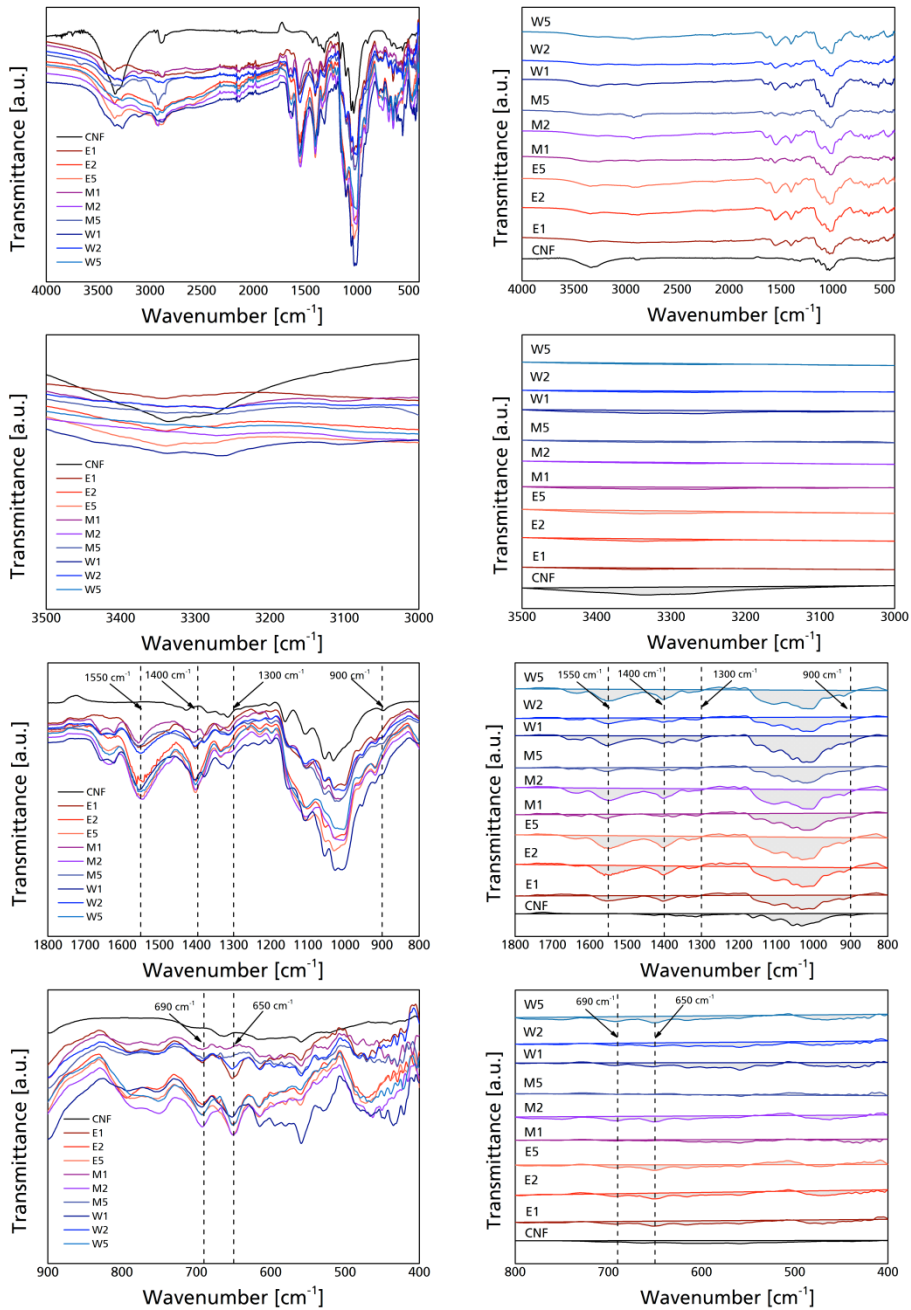
Figure IV-6 FT-IR spectra of native and silanized CNF.

For the esterified CNF, the aliphatic acid chains in the case of DDC are identified by FT-IR. Bands at ~2854 and ~2923 cm^{-1} correspond to the C-H band, belonging to aliphatic acid chains, also a new band can be observed at ~1743 cm^{-1} corresponding to the 1750-1735 cm^{-1} ester carbonyl band[168], this three bands that occur in characteristic bands of DDC prove the successful esterification of the nanocellulose.
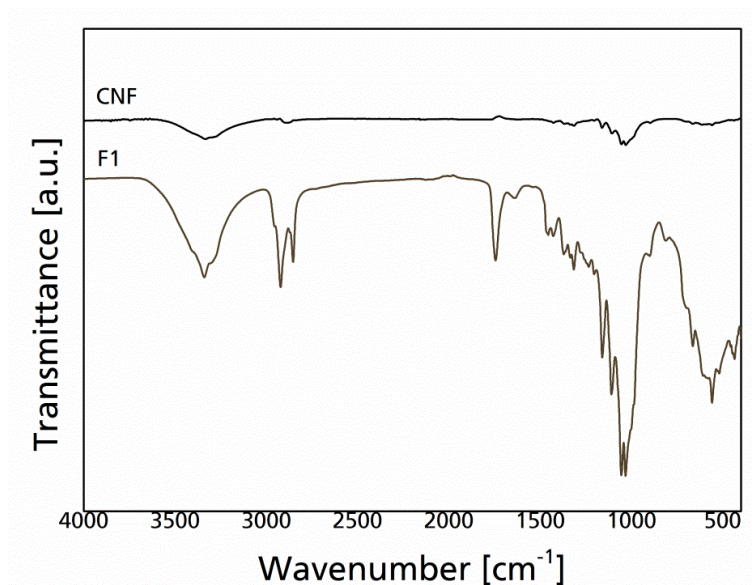
Figure IV-7 FT-IR spectra of native and esterified CNF.

Another method to analyze the influence of silanization in cellulose nanoparticles is the thermogravimetry. During thermal degradation of fibers, there are two main aspects to consider, the mass loss at key temperatures which correspond to the mass changes of a sample due to degradation of determined components as function of the temperature, time and atmosphere under which the thermogravimetry is performed; the other aspect is the final residue which correspond to ashes. Such ashes are composed of char and inorganic compounds. Figure IV-8 shows thermogravimetric curves as well as differential thermogravimetric curves of native and silanized CNF. The increase in the residue after 800 ºC is due to both, silicon and carbon presence in the silanized CNF.

With lower silane yield, there is a considerable variation between the different silanized specimens; however, with the highest amount used, differences between the final residues are not significant, regardless the solvent used.
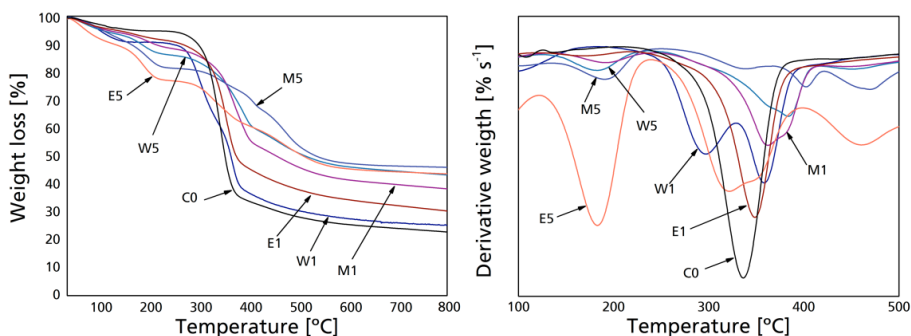
Figure IV-8 Left: thermogravimetric curves of native and silanized CNF. Right: 1st differential thermogravimetric curves of native and silanized CNF.

Cellulose is a paracrystalline polymer composed by crystalline regions attached to amorphous domains[212]. After silanization, the surface modification performed in each sample generated a new amorphous region around the paracrystalline cellulose by hydrogen bonds with the hydroxyl groups present in the exterior chains of the molecular wall. In X-ray diffractograms, the contribution made by amorphous silanes in the structure of the nanocelluloses can be appreciated.

In general, after silanizations it can be observed a slight bump as a result of the addition of amorphous materials to the paracrystalline cellulose; in Figures IV-9 to IV-11, the raw scatter, fitted curve, fitted peaks and normalized individual intensities are presented for different silanized CNF. Fitted curves show new peaks at 2θ ~ 20 degrees with low intensity and high internal breath, and sharper peaks for the diffraction of the corresponding 002 lattice planes; this phenomenon can be explained that some of the un-oriented nanocellulose chains underwent self-orientation due to their native crystalline characteristic[244]. On the other hand, as silane content was increased (W5, M5, E5), this

phenomenon is reverted by the excess of amorphous material; the scatter domain is further broadened in the 2θ region from 20° to 30° which corresponds to Si-O-C linkages between cellulose and silane as well as the amorphous silicon derivates, with local peaks varying from 20° to 21° 2θ[245,246]. After silanizations another diffraction is generated at 2θ = 35°, which in general is low in intensity and overlapped with the 004 lattice plane of cellulose, this signal is attributed to the Si-O-C generated after silanization of cellulose.

Normalized individual signals reduce the overlapping of amorphous scatter with the cellulose characteristic diffractions, as stated before, with lower amount, nanocelluloses maintaining the narrow integral breath of nanocellulose (C0) with higher intensities of the 002 lattice plane, but for celluloses containing more silane yield, there is a significant increase on the intensity at 2θ = 20°; increase on the intensity of the diffraction corresponding to determined lattice plane corresponds to an increase on the periodic arrangement in such plane, this is less visible in silanized nanocelluloses with less silane yield (W1, M1 and E1) in which the diffraction peaks corresponding to the -110 lattice plane at 2θ ~ 20° only generate a shoulder overlapped to the 002 diffraction peak, while in nanocelluloses containing more silane yield such overlapping generates a double peak from 2θ = 20° to 23°, which is also enhanced by the amorphous contribution of silanes present in the cellulose-silane network but not necessarily linked directly to the cellulose hydroxyl groups, but between each other through Si-O-Si linkages, which concurs with the presence of Si-O-Si bands in the FT-IR spectra.
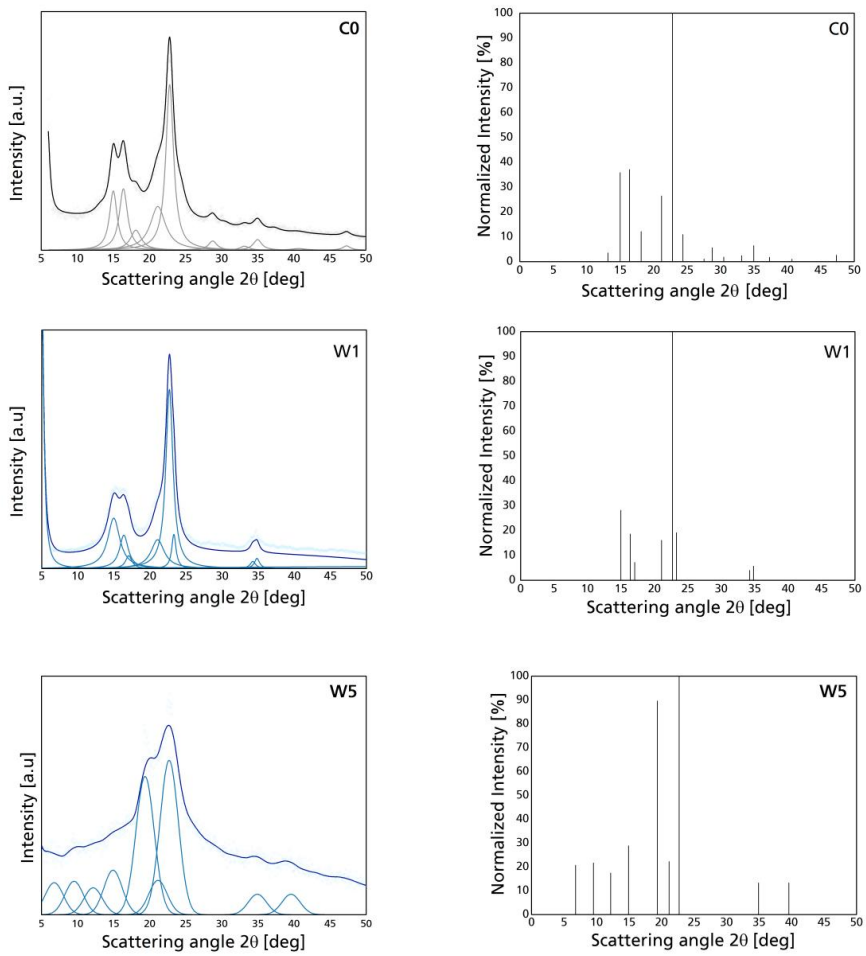
Figure IV-9 Left column: XRD diffraction patterns for water based silanized celluloses. Right column: Normalized individual signals corresponding to cellulose and modified cellulose diffraction planes.
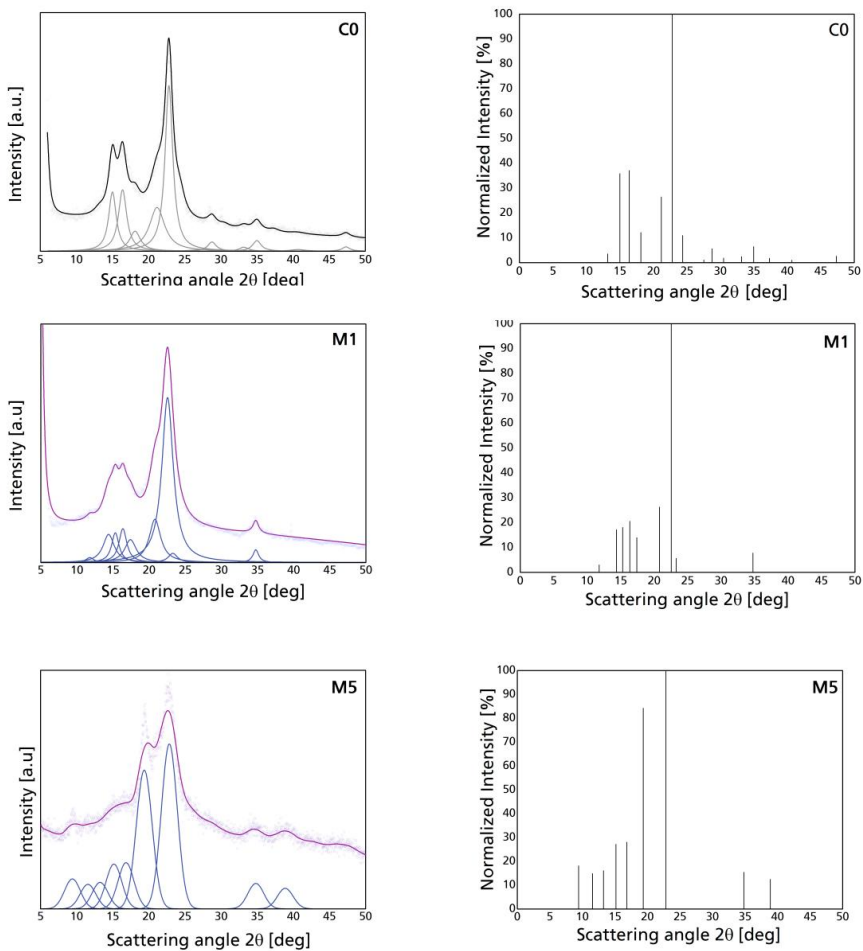
Figure IV-10 Left column: XRD diffraction patterns for water-ethanol based silanized celluloses. Right column: Normalized individual signals corresponding to cellulose and modified cellulose diffraction planes.
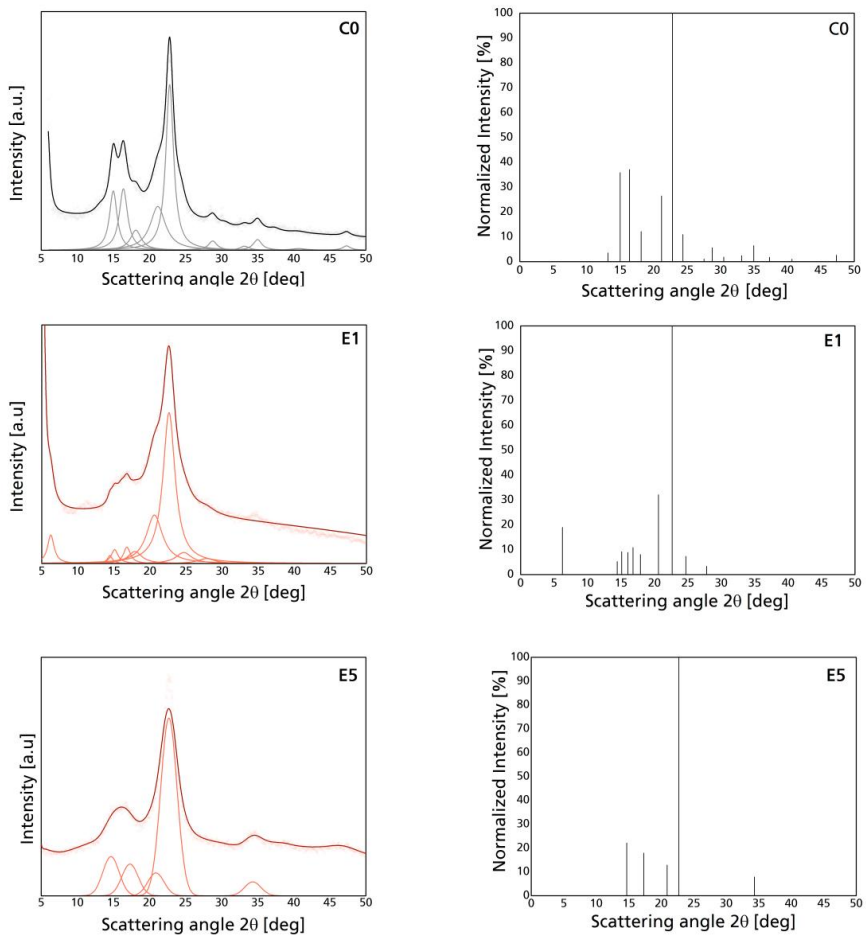
Figure IV-11 Left column: XRD diffraction patterns for ethanol based silanized celluloses. Right column: Normalized individual signals corresponding to cellulose and modified cellulose diffraction planes.

For the F1 sample, the addition of large aliphatic chains generates a whole new region around the crystal particles; this can be concluded as the estimated crystallite size is 53% bigger than the original BOS. This new aliphatic chains in the crystalline surface diminish the crystallinity of the modified cellulose as the morphology is altered[247]. In Figure IV-12, the deconvoluted peaks for the F1 sample shows a new low-intensity peak at $2\theta = 7.99$ degrees that is in the range of the associated diffraction of aliphatic chains for a number of carbons higher than 7[248]. There are also new peaks at $2\theta = 25.26$ and 28.44 degrees.
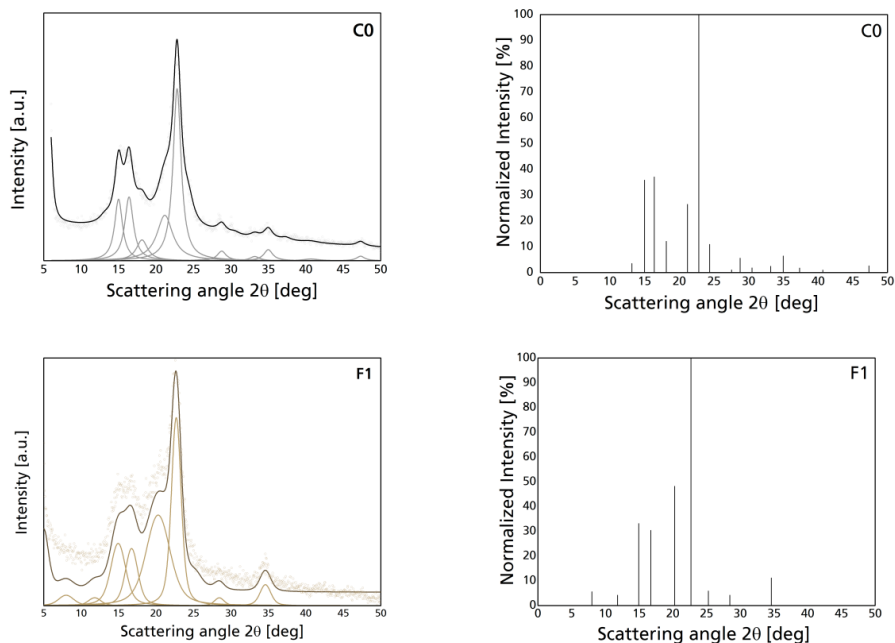
Figure IV-12 XRD diffraction patterns for F1 esterified cellulose.

Solid state NMR analysis was done studying two nuclei with magic angle spinning and cross polarization; selected nuclei were ^{13}C and ^{29}Si. Figure IV-13 shows the NMR spectra for the modified celluloses: a) corresponds to the ^{29}Si spectra, b) to the ^{13}C, c) to ^{13}C in the range in which silane carbons are situated and d) shows the identification of each silane carbon. In case of water-based solutions the reactivity of silane-cellulose interactions is higher (W series has sharper peaks for C_1 and C_4, which means that ethoxy groups are still present in the silane-CNF network. For E series, the ethoxy carbons (C_1 and C_4) are not present as during reaction, ethanol is produced from hydrolyzed silanes as byproduct and during casting such ethanol is evaporated, however the signals corresponding to propyl chains are almost imperceptible, which is theoretically the non hydrolizable organic substituent. ^{29}Si NMR shows two peaks which correspond to single SiO and Si-O-Si silicon linkages[249].
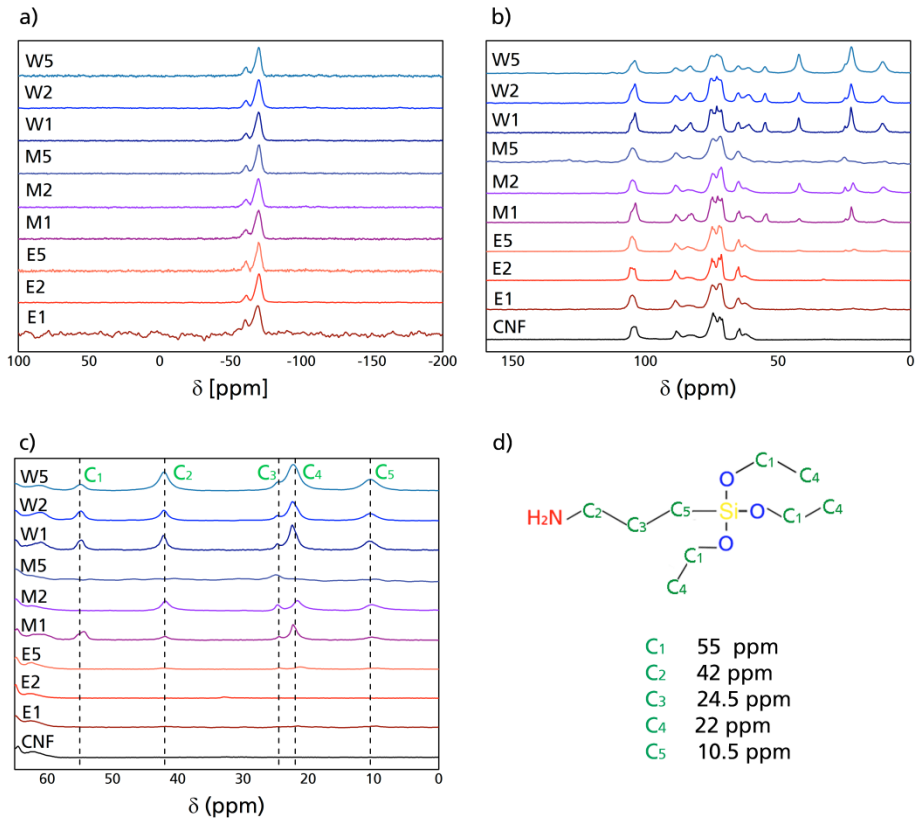
Figure IV-13 NMR spectra of cellulose nanofibers before and after silanization: a) ^{29}Si, b) ^{13}C, c) ^{13}C in the range of new signals and d) carbon identification in the ATS. The apparition of new signals at ~10, 25 and 40 ppm correspond to the propyl and ethyl carbons of ATS.

Figure IV-14 shows the deconvoluted C4 regions for ^{13}C NMR spectra of selected silanized CNF compared to neat CNF. Most changes include the reduction of the amorphous region in case of W2, while in M2 and E2 (reactions in ethanol-based solvents) there is an increase in the amorphous region, which means that when the reaction is done in water, there is a tendency to align the planes as it was explained in the XRD analysis.
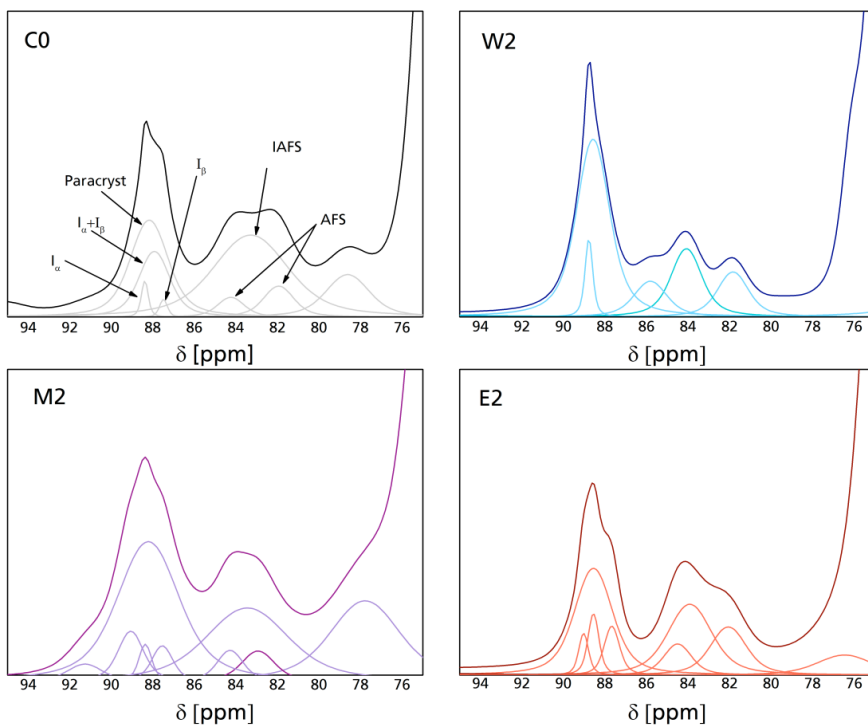
Figure IV-14 Fitted curves for C4 carbons in neat and modified CNF.

Surface modification increases the hydrophobicity of cellulose fibers; contact angle provides further information regarding the interaction between the surface of the CNC and CNF and the hydrophobic agent.

Table IV-3 presents the water contact angles (θ_w) of cellulose after bleaching as well as modified CNC and CNF.

The changes in θ_w are related to the topology of the surface, either because of the size of the particle avoid the surface roughness or because of the reaction of hydroxyl groups through hydrogen bonds. In case of modified cellulose nanoparticles, even though during surface modification not all hydroxyl groups may react, the possibility of water molecules to penetrate the substrate when dealing at nano-scale is reduced.. In case of the ATS modified celluloses, it can be observed an increase in the surface hydrophobicity as the amount of silanes is increased, this is related to the features associated with the components of the respective modification, as well as with the specific surface of the particle; nano-scale cellulose has more hydroxyl groups to react with, this groups have strong hydrogen bonding with the surface modification agent that generates a shield against water sorption[250,251].

Table IV-3 Water contact angle and surface energy values for the different silanized CNF.

Sample	θ_w [deg]	γ_s [mN m^{-1}]	γ_s^d [mN m^{-1}]	γ_s^p [mN m^{-1}]	W_a [mJ m^{-2}]
C0	82.50	39.61	36.22	3.39	81.62
W1	84.00	38.56	35.51	3.06	79.75
W2	88.00	35.88	33.62	2.25	74.72
W5	99.00	29.39	28.72	0.67	60.91
E1	88.50	35.55	33.39	2.16	74.09
E2	94.00	32.16	30.89	1.27	67.16
E5	103.00	27.39	27.06	0.33	55.96
M1	84.50	38.22	35.27	2.95	79.12
M2	85.50	37.54	34.80	2.74	77.86
M5	92.00	33.36	31.79	1.56	69.68

Figure IV-15 presents the static water contact angle after 60 seconds for the silanized CNF, as it can be seen, contact angle is related directly proportional to the silane content in the reaction, with no significant difference between the different systems, with the mere particularity that in case of M5 the contact angle is not as high as for W5 or E5 (in Table 3 polar component is also significantly higher than for W5 and E5) this phenomenon is not present in case of M1 and M2 which are very similar to their counterparts elaborated with either water or ethanol.
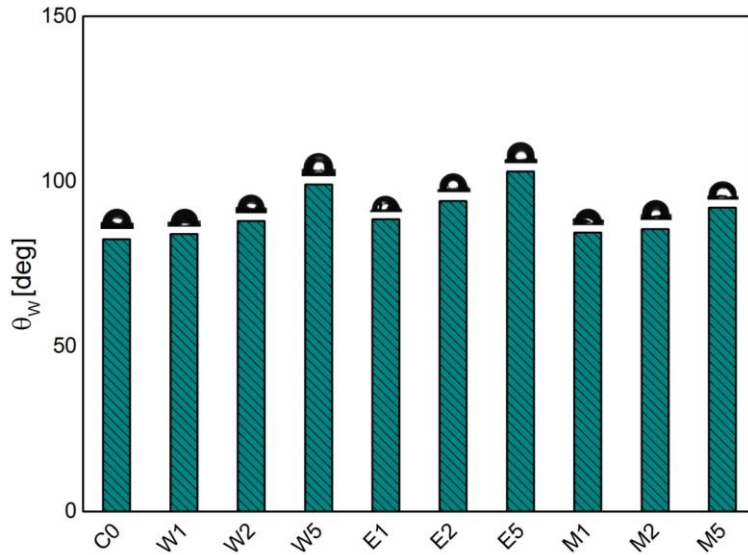
Figure IV-15 Water contact angle values for the silanized CNF after 60 s, above each column is presented a representative drop from the sample.

Conclusions

Ten different nanocellulose modifications were done to functionalize CNF or CNC from blue agave. The properties of each type were analyzed to evaluate their potential use for different applications. In general the variation in properties is directly related to the amount of silane used in the reaction, with samples containing 2 wt% silane presenting the most acceptable values, as the reaction between CNF-silane are better than those containing 1 wt%, but the interactions between silanes which are present in 5 wt% samples is avoided. The functionalization with fatty acids showed properties similar to those of previous works done elsewhere. For functional applications of CNF-silane systems, the W2 sample is going to be the most used either for wet or solid state applications, this because differences in the properties compared to CNF containing more silanes are not significant, while the reactive used is the double, therefore to optimize the use of silanes without reducing the functional properties of silanized CNF 2 wt% silane is enough. On the other hand, as for composites the temperatures used are quite elevated, the use of ethanol constitutes a risk during the elaboration processes, therefore water-based silanized CNF were preferred.

V)   Capítulum Quartum

Composite elaboration
and functional applications

Motivation

After the obtention and functionalization of cellulose nanoparticles from blue agave, four different applications were studied to verify the feasibility of using such nanocelluloses in functional applications. These applications cases are called 'work' and are numbered from 1 to 4 as follows: Work 1 PLA-Modified nanocellulose and their hydrophobic character; Work 2 Cellulose-chitin nanofilms and their antifungal activity; Work 3 Cellulose-PLA nanofilms and their mechanical-barrier properties and Work 4. Multi-layered hardboard with enhanced properties.

The first work corresponds to a series of composites elaborated using a polymeric matrix, which for this work consisted in PLA as it is one of the most commonly used biocomposites and a lot of research has been done using this polymer. This allows the elaborated composites to be compared to published works and also to contribute to the existing document archive dealing with biobased composite materials. The second, third and fourth works consist also in biobased composites. However, for these works no extra binder was added, nor a polymeric matrix. These works were prepared through hot-pressing, an elaboration process that uses the interactions between the hydroxyl groups of the nanocellulose as active binding agents for the composite elaboration. Works 2 and 3 are nanocellulose films done with the addition of extra nano or micro particles; work 3 uses chitin nanocrystals as additive in CNF-based films to contribute with antifungal properties, while work 4 uses microfibrillated PLA as additive which increases porosity and gives other properties to the film.

Work 4 is focused in the study of the elaborated modified CNF as external layers applied to hardboards elaborated with the wet-process (with no resins) these self-bonded composites were elaborated in wt state and then hot-pressed together with no extra resin nor binding agent added to the fibers.

The insistence in these works to use simple techniques and few materials is to give functional applications to the cellulose nanoparticles either modified or unmodified without increasing the production and end-of-life disposal costs in order to make price competitive alternatives for current materials. This decision sacrifices the optimal performance of the material (although is still competitive) but contributes with the environmental conscience of the author and the scope of the research done by the Bio-Refinery Processes group.

V-1. PLA-Modified nanocellulose and their hydrophobic character

Aim

The objective of this work is to develop new composites using PLA as matrix, by adding as fillers modified cellulose nanofibers and nanocrystals obtained from agricultural waste of a highly fibrous plant (Agave tequilana) in order to give value added applications to an undervalued material. On the other hand, PLA properties require improvements to compete with other plastics, making important the exploration of new surface modifications in polymer reinforcements in order to increase mechanical and hydrophobic properties of PLA and to enhance the interaction between nano fillers and the matrix, avoiding the formation of dislocations in the interaction surface. Two different surface modifications on two cellulose nanoparticles (CNF and CNC) were evaluated to determine the improvements that these modifications provide to the cellulose surface, they were also compared to raw blue agave bagasse and to bleached pulp to analyze if working on nano-scale was relevant.

Composite elaboration

Composites were prepared using a Haake Minilab twin-screw extruder. According to the capacity of the machine, total mass of 6 g for each batch was mixed during 15 min (T_M); after which the mix was extruded (T_E)[252]. Bulk filler was added dry and mixed with PLA with a share of 0.5, 1.0 and 2.0 percent. Table V-1 describes the fillers used to reinforce the PLA matrix.

Table V-1 Abbreviations used for the different reinforces used for the composites.

Sample	Matrix	Load
PLA	PLA	-
BAST	PLA	BAB
BABP	PLA	ABE
BANF	PLA	BEH
BANC	PLA	BES
BANS	PLA	BEH-W5
BADC	PLA	BES-F1

Composite characterization

Tensile tests of the composites were performed using MTS Insight 10 equipment provided with pneumatic clamps (Advantage Pneumatic Grips) and a 250 N loading cell, with a speed of 5 mm min^{-1}. Samples were prepared 60 mm long, with an average width of 5 mm and thickness of 0.7-0.9 mm. The set distance between the clamps was 20 mm. The values quoted are the average of ten measurements.

The effect of modified CNC on the crystallization behavior of PLA was studied using differential scanning calorimetry (DSC).Experiment was realized in a N_2 atmosphere with a 4 stage cycle : (1) 5-10 mg samples were heated from 25 ° to 250 °C at 5 °Cmin^{-1} (2) temperature was held for 3 min with constant temperature, (3) temperature was decreased to 25 °C at 5 °Cmin^{-1} and (4) reheated from 25 ° to 250 °C at 5 °Cmin^{-1}. Percentage of crystallinity (Xc) in the PLA-based composites was calculated by:

$$Xc\ (\%) = (\Delta Hm + \Delta Hc)\ (\Delta H°m \times XPLA)^{-1} \times 100$$

where ΔHm is the enthalpy of the sample, $\Delta H°m$ is the enthalpy of fusion of a PLA crystal of infinite size (93 J g^{-1}), XPLA is the weight fraction of PLA[253,254].

Results

Figure V-1 Visual aspect of the different composites.shows the visual aspect of the different composites compared to a pellet made of powdered fibers from the different fillers. The color contribution is related to the addition of either silanes (yellow) or fatty acid (brown). Figure V-2 shows SEM images of different composites with 2 wt% content of filler, stronger interactions can be seen between the matrix and esterified CNC, whilst in composites with silanized CNF the interaction is lower. In both unmodified cellulose particles, dislocations were observed in the surface contact between matrix and filler, thus confirming the strengthened bonds that ATS and DDC provide to cellulose nanoparticles.
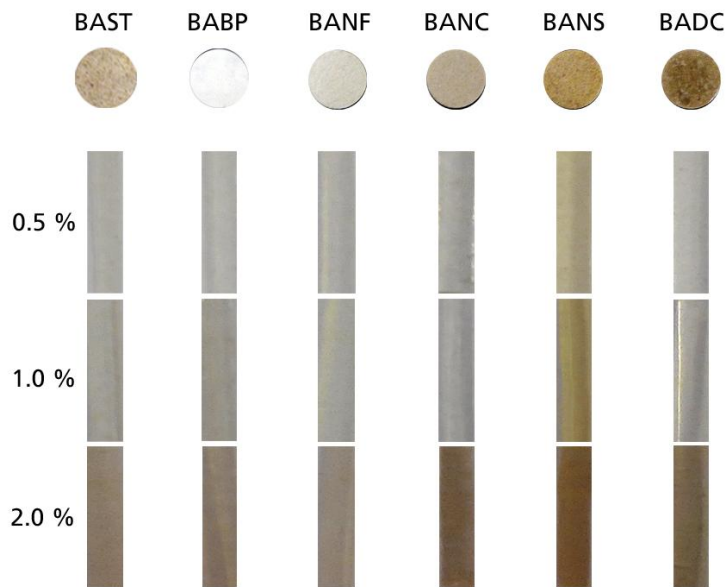
Figure V-1 Visual aspect of the different composites.

Table V-2 Ultimate tensile stress and strain at fracture of the different composites number in parenthesis is the standard deviation in percent.

Material	σ [MPa]	ε [%]	E [GPa]
PLA	45 (2.31)	11 (8.80)	2.69 (3.05)
BAST-0.5	39 (8.95)	10 (4.35)	2.47 (2.40)
BAST-1.0	36 (9.08)	9 (5.43)	2.83 (1.97)
BAST-2.0	33 (5.06)	8 (6.75)	2.99 (2.22)
BABP-0.5	41 (7.27)	9 (3.07)	3.19 (1.77)
BABP-1.0	37 (7.27)	8 (6.42)	1.20 (6.02)
BABP-2.0	31 (2.81)	6 (5.36)	4.04 (0.37)
BANF-0.5	42 (10.11)	9 (16.30)	1.39 (3.83)
BANF-1.0	36 (2.80)	8 (5.02)	2.82 (2.63)
BANF-2.0	35 (2.99)	8 (2.35)	2.95 (1.28)
BANS-0.5	43 (3.90)	14 (1.52)	1.87 (2.52)
BANS-1.0	39 (9.09)	11 (7.08)	2.06 (5.32)
BANS-2.0	34 (8.18)	8 (6.49)	2.85 (2.32)
BANC-0.5	42 (2.17)	9 (6.08)	2.81 (0.93)
BANC-1.0	37 (8.70)	8 (5.06)	3.48 (1.87)
BANC-2.0	36 (1.79)	6 (14.95)	2.04 (9.04)
BADC-0.5	43 (5.48)	13 (5.87)	1.93 (9.87)
BADC-1.0	42 (2.94)	10 (7.89)	2.82 (3.02)
BADC-2.0	37 (3.76)	9 (9.95)	2.26 (3.30)
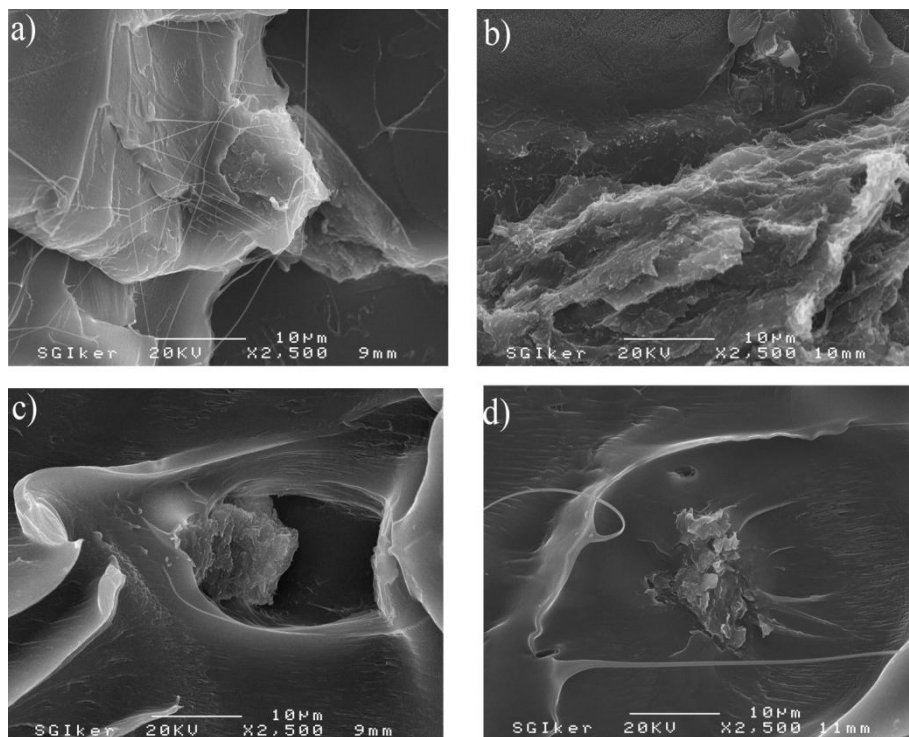
Figure V-2 SEM images of a) BANF-2.0, b) BANC-2.0, c) BANS-2.0 and d) BADC-2.0.

Table V-2 presents the data corresponding to ultimate tensile strength and strain at break results for the different elaborated composites and Figure V-3 shows characteristic Tensile-Stress graphs for each composite. The addition of anisotropic material to the polymeric matrix influences the performance in uniaxial stress[255,256]. It can be observed a considerable decrease on the mechanical properties when adding cellulose without any surface modification in composites reinforced with bleached pulp, cellulose nanofibers and cellulose nanocrystals, in which ultimate tensile strength (UTS) presents a decrease from the 45.29 MPa that has the PLA without any filler; this is accentuated as the percent of filler is increased, reaching a drop of approximately 25% when the filler reaches 2% of the composite. In general, the behavior of composites under uniaxial stress is similar to the obtained in previous publications, with an increase in the UTS and a decrease in the strain at fracture when cellulosic fillers are added[257]. Qualitative analysis shows differences with previously reported works with another type of cellulose modifications in which tensile stress and modulus are higher but the strain at break is considerably lower[258], this kind of variations and the ones presented in this wok reflect the importance that the surface modification of cellulose has in the elaboration of composites. In case of BANF and BANC, both have similar UTS values and are higher than those of bleached pulp. On the other hand, PLA composites reinforced with modified nano-particles have better UTS than

any other and are slightly better in the case of BADC. With regard to the strain at fracture, ductility of PLA is decreased when mixed with more crystalline material, this particularity can be observed with more clearness in the PLA-BANC composite in which the average maximum elongation is dropped by an average of 48% from the unfilled PLA, as the stronger bonds between the highly crystalline cellulose inhibit the elongation of the fiber. The addition of non-crystalline components to the surface of CNF and CNC enhances the interaction between the filler and the matrix, allowing a better displacement in the axial direction under tension, with strain being increased by ~18% in the case of 0.5% BADC and ~25% in the case of 0.5% BANS composites; this value gradually descends as the amount of filler represents a higher percent in the composite, as either 1% and 2% concentrations of BANS and BADC have lower values for maximum strain than PLA without fillers. The behavior of all composites shows a mechanical decay when the amount of filler is increased, this situation can be related with the morphology and the composition of the filler as amorphous parts of BABP, BANF and BAST; lignin content in BAST and coupling agents in BADC and BANC benefit the interactions between crystalline cellulose and PLA; but when the share of the filler inside the composite is increased, the anisotropy characteristic to organic fillers in polymeric matrices, gets a major role in the response of the composite to uniaxial stress, generating more dislocations inside the composite. Furthermore, higher amount of filler material can generate agglomerations that result in a deterioration of tensile stress transfer between matrix and filler, generating a more brittle structure[259].
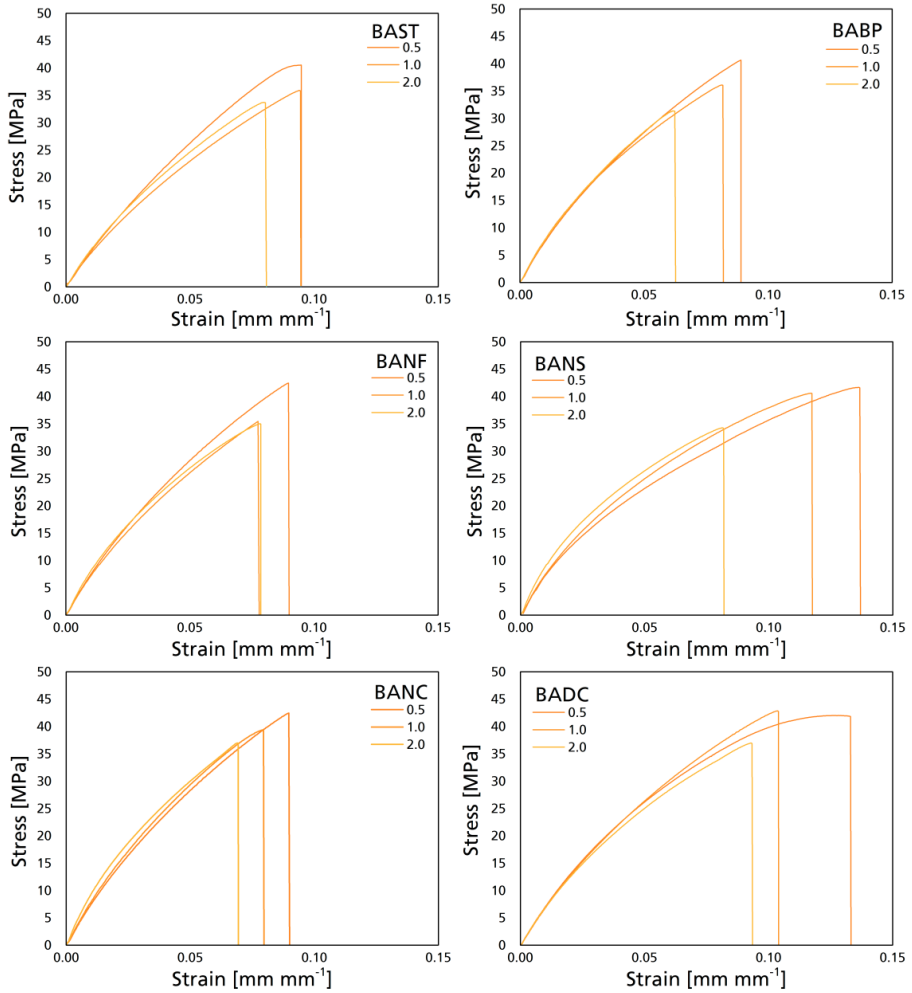
Figure V-3 Characteristic Tensile-Stress graphs for each composite.

Table V-3 Thermal properties of PLA and PLA with 0.5% of nano-fillers.

	T_g (ºC)	T_c (ºC)	T_m (ºC)	ΔH_m (J g⁻¹)	ΔH_c (J g⁻¹)	X_c
PLA	63.22	97.54	175.66	70.76	34.29	39.32
BANF-0.5	62.05	92.06	174.45	67.89	37.57	32.55
BANC-0.5	62.35	94.51	175.69	68.13	33.59	37.08
BANS-0.5	63.02	92.78	176.14	70.62	33.97	39.35
BADC-0.5	62.46	96.97	175.75	69.54	33.19	39.03

In Table V-3, glass transition temperature (Tg), melt temperature (Tm), crystallization temperature (Tc), enthalpy of melting (Hm), and enthalpy of crystallization (Hc) of the different composites are presented. Bulk PLA presents a Tg of 63.22 °C and Tm 175.66 °C this results are similar to those reported in previous works[185,260] changes in Tg are not significant between different composites, in more crystalline reinforcements such as silanized nanofibers or cellulose nanocrystals it can be observed a slight variation in the Tc (between 3-5 °C) this changes and the increase of the enthalpy of fusion show a good nucleation of the cellulose crystallites enhancing the chain flow of PLA around the crystals whilst the crystallinity and the melting temperature is not highly affected.
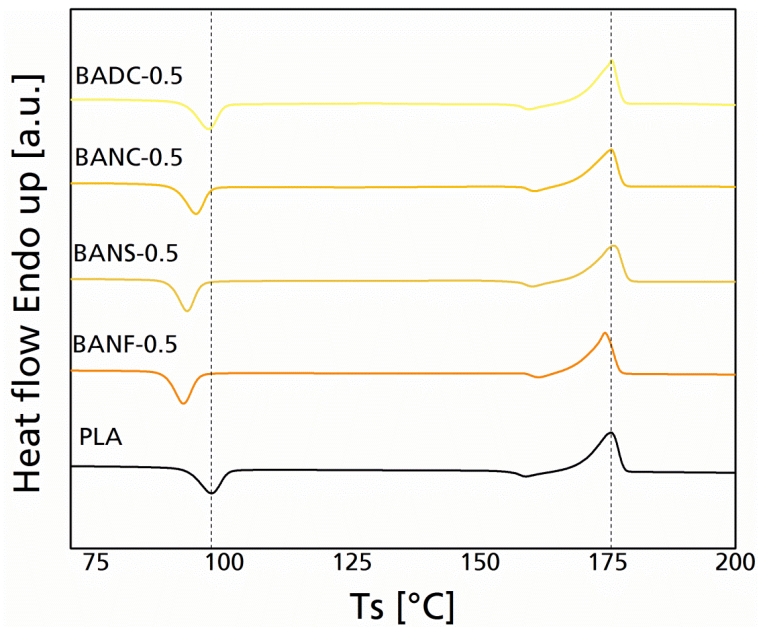
Figure V-4 DSC thermograms of PLA as well as PLA reinforced with nano-fillers.

Conclusions

Six different composites were elaborated using PLA as a matrix and blue agave bagasse as raw material. To study the relevance of composition and surface modification in natural fibers, different chemical and mechanical treatments were performed, the analysis of composites made with the same material throughout the complete process can help to determine the relevance and feasibility of the treatments and then decide if whether or not is worthy. Hydrophilic character of cellulose surface was modified with 3-aminopropyl triethoxysilane in case of nanofibers and dodecanoyl chloride in case of nanocrystals. The behavior towards contact angle and tensile tests showed the potential of these modifications as suitable methods to enhance mechanical properties and hydrophobicity because of the formation of non-polar covalent bonding between free hydroxyl and coupling agents, also

enhancing dispersion inside the matrix, this has an important potential in creating barrier materials to avoid contact with water. Exists an inversely proportional relation between the amount of filler and the uniaxial mechanical properties, this can be related to agglomerations and the anisotropy of the filler inside the matrix, also the addition of nano-scale particles enhanced the interaction between matrix-filler. Thermal properties showed a better crystallization of the PLA chains when reinforcements were added without affecting the final crystallinity of the polymer.

V-2. Cellulose-based films: Cellulose-chitin nanofilms and their antifungal activity

For self-bonded composites elaboration cellulose nanofibers and chitin nanocrystals were mixed at different percentage contents inside of a beaker with a 3 wt% total concentration; the mixture was stirred using a Heidolph Silent Crusher M at 15 000 rpm for 10 minutes to ensure well-dispersed slurry. Water was vacuum extracted with a glass filter funnel using a 0.22 µm Durapore membrane. The wet mats were oven dried at 50 ºC until water content of 10 wt% was obtained. Self-bonded composite films were hot pressed for 15 minutes with a curing pressure of 180 bar at 110 ºC[127]. Table V-4 presents the identification of the samples according to its composition.

Table V-4 Identification, grammage and porosity of the different composite films, values in parenthesis represent relative standard deviation in percent (%RSD).

Sample	Cellulose type	Cellulose [%]	Chitin [%]	G [g m^{-2}]	P [%]
0S	BEH	100	0.0	71.10 (3)	31(3)
1S	BEH	99	1.0	73.04 (6)	23 (1)
3S	BEH	97.5	2.5	77.50 (7)	23 (1)
5S	BEH	95	5.0	70.98 (4)	25 (3)
7S	BEH	92.5	7.5	69.73 (2)	27 (3)
9S	BEH	91	9.0	70.09 (7)	21(2)
10S	BEH	90	10.0	71.08 (3)	23 (4)

Composite films characterization

Atomic Force Microscopy (AFM): Atomic force microscopy images were obtained operating in tapping mode with a NanoScope IIIa, Multimode TM-AFM from Digital Instruments-Veeco scanning probe microscope equipped with an integrated silicon tip cantilever with a resonance frequency of 300 kHz. To obtain representative results, different regions of the samples were scanned.

Scanning Electron Microscopy (SEM): Scanning electron microscopy images were obtained with a Scanning electron microscope JEOL JSM-6400F with field emission cathode, with a lateral resolution of 10-11 Å at 20 kV.

Attenuated-Total Reflectance Infrared Spectroscopy (ATR-FTIR): Infrared spectra were recorded on a PerkinElmer Spectrum Two FT-IR Spectrometer equipped with a Universal Attenuated Total Reflectance accessory with internal reflection diamond crystal lens. The defined range was from 800 to 4000 cm^{-1} and the resolution 8 cm^{-1}. For each sample 10 scans were recorded.

Dynamic Light Scattering (DLS)

The dynamic light scattering measurements were performed in a Brookhaven BI-200SM goniometer with a 9000AT correlator with a He–Ne laser light beam (Mini L-30, wavelength $\varkappa$ = 637 nm, 10 mW) directed to a pot with a glass vat with a refractive index matching liquid surrounding the scattering cell and set at 25 °C was used. The scattered light intensity was measured at 90 deg with respect to the incident beam. Size distributions were analyzed with a 0.018 wt% concentration in water; samples were kept for 24 h at room temperature to stabilize dispersion.

X-Ray Diffraction (XRD): X-ray powder diffraction was performed with a Panalytical Phillips X'Pert PRO multipurpose diffractometer, with samples mounted on a zero background silicon wafer fixed in a generic sample holder, using monochromatic CuKα radiation (λ = 1.5418 Å) in a range from 5 to 50 2θ with step size of 0.026 and time per step of 80 s at room temperature. Apparent crystallinity was calculated using pseudo Voigt functions for peak fitting.

Grammage and porosity: Grammage of the cellulose-chitin reinforced papers were determined according to ASTM D646-13 standard method. Then, to obtain the porosity (P), densities were related to the content of each composite following the equation:

P= 1-[ϱn/(ϱCe + ϱCh)]

In which ϱn is the density of the composite film, ϱCe is the density of cellulose nanofibers multiplied for the corresponding fraction contained in each composite and ϱCh is the density of the used chitin multiplied for its corresponding fraction.

Contact angle: Sessile drop contact angle was measured with a DataPhysics video-based measurement contact angle system OCA20 with a software controlled dosing volume weight-drop to determine surface energy by using 3 different liquids: water, ethyleneglycol and diiodomethane. The results presented are the average of eight measurements, to determine the surface free energy Owens, Wendt, Rabel and Kaelble (OWRK) method was used.

Tensile stress test: Tensile tests of the composites were performed using MTS Insight 10 equipment provided with pneumatic clamps (Advantage Pneumatic Grips) and wit a 250 N loading cell, with a speed of 5 mm min^{-1}. Test specimens were prepared as established by ASTM D 585 – 97 standard methods. The set distance between the clamps was set at 20 mm. The values quoted are the average of ten measurements.

Thermogravimetrical analysis (TGA-DTG): Thermogravimetric analysis (TGA) assays were carried out in a TGA/SDTA 851 Mettler Toledo instrument according to standard test method[238], this consisted in putting ~5 mg of sample under 20 ml min^{-1} nitrogen atmosphere from 0 to 900 °C at 10 °C min^{-1}. The thermal decomposition temperature was taken as the onset of significant weight loss, after the initial moisture loss.

Antifungal activity: Antifungal activity of the composites was evaluated to determine the effect of chitin nanocrystals as well as the nano- and micro-scale of the cellulose content. To evaluate the influence of nano-scale of cellulose samples were prepared by using cellulose microfibers instead of nanofibers. Aspergillus sp. was previously cultured in solid substrate of malt extract agar (MEA, Sharlau) and incubated in sealed Petri dishes for 72 h at 25 ± 1.5 °C within a Selecta Medilow climatic chamber. After growing, an aliquot of spores was diluted in Ringer solution and aseptically inoculated using a glass rod (40 µL of dissolution at 1.21·106 Spores·mL^{-1}) on the MEA surface containing film.

After 7 days of incubation at 25 ± 1.5 °C, composites were gently extracted from the agar and washed with Ringer solution. The obtained spore solution was vortexed and stained with LPCB to count spores concentration and using trypan blue solution for viability analysis. The cell concentration and life viability was determined with a Cellometer® Mini (Nexcelom Bioscience LLC) automated cell counter by putting 20 µL of each spore solution inside Cellometer® Counting Chambers and using Cellometer® Mini software for the analysis. The values obtained for the concentration of each sample correspond to the average of four independent experiments. The fungal growth inhibition (FGI) was calculated as concentration of spores (conidia) per milliliter, according to equation (3):

$$FGI\ (\%) = 100 \times Cg\text{-}Tg \times Cg^{-1}$$

In which Cg is the average concentration in the control samples set (0S) and Tg is the average concentration in the treated set.

Water Vapor Transmission Rate (WVTR): Water vapor permeation was measured with a thermohygrometer using deionized water according to standard tests[261]; measurements were performed at least three times.

Characterization of the composite films

Morphological and physical properties: Figure V-5 shows SEM images of 0S (a and d), 5S (b and e) and 10S (c and f) corresponding to the cross-section (fracture cut after tensile analysis (a-c)), and surface (d-f) of the self-bonded composite films. Figure V-6 presents the AFM images of the surface for the same samples. When compared with Figure V-5-d, in Figures V-5-f and V-5-c it can be perceived a considerable increase in chitin nanocrystals as their mass contribution is higher, and chitin nanocrystals can be appreciated in the surface. Figure V-5-e shows clearly a chitin nanocrystal as part of the disposition of larger and broader cellulose nanofibers this phenomenon can be also observed at less increases in Figure V-5-c.
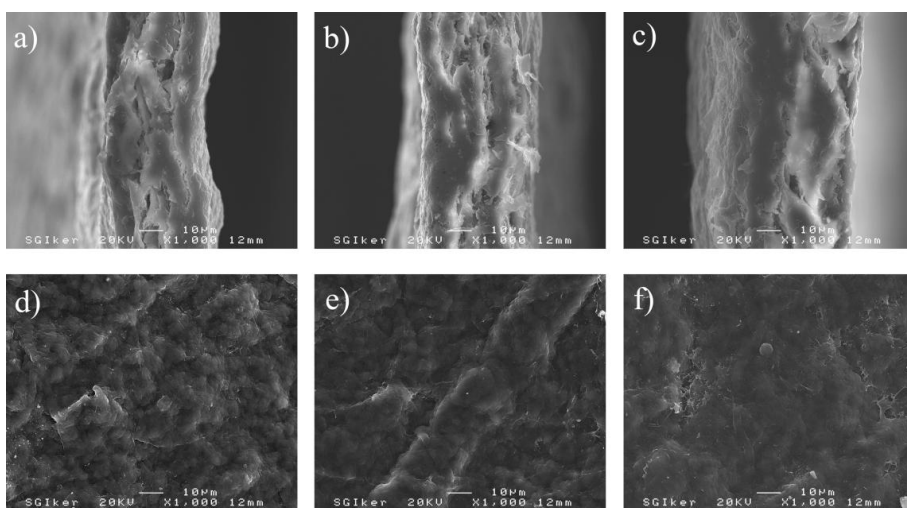
Figure V-5 SEM images of 0S (a and d), 5S (b and e) and 10S (c and f); first row presents images for fracture region after mechanical tensile tests and second row corresponds to surface of the composites.
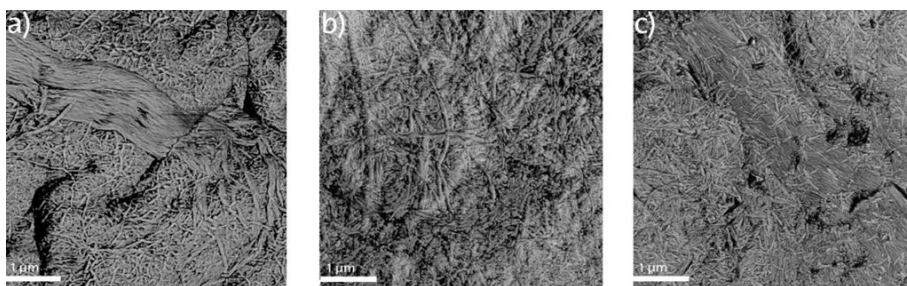
Figure V-6 AFM images of a) 0S, b) 5S and c) 10S composites.

Grammage and porosity values (Table V-4) showed similar results for all the composites, with grammage being similar in all cases and porosity changing with the addition of chitin nanocrystals, as smaller particles prompted higher packing properties of the film composites. Figure V-7 shows the general aspect and flexibility of one of the elaborated composites (5S). All composites were visually similar.
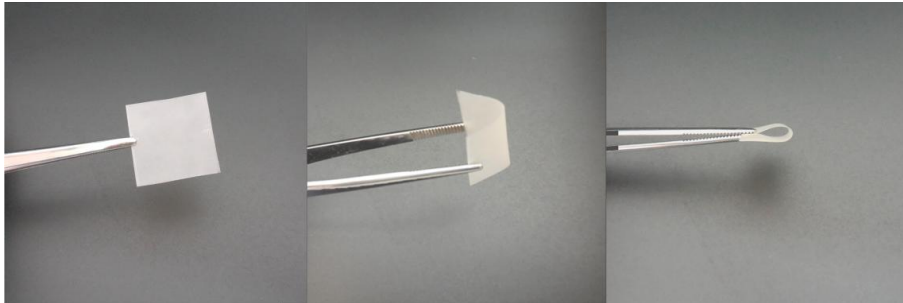
Figure V-7 Visual aspects of 5S composite film.

Mechanical properties

The mechanical standard tests under uniaxial stress were carried out to determine the tensile stress (σ), strain at break (ϵ) and the Young modulus (E) of each composite film, the results are shown in

Table V-5. The origin and morphology of the components, as well as the selected process for the elaboration played significant roles in the behavior of the composites. Chitin nanocrystals have lesser resistance to tensile stress, which is common in particles with high crystallinity[262]; on the other hand cellulose films processed with hot pressing method tend to have lower Young modulus than those elaborated with vacuum sheet former or by low oven drying as reported by Sehaqui in 2010 and by our group in 2014[127,263]. Composites corresponding to cellulose nanofibers without chitin nanocrystals (0S) achieved a mean strain at break of 7.57 % that is clearly lower than previous results for similar materials made from new resources, but considering the fact that in this work fibers that were previously subjected to chemical and mechanical treatments were used, this results can be considered satisfactory[127,264]. The addition of chitin nanocrystals with high crystallinity diminished the elongation of the papers but did not affect significantly their modulus. Behavior of the composites while varying the chitin nanocrystal content presents a non-linear tendency in strain at fracture, this can be related with the unequal distribution of chitin nanocrystals causing defects in the formation of the composite that generate disadvantages in the mechanical behavior, overall, the low amount of chitin nanocrystals added did not diminished UTS or Young modulus.

Table V-5 Ultimate tensile stress (σ), strain (ε) and Young modulus (E) of the different composites, number in parenthesis represents %RSD.

Sample	σ [MPa]	ε [%]	E [GPa]
0S	56.63 (3)	7.57 (5)	2.73 (7)
1S	55.11(4)	3.91 (10)	3.02 (7)
3S	57.99 (3)	4.01 (9)	2.95 (4)
5S	55.42 (2)	3.22 (6)	2.87 (7)
7S	57.22 (1)	3.75 (9)	2.98 (4)
9S	57.19 (2)	3.81 (5)	3.19 (5)
10S	54.77 (2)	3.92 (6)	2.31 (2)

Antifungal activity

For a better understanding of the role that nano- and micro-scale cellulose plays on the antifungal activity in self-bonded composites, *Aspergillus sp.* cultures were inoculated. Previous works have highlighted the differences between chitin nanofibers and chitin nanocrystals in fungal inhibition[265] but the importance of the substrate morphology has never been studied. In this case, cellulose microfibers and cellulose nanofibers were mixed with different amounts of chitin nanocrystals and subjected to the action of *Aspergillus sp.* Table V-6 presents the concentration, fungal inhibition, viability and the mean diameter of the colonies after 7 days incubation as obtained from Cellometer® Mini software, Figure V-8 shows a digital image after test. Results show higher spore concentration (up to 10 times higher) in case of cellulose microfiber than in cellulose nanofiber self-bonded composites.
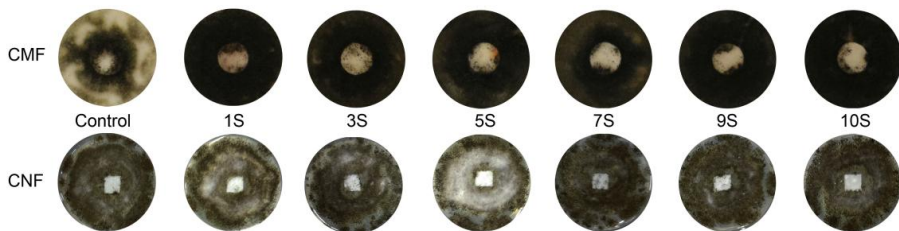
Figure V-8 Images of different composites after Aspergillus sp. incubation

Biochemical behavior of chitin against fungi and microbial agents has been studied in several works[266–269], other works have highlighted the benefits of the nano scale of chitin, as the higher surface area leaves, which increases the interaction between residual NH_2 groups in the surface and fungal agents than native α-chitin, and thus enhancing inhibition against Aspergillus sp[270]. Although in other works there has not been seen any difference

depending on the subtract used as reference[271], in this work it becomes clear that not only the properties of the inhibitor component but also those of its matrix affect the fungal growth by increasing the surface energy and surface area particularly with nano- cellulose matrix; The amount of spores present in the surface of each composite, show a drastic reduction in every nano-composite with respect to micro-scale composites containing the same amount of chitin, even with no chitin content the concentration was reduced up to 65%. The fungal inhibition is increased with 10% chitin content until 76% regarding the chitin-free film, and every cellulose nanofibers-chitin nanocrystals composite has a concentration reduced in more than 50% confirming the importance of nano-scale to inhibit fungal growth.

Table V-6 Results of antifungal activity of cellulose-chitin nanocrystals materials.

Sample		Concentration [Spores·mL^{-1}]	Diameter [μm]	FGI^a[4] [%]	FGI^b [%]	Viability^c [%]
Control		1.24·10^7 (8)	14.10 (12)	-	-	95.12 (3)
CMF-CH (ABE-CH)	0S	3.04·10^6 (28)	9.17 (3)	75.48	-	72.23 (4)
	1S	3.56·10^6 (8)	5.85 (8)	71.13	NFI*	63.01 (8)
	3S	2.34·10^6 (43)	5.50 (2)	81.12	23.02	59.78 (3)
	5S	1.10·10^6 (41)	5.80 (17)	91.13	63.81	58.95 (3)
	7S	1.08·10^6 (5)	5.67 (7)	91.29	64.47	53.97 (7)
	9S	2.79·10^6 (9)	3.93 (14)	77.50	8.22	35.56 (3)
	10S	1.13·10^6 (14)	3.10 (3)	90.89	62.82	32.49 (21)
CNF-CH (BEH-CH)	0S	1.08·10^6 (38)	8.38 (4)	91.29	-	39.93 (5)
	1S	4.52·10^5 (26)	7.90 (8)	96.35	58.14	30.73 (8)
	3S	3.78·10^5 (8)	8.06 (4)	96.85	65.00	25.62 (9)
	5S	1.52·10^5 (19)	7.10 (3)	98.87	85.82	28.09 (29)
	7S	2.00·10^5 (15)	7.23 (2)	98.38	81.48	28.37 (21)
	9S	4.33·10^5 (21)	7.59 (3)	96.50	59.90	21.41 (8)
	10S	2.55·10^5 (25)	7.36 (5)	97.78	76.38	18.32 (5)

The results of viability shown a different behavior when chitin is added to the composites with high decay from the samples containing no chitin to those that present even a small

---

[4] CMF-CH= cellulose microfibers-chitin nanocrystals; CNF-CH= cellulose nanofibers-chitin nanocrystals; a Fungal growth inhibition relative to control only with fungi; b Fungal growth inhibition relative to control with OS; c live spores/total spores; * No Fungal Inhibition; Values in parenthesis represent %RSD.

amount, in which the fungus viability is reduced significantly. In addition, the stability of the viability values is high with most of them having relatively low %RSD and few of them present high %RSD values (10S microfibers, 5S and 7S nanofibers). Also, the decay of the viability is drastic with the lowest amount of chitin (1%) in which viability falls 9 %; with the highest chitin content the viability is a 50% reduced, showing that chitin is acting to inhibit the development of *Aspergillus sp* mold fungi. Another phenomenon observed is relative to the mean diameter of the spores, with cellulose microfibers the diameter is reduced up to 30% with addition of 1S, and is going up to 60 % with addition of 10S. In case of nano-scale cellulose, the mean diameters present high %RSD, this means that the spore size varies significantly on the film surface and that differences between different composites is not significant.

Thermal properties

Thermal analysis (Figure V-9) shows that chitin nanocrystals increase the thermal resistance of the composites, although there is no significant difference between 5S (345.1) and 10S (342.4), with both curves overlapping after degradation was completed and 10S having just a slight increase in the thermal resistance before decaying (less than 5 degrees) than 5S. Overall, all of them show typical maximum temperature degradation results for cellulose[272] with just a small thermal lag caused by the chitin at the first mass decay that can be better appreciated in dTGA graph degradation peak for cellulose was 336.4 and for chitin 348.8, as the composites are >90% cellulose, final weights of all composites are comparable to cellulose final weight, differences between cellulose nanofibers and chitin nanocrystals are justified by the different origin of the materials as well as the extraction processes.
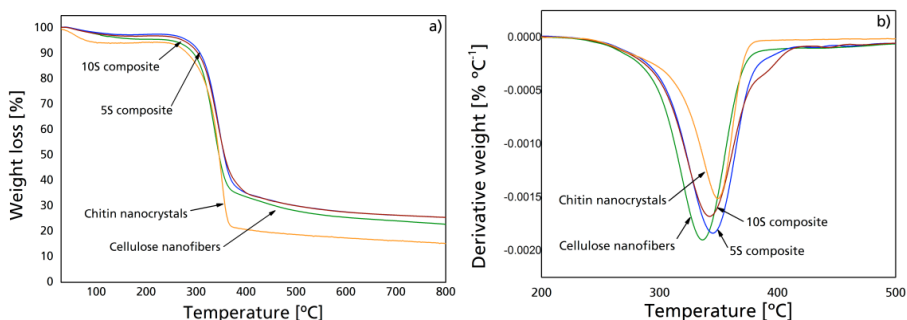
Figure V-9 TGA and DTG graphics for 0S, 5S and 10S composites.

Barrier properties

Water vapor transmission rate was measured to determine barrier properties of three selected films (Table V-7); in general the addition of chitin nanocrystals reduced the vapor transmission rate. Previously reported works[273] have shown good properties of cellulose nanofibers in WVTR tests, with 234 g m-2 day for a 42 μm film, the same study suggested

that the use of cellulose nanocrystals can potentially reduce WVTR situation demonstrated in this study with chitin nanocrystals. As the smaller particles leave less space for water molecules to pass through the composite films, fiber homogeneity as well as the distribution of chitin nanocrystals may have played an important role in the film performance against water vapor transmission; this situation can also be seen in the contact angles results (Table V-8).

Table V-7 Water vapor permeability for selected samples, numbers in parenthesis correspond to %RSD.

Sample	WVTR [g mm m^{-2} day^{-1}]	P [mL mm m^{-2} day^{-1} atm^{-1}]	Average thickness [μm]
0S	102 (9.8)	3410 (9.5)	70 (3)
5S	89 (3.4)	2967 (3.9)	64 (2)
10S	79 (3.8)	2643 (4.3)	59 (3)

Surface properties of the elaborated films were measured with the contact angle sessile drop method by using water as well as ethylene glycol to evaluate the polar component and diiodomethane to evaluate the dispersive component. Surface free energy is not considerably altered, presenting small variations between all the composites and with the dispersive component maintained in general unaltered. Polar component increases when the chitin content is higher because of the hydrophilic character of generated NH_2 and OH groups, as it is a polar component. The gradual reduction of the water contact angle from 0S to 10S was assigned to the increase of the number of residual NH_2 groups present at the surface of the chitin nanocrystals, as amino groups have more affinity to water than OH groups, this properties of the chitin nanoparticles have been studied in other works[274].

Table V-8 Contact angle and surface free energy values for all the films, numbers in parenthesis correspond to %RSD.

Sample	Water [deg]	Diiodomethane [deg]	Ethylene glycol [deg]	γ_s^p [mN m^{-1}]	$\gamma\gamma_s^d$ [mN m^{-1}]	$\gamma\gamma_s$ [mN m^{-1}]
0S	100.7 (1.4)	55.2 (1.3)	64.1 (1.3)	0.26	32.74	33.00
1S	90.4 (2.7)	59.7 (1.3)	67.0 (1.4)	2.40	27.28	29.68
3S	101.2 (2.3)	55.0 (1.7)	61.8 (1.7)	0.21	33.57	33.78
5S	92.0 (1.2)	58.7 (1.9)	58.2 (1.6)	1.92	30.25	32.17
7S	90.6 (0.6)	56.4 (1.2)	55.1 (1.1)	2.05	31.76	33.81
9S	88.4 (1.5)	57.9 (0.9)	63.9 (1.0)	2.76	28.41	31.17
10S	84.3 (1.6)	55.8 (0.6)	58.4 (0.9)	3.84	29.69	33.53

Conclusions

Chitin nanocrystals and cellulose nanofibers were used to elaborate self-bonded nanocomposite films. The properties of such composites were studied with different characterization methods. The addition of chitin nanocrystals affected strain at fracture, leaving ultimate tensile strength and Young modulus almost unaltered. Permeability was decreased while surface energy was reduced because of the polar character of NH_2 groups present in the surface of chitin nanocrystals. The growth of *Arpergillus sp.* was influenced by de-acetylation on the surface of the chitin nanocrystals providing to these composites good fungal inhibition properties.

V-3. Cellulose-based films: Cellulose-PLA nanofilms and their mechanical-barrier properties

Aim

The objective of the present work is to evaluate a new approach to the symbiosis between the most abundant biopolymer, cellulose, and the most popular synthesized bio-based polymer, PLA, to produce more applications and therefore open newer markets, in turn increasing the demand for these polymers in the industry. This will promote an increase in their production, particularly for PLA, making them more competitive in the global markets. The results obtained have confirmed the favorable affinity of these two polymers as well as the complementary properties that they contribute as composites.

Materials

Blue agave leaf-fibers were kindly provided by Finca Noctitlan, (México); fibers were pulped with an organosolv treatment and then bleached with a Total Chlorine Free Bleaching (TCF) sequence consisting in double alkali oxygen and double peroxide stages (LOH). Poly(lactic acid) fibrils were provided by Tianjin Glory Tang Co., Ltd. (China) with nominal dimensions: Finess:0.6-1.2 D and Length: 5-12 mm.

Composite elaboration

Native cellulose (Cellulose α-I and -II) fibers were defibrillated through high-pressure homogenization at ~1000 bar over 90 minutes (1:10 w/v) using a Niro Soavi Panda homogenizer, and then kept inside a freezer for their preservation. Cellulose nanofibers (LOH) and PLA fibrils (LAF) were mixed inside a beaker at 15,000 rpm with a paper blender; then, the suspension was sonicated over 15 minutes to allow PLA oligomers to defibrillate from the main polymer fibril and enhance the bonding with CNF. Water was extracted with a nylon membrane inside a glass funnel and hot-pressed with a hydraulic press at 110 ºC for 5 minutes (185 kPa). The ratio between CNF and LAF for the elaborated composites were 100/0, 75/25 and 50/50 (further referred to as 100C, 75C and 50C respectively). Figure V-10 shows the optical appearance of the different composites. As it can be seen, the addition of LAF increases the opacity of the composite films, while 100C has the typical translucent aspect of the CNF porous films (or nanopapers).
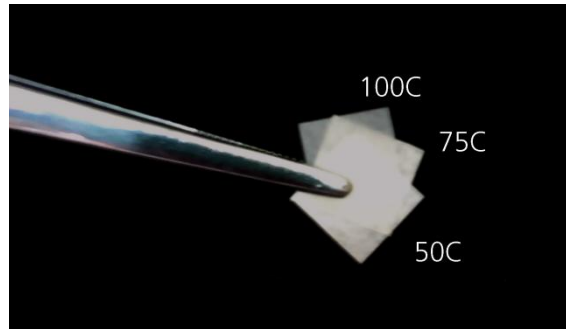
Figure V-10 Appearance of the elaborated composite films.

Composite characterization

Material conditioning and sampling: Samples were kept at 50 ºC for 24 hours before weighting and mixing to better control their content in the films. Elaborated films were conditioned according to TAPPI standards (T404).

Scanning Electron Microscopy: SEM images of the CNF, PLA fibrils as well as the surface of the elaborated films were acquired with a scanning electron microscope Hitachi S-3400N, to achieve information about the morphology of the raw material as well as the films.

Fiber length measurement: Fibers were first measured with optical microscopy to have their initial dimensions and to locate them within the elaborated films. Cellulose nanofibers were measured using an atomic force microscope Veeco NanoScope IV in tapping mode with a Cu tip.

Grammage and porosity: Grammage of the cellulose-chitin reinforced papers were determined according to ASTM D646-13 standard method. Then, to obtain the porosity, densities were related to the content of each composite by the following equation:

Porosity$= 1-[\varrho_n/(\varrho_{Ce} + \varrho_{Ch})]$

In which ϱ_n is the density of the composite film, ϱ_{Ce} is the density of cellulose nanofibers multiplied for the corresponding fraction contained in each composite and ϱ_{Ch} is the density of the used chitin multiplied for its corresponding fraction.

Tensile test method: Tensile test methods were carried out according to ASTM D3039 M-14 which is focused in determining the tensile properties of polymer matrix composite materials.

Bursting Strength Tester: Used as a measure of resistance to rupture, burst strength depends largely on the tensile strength and extensibility of the material and because of that is a good complementary analysis to tensile test and resonance stiffness. It can be determined by a Lorentzen &Wette Autoline Bursting Strength meter.

Internal tearing resistance of paper: Tearing test was performed with a Lorentzen & Wette Autoline tearing tester according to TAPPI standard (T414).

Parker Print-Surf roughness: Parker Print-Surf (PPS) roughness is sometimes called a kind of printing roughness because it correlates well to print quality as its clamping pressure makes it apt to determine surface compressibility, that is important in practical printings (Enomae and Onabe, 1997); it was measured with a Parker Print-Surf tester PPS 78 H. E. Messmer ltd. (Britain), according to TAPPI standard (T555) with a clamping pressure of 0.98 MPa.

Resonance stiffness: The correlation between the resonance length of a vibrating test strip of paper and its bending stiffness can be considered as an elastic property of papers and composite-papers. The bending stiffness of the films was measured with a RM.01 Kodak-Pathè type stiffness tester, by Adamel Lhomargy instrument, (France), according to TAPPI standards (T535). With frequency of vibration of: 25 Hz and constant 1.875.

Surface Energy: Contact angle of sessile drop was measured with a a PG-X portable contact angle meter with a software controlled dosing volume weight-drop (5 µL) with ethyleneglycol and diiodomethane to calculate the surface energy and to identify any changes in the hydrophilic character of the films with the addition of PLA. The results presented consider the measurements during 1 min (arpox 20 measurements each); to determine the surface free energy Owens, Wendt, Rabel and Kaelble (OWRK) method was used.

Water Vapor Transfer Rate: Water vapor permeation was measured with a thermohygrometer using deionized water according to standard test ASTM E96/E96M-14; measurements were performed at least three times.

Differential scanning calorimetry: Thermal behavior of the films with the addition of PLA was studied using differential scanning calorimetry (DSC).Experiment was realized in a N_2 atmosphere with a 4 stage cycle: (1) 5-10 mg samples were heated from 25 ° to 250 ºC at 5 ºC min^{-1} (2) temperature was held for 3 min with constant temperature, (3) temperature was decreased to 25 ºC at 5 ºC min^{-1} and (4) reheated from 25 to 250 ºC at 5 ºCmin^{-1}.

Results and Discussion

Fiber characterization

Morphological and optical analysis of the fibers can be appreciated in Figure V-11, which shows both SEM images and visual aspects of the two different raw materials. Bleached fibers were around 4 mm length with diameters between 6-10 µm, some fibers presented a

rectangular-tubular shape, with most of them being round-tubular. PLA microfibers were around 5 mm length with diameters ranging between 10 and 20 µm, PLA microfibers were smoother in their surface and tended to be more straight. Both fibers were light in color at simple sight, with bleached cellulose fibers being whiter. After high pressure homogenization cellulose nanofibers formed a translucent gel which depending on the concentration could reach more solid white tones.
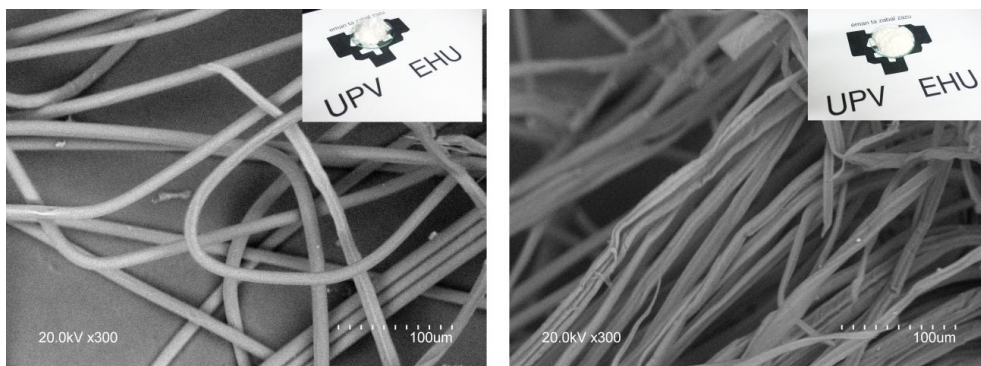
Figure V-11 SEM images of LAF (left) and ALO (right).

Film interaction and visual evaluation

Morphological and physical properties

Figure V-12 presents SEM images of the elaborated composites surface with 300x magnification, as well as an image of the breaking edge after tearing burst essay with a 55x magnification. The surface of 100C film presents the traditionally smooth surface of nanocellulose-based films; some rugosities can be observed and are attributed to the nonstick paper used during hot-pressing. When PLA microfibrils are added to the films, there is an evident anisotropic distribution, with entanglements and an increase in the pores due to entanglements, overlapping and the low compatibility of the composite films which leads to a porous rough material.

The surface topography of each composite was further characterized by AFM (Figure V-13). The dense and aggregated cellulose nanofibril and PLA microfibrils structure on the films is more apparent on by AFM microscopy, with the randomly oriented and overlapped fibrils producing the aggregated web structure. It can be seen from the inset images that the increased PLA microfibrils content reduce the contact angle, hence the polarity and hydrophilicity of the films increased.
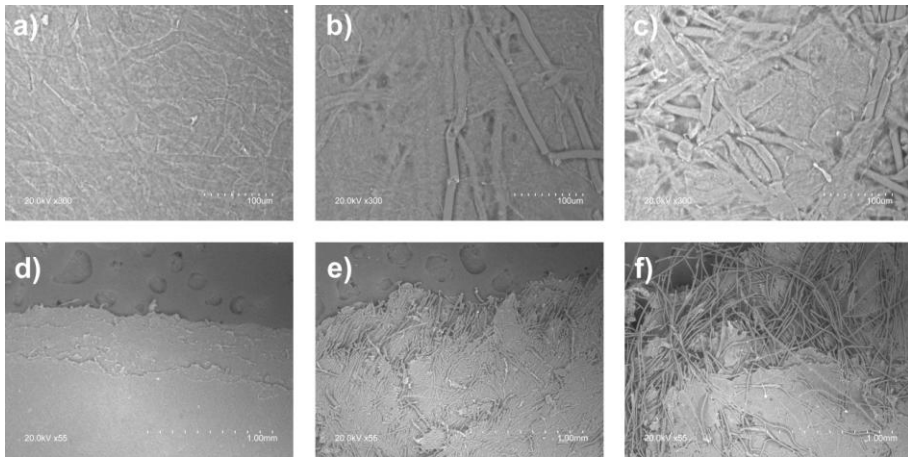
Figure V-12 SEM images of film composites a) 100C, b) 75C and c) 50C); first row presents images of the surface of the composites and second row corresponds to fracture region after mechanical tests.
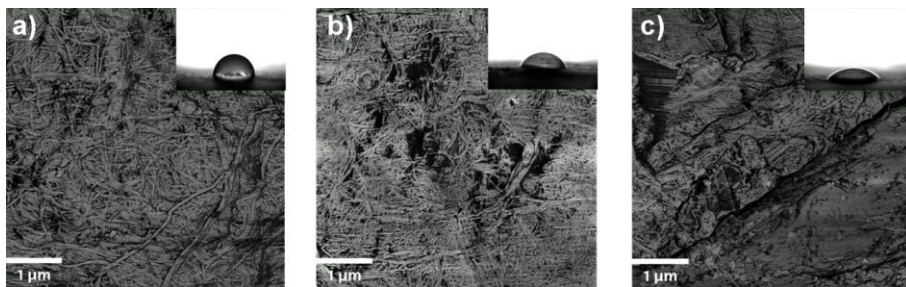
Figure V-13 AFM images of film composites a) 100C, b) 75C and c) 50C.

Mechanical properties

Tables V-9 and V-10 show inherent mechanical properties of the elaborated film composites, Table V-9 focuses in the material properties under uniaxial stress, ultimate tensile strength, strain, modulus, grammage and porosity, while Table V-10 is an approach to potential applications, grouping properties such as density, Parker printing surface roughness, bursting strength, tearing strength and bending stiffness. As chemical bonding is low because of the pressing temperature and the lack of any type of compatibilizer, the increase of LAF in the composition of the composite films has direct implications in their mechanical behavior, in any case, the strain achieved in all composite films is over other publications, which is usually related to the hydrogen bonding occurring between free hydroxyl groups of CNF. These results (average strain ~10 %) are higher than other nanopapers made with the same preparation method (filtration+hot pressing) as other works have reported strains around 4-7 %[127,275], moreover, in case of cellulose-chitin composite films (previous section)[275] it was shown that the addition of non-cellulosic

particles to the composition of the paper has reduced the overall tensile-stress properties of the films. It is also worth noting that the results are lower to other publications who reach strong an tough nanopapers mostly due to three factors: the origin of the lignocellulosic matter, the cellulose extraction method and the elaboration process, reported substantial differences between different cellulose based nanopapers depending on the elaboration method, with sheet-forming devices and solvent casting had overall higher values. On the other hand, reported differences between nanopapers elaborated from the same raw material and by the same elaboration process (hot-pressing) but with different cellulose extraction method. Therefore, results for only-cellulose nanopapers of films obtained from this work are consistent with published works dealing with nanopapers, while results for composites containing LAF behave as expected, with low chemical interaction between surface oligomers and free hydroxyl groups, mostly because of the processing which was performed under the PLA Tg and with no further surface compatibilizer, but both circumstances were intended as the aim of this work was not to elaborate strong and tough composites, but rather a biobased polymer film or membrane in which the different constituents can provide properties which are inherent to their natural conditions.

Table V-9 Ultimate tensile stress (σ), strain (ε) and Young modulus (E) of the different composites, number in parenthesis represents %RSD.

	σ_{max} [MPa]	ε [%]	E [MPa]	G [g m^{-2}]	P [%]	Average thickness [μm]
100c	72.47±10.99	10.38±1.11	3222.93±243.37	68.00±7.94	87.39	70±6.8
75c	21.39±0.48	4.38±0.53	1828.56±98.18	84.00±6.56	84.05	70.9±7.9
50c	15.36±0.97	3.25±0.65	1400.98±39.94	50.33±1.53	82.06	75.5±1.9

Table V-10 Medium density, Parker print-surf, bursting strength, tearing resistance and bending stiffness of the different composites, number in parenthesis represents %RSD.

	ϱ_m [g cm^{-3}]	PPS [MPa]	X_m [kPam^2 g^{-1}]	T_i [mNm^2 g^{-1}]	S^b [mNm]
100c	0.2691	0.7907	14.9205	5.4040	0.6192
75c	0.2278	0.8228	7.3302	4.2 690	0.5708
50c	0.1709	0.8581	4.0637	2.7647	0.2531

The surface properties of the elaborated films were measured via the contact angle sessile drop method by using water, diiodomethane, and ethylene glycol as testing liquids. For further water-interaction information, the water vapor transmission rate, and the water

contact angle are presented, the resulting values are presented in Table V-11. As stated earlier the increasing content of LAF increase the surface polarity by almost 7 times compared to the pure CNF sheet, which reduce the contact angle values and the films become highly hydrophilic. The dispersive component of the surface energy remained stable with negligible variation and 20% lower than the maximum theoretical value. The composite films can be easily printed and glued as the surface energy values are over the critical 38 mNm^{-1} value. The surface roughness of the films evaluated from the PPS value show that it is slightly increased as the microfibrils make it more porous network. The burst strength is influenced by mainly the fibril bonding, indicating that the there is not significant chemical bonds between the nano and microfibrils. The tearing strength of the sheets is generally depending on the fibril length and bonding degree between them. As the nanofibril content increases in the composite the tearing strength also increases significantly. The fibrillar composite sheets show interesting bending stiffness strength. In case of 75C, bending stiffness is till over bond paper average values, even though there is a decrease regarding 100C samples; in case of 50C values are lower than bond paper. This value is further increased when the purely CNF composed the sheets. The bending stiffness is related mainly to the fibril length and sheet thickness, which was the same in the 100C and 75C composites.

Table V-11 Contact angle; surface free energy values, water vapor transmission rate and oxygen permeability for all the films, numbers in parenthesis correspond to %RSD.

	θ_w [deg]	γ_s [mN m^{-1}]	$\gamma\gamma_s^d$ [mN m^{-1}]	γ_s^p [mN m^{-1}]	WVTR [g mm m^{-2} day]
100c	88	45.0	39.2	5.8	136.00±5.66
75c	47	73.3	40.4	33.0	117.50±6.36
50c	45	77.0	42.7	34.3	112.00±7.07

The thermal mass loss of a certain material through a single layer corresponds to the heat loss due to the specific heat of the material. The evaluation of the thermal mass loss through a ~70 µm thick film of the elaborated composites is provided in Figure V-14a. The presence of LAF has an important contribution to the thermal mass loss at increased temperatures, but the main contribution is due to the presence of CNF.

In anisotropic materials, the thermal conductivity typically varies with orientation, therefore, in order to acknowledge the performance of the composite films under changing thermal circumstances the dynamic thermal conductivity was measured (Figure V-14) with the theoretical thermal conductivity at 20 ºC (k20ºC) highlighted inside the graphic. The presence of LAF in the composite reduces the thermal conductivity (k20ºC for PLA is 130

mW m^{-1} K^{-1}). To contribute to the elucidation of the thermal properties, Figure 5c also displays the DSC thermograms, whereby the CNF film can be considered as a baseline, while the addition of PLA led to an increased integral signal at the region at which the melting point of PLA was located. The onset of melting was at ~165 °C for the PLA used in this work, but for different PLA this value can vary between 150-200 °C and in some cases be above 200 °C depending on the grade.
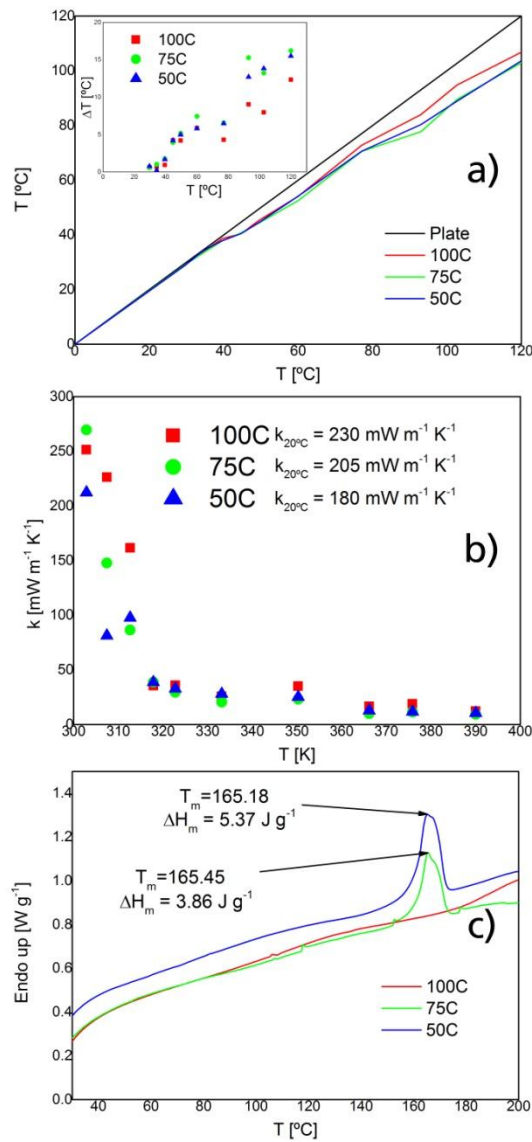
Figure V-14 a) Thermal loss of the different composites at different temperatures b) DSC thermogram with dynamic thermal conductivity.

V-4. Multi-layered hardboard with enhanced properties

Aim

The aim of this work was to analyze the influence of small fibers mixed with the traditional industrial fibers as well as the contribution of different types of nanocellulose in the external layers to the mechanical and physical properties developed within multilayer self bonded lignocellulosic composites.

Composite elaboration

In order to facilitate the understanding of further text, Table V-12 gives information regarding the codes used to identify the different composites.

Table V-12 Description of the different composites.

Sample	Base layer			External layers			ϱ_{calc} [g cm^{-1}]
	Composition [%]		Average Thickness [mm]	Second layer	Third layer	Average Thickness [mm]	
	Industrial fibers	Blue agave bagasse					
IB	100	0	~3.00	-	-	-	0.90
IC	100	0	2.80-2.90	ABO	-	~0.15	0.90
IN	100	0	2.80-2.90	ABO	BOH	~0.15	0.90
IS	100	0	2.80-2.90	ABO	BOH-W2	~0.15	0.90
BB	80	20	~3.00	-	-	-	0.90
BC	80	20	2.80-2.90	ABO	-	~0.15	0.90
BN	80	20	2.80-2.90	ABO	BOH	~0.15	0.90
BS	80	20	2.80-2.90	ABO	BOH-W2	~0.15	0.90
BN	80	20	2.80-2.90	ABO	BOH-F1	~0.15	0.90

Base layer industrial fibers (I), mixed industrial-bagasse fibers (B) and cellulose fibers (C) were suspended in water (1:60 w/w) and stirred at 700 rpm for 20 min with a CAT R100S-D mechanical stirrer, cellulose nanofibers (CNF) and modified cellulose nanofibers (BEH-W2/F1) were suspended in a plastic beaker with a 1 wt% concentration. The industrial and mixed fibers were filtered with a 0.25×0.16 mesh steel cloth. Water was discharged at 3.57×10^{-5} m^{3}s^{-1} flow rate using atmospheric pressure and gravitational force to generate the flux. When no more water was observed, fibers were pressed following the sequence in Fig. 1: 1) hand-pressing until no further water was extracted; 2) cold pressing with a ZUP-NYSA PH-1LP25 hydraulic press at 142 kN for 5 minutes for further water extraction, this was made to gain the mat absolute moisture content under 60 wt% and thus avoid the

formation of isolated water spheres that could explode during hot pressing; 3) hot pressing at 200 ºC with a ZUP-NYSA PH-1P125 hydraulic press at 684 kN for 7-9 min.

Composites with extra layers were made as described above, with the following modifications: 4) Cellulose layer was deposited over the baselayer in aqueous suspension after 1) and then lignocellulosic mat with cellulosic layer was processed as described in 2) and 3); 5) Cellulose nanofibers (either modified or unmodified) were deposited in liquid suspension over the cellulose layer after being cold pressed in 2) with an industrial-type spraying system to form a uniform layer, after this composites elaboration process followed 3); a visual description of the elaboration of the composites is presented in Figure V-15.
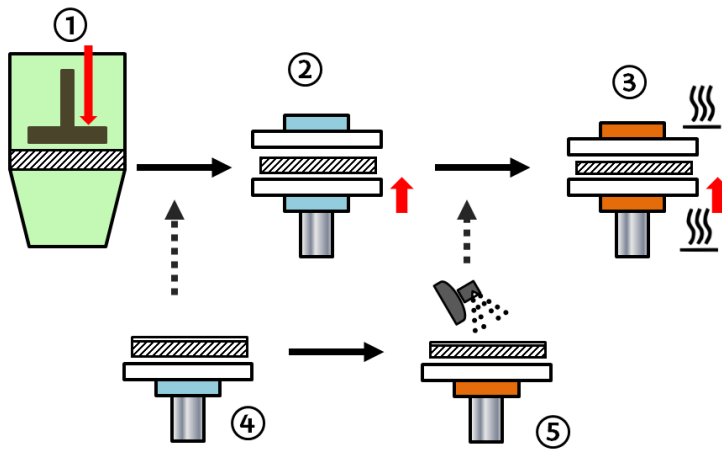
Figure V-15 Schematic description of the composite elaboration.

Composite characterization

Mechanical test methods: Three point flexural tests were measured according to standard methods, with an INSTRON 3369 universal testing machine in order to obtain the Modulus of Rupture (MOR) and Modulus of Elasticity (MOE) of each composite.

Contact angle: Contact angle measurements were performed with contact angle analyzer PHOENIX 300 (SEO) equipment using 4 μL drops with water, formamide and diiodomethane to determine surface tension, results correspond to at least 6 measurements. To determine the surface free energy Owens, Wendt, Rabel and Kaelble (OWRK) method was used for each composite.

Vertical density profile: To determine the vertical density profile (VDP), all samples were cut into 50x50x3 mm test specimens and were analyzed in a Grecon DA-X measuring instrument with direct scanning X-ray densitometry across the layer thickness with an incremental step of 0.02 mm.

Surface Water Absorption: Surface water absorption of the panels was determined with a "Cobb Ring" apparatus according to standard methods[276]; in all the composites the layer used as surface for this test was always the external one.

Water uptake and thickness swelling: Water uptake (WU) was measured following standard methods[277]. The samples were weighted before the test, and then soaked in distilled water at room temperature for 2 h after which they were removed from water, cleaned from water drops, weighted, and then soaked again for a 24 h total soaking time. After that, samples were dewatered again and the weight of them was measured. The water uptake was calculated according to:

$$WU = m_f\text{-}m_o/V_o \ [\text{mg mm}^{-3}]$$

The thickness swelling (TS) was determined on the same soaked samples, but the thickness of the samples was measured instead of weight. The thickness swelling was calculated from equation:

$$TS = t_f\text{-}t_o/t_o \ [\text{mm mm}^{-1}]$$

In which WU represents water uptake [mg mm^{-3}], m_o is weight of sample before soaking [g], m_f the weight of sample after soaking [g], TS is thickness swelling [mm mm^{-1}], t_o is the thickness of sample before soaking [mm] and t_f the thickness of sample after soaking [mm].

Colorimetry: Color properties of the different composites were measured to determine the influence of the composition of the final layer in the optical properties. This was elaborated with an X-Rite 500 series colorimeter over 10 different regions of each composite, mean RGB profile was made for the final surface layer of each composite. Color change between composites was calculated with equation:

$$\Delta E^* = (\Delta L^{*2} + \Delta a^{*2} + \Delta b^{*2})^{-2}$$

In which ΔE* represents the color change and L* represents the lightness from 100 to 0 (being 100 total lightness: white and 0 total darkness: black). On the other hand a* and b* represent chromate coordinates from which color combination can be determined; being the three colours that determine RGB values defined as follows: red is +a*, green is –a*, blue is –b* and yellow corresponds to +b*.

Table V-13 shows the mechanical properties after bending tests. In general, industrial fibers show better properties than mixed fibers as the bonding between the larger fibers in binderless materials is good. These properties are enhanced when adding cellulose of high purity and large fibers (IC and BC), but are further improved with the addition of modified cellulose nanoparticles (IS) as aminosilanes act as coupling agents. In all the composites MOR results do not fulfill the least acceptable minimums required by European Standards (EN) that is 30 N mm^{-2} for panels with thickness under 3.5 mm[278] but are in the same range of previously reported results for binderless lignocellulosic composites[279,280].

Table V-13 Mechanical properties of the composites under flexural stress: Mean density (ϱm) Modulus of Rupture and Modulus of Elasticity (numbers in parenthesis represent %RSD).

Sample	ϱ$_m$ [g cm^{-3}]	MOR [N mm^{-2}]	MOE [N mm^{-2}]
I	0.90 (4)	17.44 (13)	3423.00 (14)
IC	0.91 (5)	20.20 (10)	3528.63 (17)
IN	0.86 (2)	17.05 (09)	2969.50 (11)
IS	0.91 (4)	22.49 (12)	4139.50 (12)
B	0.88 (4)	17.05 (16)	2738.25 (21)
BC	0.90 (2)	16.57 (11)	2774.75 (14)
BN	0.93 (4)	18.37 (17)	3236.63 (14)
BS	0.86 (4)	17.32 (19)	2837.63 (16)
BF	0.92 (3)	18.68 (13)	3494.25 (14)

Compared with typical lignocellulosic composites from agricultural waste fibers, both MOR and MOE present significant increase; composites with formaldehyde-urea resin in previous works[281–283] have reported values that range between 15-36 N mm^{-2} MOR and 1300-2300 N mm^{-2} MOE, they have highlighted the importance of chemical composition of fibers, as high lignin content benefits bonding between fibers but high cellulose content increases the final resistance of the composites, this particularity is specially visible when resins are added during the process. In reported works focused on self-bonded fibers a significant increase has been achieved in mechanical properties when fibers are extracted with organic solvents, as this allows hydrogen bonds prompting stronger adhesion. This same phenomena is present in other materials that require self-bonding from fibers[284], besides, the addition of regenerated cellulose particles resulted in a decrease of mechanical properties, as this fibers

have a more hydrophilic character and act as density homogenizers, reducing the strength of the fiber bonds, MOE is decreased from 2750 to 2400 N mm^{-2} (a 15% decrease) and MOR from 14 to 10 N mm^{-2} [285]. The presence of bagasse fibers (with average length of 3 mm) reduced both MOR and MOE, being more significant the MOE reduction which implies a ~20% decrease, this can be related to two main factors: 1) the stiffness provided by the presence of smaller fibers, which fills in the interstices left by the larger fibers during self-bonding, but also generates punctual defects in the fiber network and 2) the extraction to which agave fibers are subjected during tequila production leads to degraded fibers with less natural compounds that can prompt bonding between fibers [19]. After the addition of nanocellulose layer (N) and in particular of surface-modified nanocellulose (S and F), this drawback is surpassed with a ~10% increase in case of BF and ~2% in case of BS. On the other hand, the addition of extra layers with only industrial fibers as baselayer generated an increase of ~30% when silanized nanocellulose was added (IS).

Density profile

In Figure V-16 the mean density profiles of the elaborated composites can be observed. Single-layer composites (I and B) present lower densities in the surface than multi-layered composites and similar tendencies to those published in other works[286,287]. It can be noticed that the addition of bagasse fibers, which are stiffer and smaller than those of softwood origin generate an irregular distribution of the densities, this can be a reason for the MOR and MOE decay as it has been stated before. Composites with cellulose in the final layer (IC and BC) present higher densities (around 1000 kg m^{-3}) because of the higher compression achieved by thinner cellulose fibers, as well as the cross-linking that occurs between cellulose free hydroxyl groups. In case of nanocellulose this packing properties are increased just slightly and is until coupling agents addition (IS and BS) that an increase in the density can be defined more clearly. Central regions present lower densities in every composite, characteristic of self bonded wet-technology composites. Figure V-17 shows the cross sections of all composites, in which the layer deposition can be clearly appreciated, because of the higher packing prompted by the shorter bagasse fibers. In B series composites layer formations are visibly more defined, while in three-layer composites face-layer is better defined regardless of the baselayer.
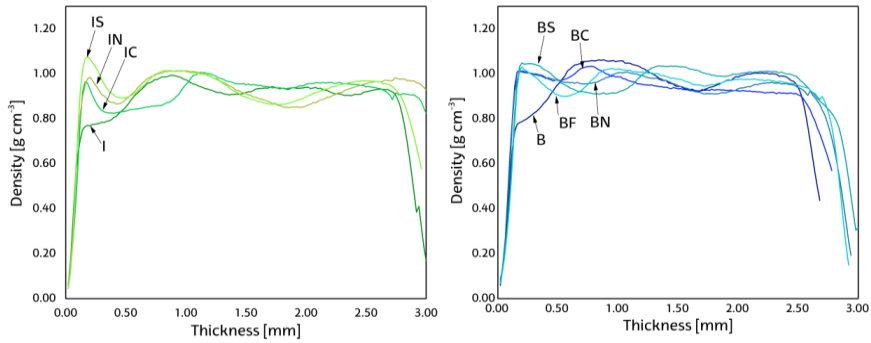
Figure V-16 Initial density profiles of the elaborated composites
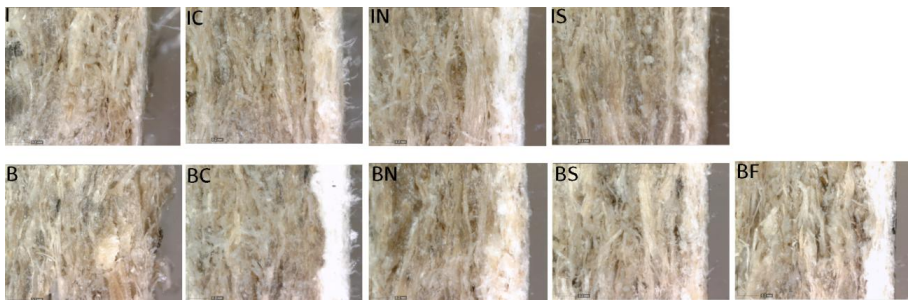
Figure V-17 Optical appearance of lateral cut of each composite at 230x.

Surface interaction with liquids

Contact angle against water sessile drop (Table V-14) shows better hydrophobic behavior when modified cellulose nanoparticles are added in the final layer. Among all the composites, BF presented the highest angle, while composites containing native cellulose: IC and BC present the worst values. Cellulose-based surface layer present higher polar component, while modified nanofibers have the lowest surface tensions in general and also the lowest polar components being BF the least polar and IS the one with lower surface tension. Table V-14also presents different methods to study the interaction of lignocellulosic composites with water during elapsed time like surface water absorption, water uptake and thickness swelling. The first one is used to evaluate the properties with whom surface layer contributes to the stability of the composites, in this case modified nanofibers contribute to slow down the amount of water that penetrates the composite from outside through the surface layer, with a ~44 % reduction between I and IS and ~23 and ~42 % reduction in case of BS and BF with respect to B; overall BF has the highest resistance to surface water absorption, as only allowed 2.654 mg m^{-2}. Water uptake and thickness swelling evaluate the water absorbed by the whole volume when interacting with external humidity, the first one is focused on the amount of water absorbed by the whole

composite when exposed to high humidity environments, while the second one focuses on the dimensional stability of the composites after elapsed contact with highly humid environments, the different composition of the composite layers played a significant role in this issue, as cellulose is highly hydrophilic and the fibrillation of both industrial fibers and cellulose fibers resulted in higher surface area.

Table V-14 Surface interaction with liquids, numbers in parenthesis represent %RSD.

Sample	γ_s [mN m^{-1}]	$\gamma\gamma_s^d$ [mN m^{-1}]	γ_s^p [mN m^{-1}]	θ Water [deg]	Surface Water Absorption [mg mm^{-2}]	Water uptake [mg mm^{-3}]		Thickness swelling [mm mm^{-1}]	
						t = 2 h	t = 24 h	t = 2 h	t = 24 h
IB	47.67	43.36	4.31	72.90 (5)	5.19 (8)	6.08 (6)	7.43 (7)	1.23 (9)	1.44 (9)
IC	42.93	33.59	9.33	66.03 (3)	5.05 (6)	5.42 (4)	6.27 (5)	1.00 (9)	1.21 (10)
IN	46.00	34.94	11.06	62.70 (3)	3.55 (5)	4.59 (5)	5.12 (6)	0.79 (6)	0.91 (6)
IS	37.98	31.84	6.13	76.97 (4)	2.90 (4)	3.61 (2)	3.98 (3)	0.61 (11)	0.69 (11)
BB	45.37	42.24	3.13	73.47 (1)	4.59 (8)	5.07 (9)	5.58 (10)	0.89 (12)	0.97 (18)
BC	49.73	34.85	14.88	57.23 (5)	4.45 (6)	5.61 (6)	6.48 (6)	1.05 (6)	1.19 (6)
BN	46.31	36.03	10.28	63.73 (2)	3.10 (15)	4.13 (14)	4.63 (15)	0.76 (15)	0.83 (18)
BS	41.41	37.84	3.57	79.43 (4)	3.55 (6)	5.95 (2)	6.60 (1)	1.10 (11)	1.21 (7)
BF	39.60	36.35	3.24	81.73 (3)	2.65 (6)	4.64 (4)	5.21 (4)	0.84 (4)	0.95 (5)

Another physical aspect involved in the interaction between binderless composites and water can be observed in Figure V-18 and Figure V-19, in which density profiles of dry composites before soaking and wet composites after 2 h and 24 h soaking are compared. In case of industrial fibers based composites (I series, Figure V-18), physical changes can be observed in both density and thickness. While thickness is increased in all cases, density is only increased when extra layers are added; this can be caused because of the compacting of the surface layers acts as a retainer for the wet industrial fibers but especially because of the more hydrophilic character of cellulose fibers, thicknesses are specially increased when no nanocellulose is present in the surface, as it has been seen before in Table V-14, for I thickness swelling is 1.44 mm mm^{-1}, which is approximately a final thickness of 7.52 mm, compared to results in figure 4 it can be seen that this increase is also observed. Hydrogen bonding provokes stronger interactions between smaller particles, thus reducing the amount of water in the internal structure of the composites, as it can be seen in IS and IN, composites with modified nanofibers (IS) have the smaller variations as the change between 2 and 24 h is less than 10% thus showing a better dimension stability of the samples and an increase in the hydrophobicity of the composite.
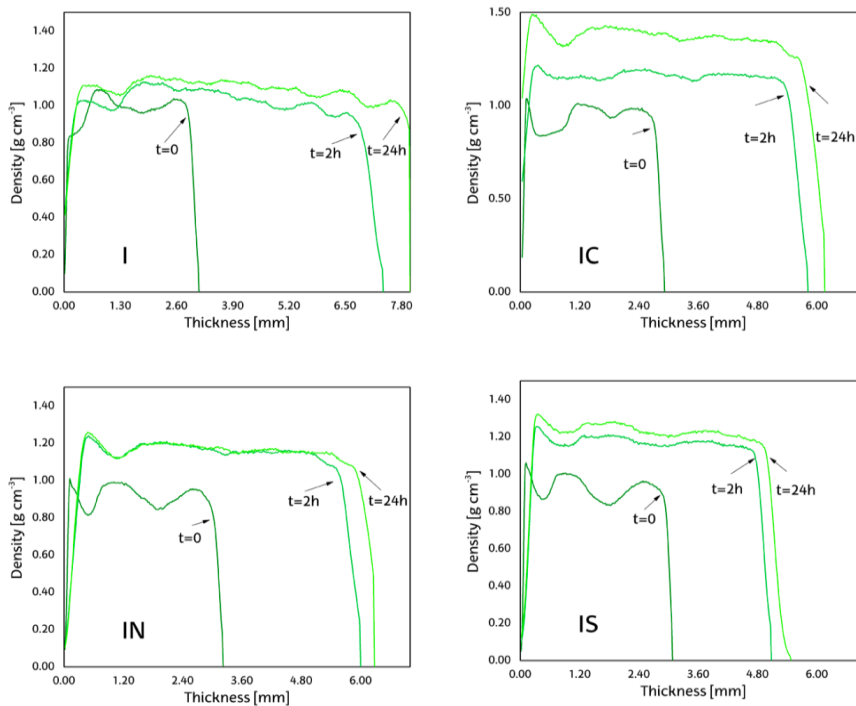
Figure V-18 Comparison of the density profiles of composites containing industrial fibers (I) before soaking, after 2 h soaking and after 24 h soaking.

In case of composites with bagasse fibers added to the baselayer (B series), dimensional stability in single layer (B) was in general higher than for industrial fibers (I) because of the higher compacting of smaller particles inside the baselayer structure, while with cellulose layer sample (BC) was unable to be measured in the equipment after 24 h of soaking, but did not represent a significant variation with respect to I series after nanocellulose layers were applied (BN, BS) with both presenting little spans after 24 h with respect to the 2 h measurement, difference after 24 h is between 4-6 % in all thicknesses for B series containing cellulose nanofibers in any form (see table 4) water absorption, thickness swelling as well as density profiles after 2 and 24 h soaking presented consistently the contribution of cellulose nanofibers in external layers to reduce the water content inside the composites.
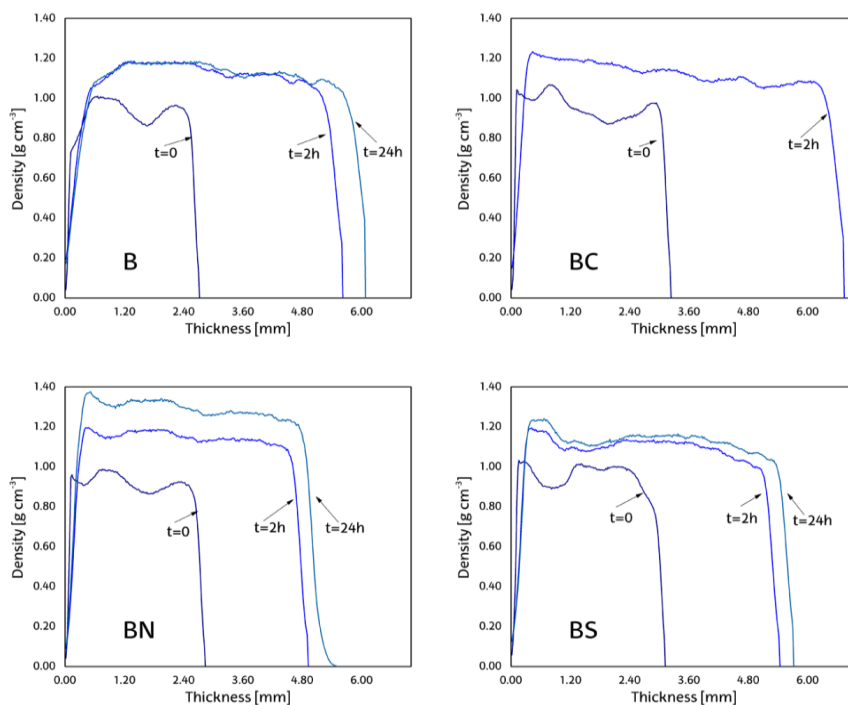
Figure V-19 Comparison of the density profiles of composites containing mixed fibers (B) before soaking, after 2 h soaking and after 24 h soaking

Colorimetry

Table V-15 shows the CIELab standard color space for each composite, on the other hand in Figure V-20 it can be observed the visual aspect of the surface layers at 0x (left) 230x(upper right) as well as the simulated RGB pattern that corresponds to the CIELab values measured (lower right). ΔE* corresponds to the color change observed between the single layer composite and the different multilayer composites made with that same baselayer (either I or B). Higher color changes are visible in case of cellulose fibers because of the characteristic white color of this material with ΔE* going as far as 20 in case of BC composites, in general mixed-fiber baselayers (B) have higher ΔE* because their more compact surface prompted a better assembly of the exterior layers, this can be seen in L* values of BC and BN, as well as BN, b* values increased with the addition of silanized nanofibers because of their characteristic yellowing effect, being higher values of b* associated with an increase of the yellow color, in BN the value of b* is increased almost 50% while IN increased 30%. Respecting the homogeniousness of the surface, single layer composites present less color variation, with %RSD ~1%, double layer composites (IC and BC) have the highest %RSD as there could be homogenity inacccuracies during layer deposition, thinner white regions may become translucent and the appeareance of brownish

baselayer through traslucent face layer results in variations through the green coordinate (lower a*) this phaenomena is not present in three-layer composites as the color influence of the baselayer is compleatly discarded because of the ammount of added material and the higher homogeneity of cellulose nanofibers.

Table V-15 Optical properties of each composite.

Sample	L*	a*	b*	C^*_{ab}	h	ΔE^*
I	72.53 (1)	8.27 (1)	20.51 (1)	22.12 (2)	1.19 (3)	-
IC	85.27 (1)	4.63 (5)	16.53 (4)	17.16 (9)	1.30 (10)	13.83 (22)
IN	83.09 (2)	6.76 (6)	21.86 (2)	22.88 (8)	1.27 (8)	10.75 (30)
IS	73.69 (2)	10.13 (7)	26.19 (4)	28.08 (11)	1.20 (11)	6.08 (68)
B	67.76 (1)	8.62 (1)	20.29 (1)	22.05 (2)	1.17 (3)	-
BC	86.95 (1)	4.03 (10)	16.19 (5)	16.68 (15)	1.33 (16)	20.15 (16)
BN	85.01 (6)	4.74 (6)	18.08 (4)	18.69 (10)	1.31 (11)	17.82 (18)
BS	74.23 (2)	12.23 (4)	30.49 (3)	32.85 (7)	1.19 (7)	12.60 (30)
BF	76.22 (3)	7.11 (4)	20.62 (3)	21.81 (7)	1.24 (7)	8.60 (54)
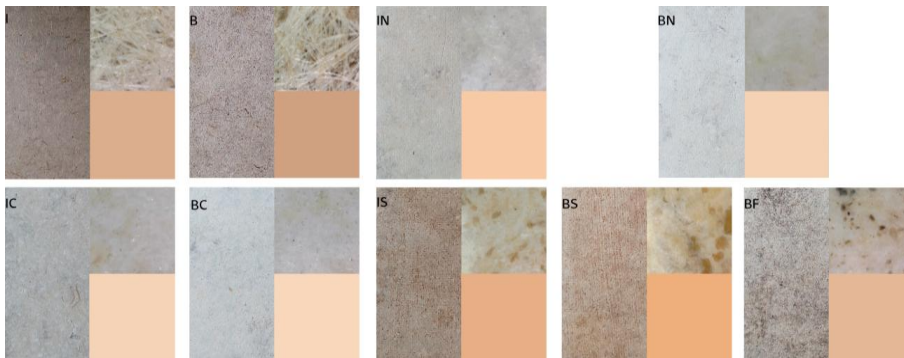
Figure V-20 Optical appearance of each composite; left: visual aspect, upper right: 230x microgram and lower right RGB color simulated with L*a*b* parameters.

Conclusions

Binderless materials represent a high opportunity for industrial applications as they represent no harm for human life regarding VOC emissions. The mechanical properties as well as the behavior of multi-layered composites under different circumstances were evaluated to study the influence of such layers in the physical properties of binderless fiber composites. The addition of smaller particles had minor influence in the surface slightly increasing water absorption in B respect I, but heavily decreased mechanical properties (more than 20% in case of MOE), this is counteracted by the addition of modified CNF to

the external layers who act as a reinforcement to the composites under flexural stress as well as a barrier against water, this is further enhanced with surface modifications, the surface modification which proved to be more versatile under mechanical surface tests is the one with fatty acids (BF), as it acts both as a bonding agent between modified nanofibers and the lower layer, and as a surface protector for the composite.

VI) General Conclusions and Future Works

General Conclusions

The present work pretends to contribute to the utilization of by-products from the tequila industry by obtaining value-added functional materials. For this purpose, blue agave leaves and bagasse were collected and treated to extract their native cellulose with environmentally friendly processes; with such native cellulose, nanoparticles were elaborated via chemical or mechanical methods. The obtention of competitive nanocelluloses from blue agave by-products and their characterization represents an alternative market to the blue agave cultivars, which are currently oriented exclusively to the tequila production.

The design of the pulping and bleaching sequences was done according to current trends in the industry as well as the know-how the Biorefinery Processes research group, complemented by state-of-art publications by experts in the topic. The selected methods are based in economical and environmental aspects of the available technologies, therefore, pulping was done either with soda or with organosolv processes, instead of more used sulfite and Kraft, while bleaching was done with elemental chlorine free and total chlorine free sequences, which means that the resulting celluloses would be considered "green" as reagents are of low environmental impact. This of course implies an increased processing cost, but such drawback is countered by the fact that the raw material is a by-product, which makes the obtained celluloses competitive both in quality and price to those obtained from similar plants but harvested from fiber-oriented cultivars, for example sisal.

Cellulose nanoparticles (CNF and CNC) were elaborated with methods similar to state-of-art literature, with the only particularity being the integration of cavitations during acid hydrolysis instead of mechanical stirring and the separation of un-hydrolyzed fractions. Yields were quite competitive, in particular for CNF, while the morphology and physical properties of CNF and CNC was within the expectations.

Modification with organosilanes or with fatty acids gives different functionalities to the cellulose nanoparticles; such properties include colloidal stability, hydrophobicity, or coupling enhancement. The selection of such reagents to perform the functionalizations was due to their nature or their processing properties. In case of silanes, the by-product generated during the reaction is ethanol, which is then evaporated during curing and does not represent a harmful volatile compound, as could be the case of methoxysilanes. Moreover, silanized nanoparticles in after-service life could be composted with no particular harm to the environment. Esterified cellulose nanoparticles are also compostable and nature-based, however during the reaction toluene and pyridine are involved, which cannot be considered a "green" process. However both reagents can be recovered after the modification and reused in further reactions, which reduces the negative impact of such products. In any case, the present work focused more in the use of organosilanes than in the fatty acid.

The processing and potential applicability of cellulose nanoparticles before and after modification of cellulose-based biocomposites was studied in Chapter 4. In such works, both CNC and CNF showed significant contributions to the properties of the composites, either neat or modified. The other materials used to elaborate composite materials consisted also in bio-based polymers e.g. chitin, polylactide or natural fibers. This resulted in fully biodegradable or compostable composites, which was a significant aspect of the present work. The most studied properties were mechanical, but other functional aspects were studied as surface properties (surface energy, water uptake, water vapor permeability, color, etc.), visual aspects, or even antifungal activity. In general the use of functionalized nanoparticles implied an enhancement of the surface properties, but not necessarily mechanical properties, this could be further improved with the addition of a plasticizer to the composites, if needed.

Future Works

Further works involving the use of blue agave include the complete fractioning of the lignocellulosic biomass to recover lignin and hemicelluloses, so the exploitation of such by-products would imply the obtention of more value-added components and therefore a better economical profit from the same process. Another aspect in mind is the use of more effective methods for the elaboration of cellulose nanoparticles from blue agave to reduce the energy consumption and to avoid the use of reagents such as sulfuric acid; this could be done by the use of carboxylic acids and maybe by the use of environmentally friendly pretreatments to oxidize the cellulose before fibrillation as it is done with carboxymethilation or TEMPO oxidation. And of course, the elaboration of bio-based composites will still be a major objective in the use of cellulose nanoparticles from blue agave, as the applications of silanized cellulose are diverse and promising.

References

References

1.   Euripides. *The Bacchæ*. (P.F. Collier & Son, 2001).

2.   Linnaeus, C. in (ed. Salvius, L.) 323 (1753).

3.   Weber, F. A. C. Agavaceae Agave tequilana F.A.C.Weber. *Bulletin du Muséum d'Histoire Naturelle* **8,** (1902).

4.   The Angiosperm Phylogeny Group III. An update of the Angiosperm Phylogeny Group Classification for the orders and families of floweringplants: APG III. *Botanical Journal of the Linnean Society* **161,** 105–121 (2009).

5.   Humboldt, A. von. *Essai politique sur le royaume de la Nouvelle-Espagne*. (Chez J. H. Stône, 1811). at <http://www.biodiversitylibrary.org/item/85270>

6.   Mexican Direction of Industrial Property. General declaration of protection of the designation of origin 'Tequila'. *Official Journal of the Federation* **127,** 15 (1974).

7.   Mexican Government. Lisbon International System of Apellations of Origin (669) Tequila. *Bulletin 'Les appellations d'origine"* **12,** 669 (1978).

8.   Mexican Secretariat of Economy. Norma Oficial Mexicana NOM-006-SCFI-2005, Bebidas Alcohólicas-Tequila-Especificaciones. *Official Journal of the Federation* **628,** (2006).

9.   Mexican Secretariat of Commerce and Industrial Development. Norma Oficial Mexicana NOM-070-SCFI-1994, Bebidas Alcohólicas-Mezcal-Especificaciones. *Official Journal of the Federation* **525,** (1997).

10.   Valenzuela-Zapata, A. G. & Nabhan, G. P. *Tequila: A Natural and Cultural History*. (The University of Arizona Press, 2004).

11.   Royal Botanical Gardens. World Checklist of Selected Plant Families. at <http://apps.kew.org/wcsp/incfamilies.do>

12.   Missouri Botanical Garden. Tropicos.org. at <http://www.tropicos.org/>

13.   Satyanarayana, K. G. *et al.* Characterization of blue agave bagasse fibers of Mexico. *Composites Part A: Applied Science and Manufacturing* **45,** 153–161 (2013).

14.   National Regulator Council for Tequila Industry. CRT. at <https://www.crt.org.mx/>

15.   Octave, S. & Thomas, D. Biorefinery : Toward an industrial metabolism. *Biochimie* **91,** 659–664 (2009).

16.   Pauly, M. & Keegstra, K. Cell-wall carbohydrates and their modification as a resource for biofuels. *The Plant Journal* **54,** 559–568 (2008).

17.   Vogel, J. Unique aspects of the grass cell wall. *Current Opinion in Plant Biology* **11,**

301–307 (2008).

18.   Carpita, N. C. & Gibeaut, D. M. Structural models of primary cell walls in flowering plants : consistency of molecular structure with the physical properties of the walls during growth. *The Plant Journal* **3,** 1–30 (1993).

19.   Carpita, N. C. STRUCTURE AND BIOGENESIS OF THE CELL WALLS OF GRASSES. *Annual Review of Plant Physiology and Plant Molecular Biology* **47,** 445–76 (1996).

20.   Aspinall, G. O. in *The Biochemistry of Plants, Vol. 3* (ed. Preiss, J.) (Academic Press, 1980).

21.   Capek, P., Alföldi, J. & Lišková, D. An acetylated galactoglucomannan from Picea abies L. Karst. *Carbohydrate Research* **337,** 1033–1037 (2002).

22.   Boerjan, W., Ralph, J. & Baucher, M. Lignin Biosynthesis. *Annual Review of Plant Biology* **54,** 519–546 (2003).

23.   Pattathil, S., Hahn, M. G., Dale, B. E. & Chundawat, S. P. S. Insights into plant cell wall structure , architecture , and integrity using glycome profiling of native and AFEX TM -pre- treated biomass. *Journal of Experimental Botany* 1–16 (2015). doi:10.1093/jxb/erv107

24.   Nägeli, K. *Die micellartheorie.* (1928).

25.   Frey-Wyssling, A. Der Aufbau der Pflanzlichen Zellwände. *Protoplasma* **25,** 261–300 (1936).

26.   Frey-Wyssling, A. Röntgenometrische Vermessung der submikroskopischen Räume in Gerüstsubstanzen. *Protoplasma* **37,** 372–411 (1937).

27.   Frey-Wyssling, A. Über die submikroskopische Morphologie der Zellwände. *Berichte der Deutschen Botanischen Gesellschaft* **55,** 119–132 (1937).

28.   Clarke, S. Fine structure of the plant cell wall. *Nature* (1938). at <http://www.nature.com/nature/journal/v142/n3603/abs/142899a0.html>

29.   Anderson, D. B. The Structure of the Walls of the Higher Plants. *Botanical Review* **1,** 52–76 (1935).

30.   Gibson, L. J. The hierarchical structure and mechanics of plant materials. *Journal of the Royal Society, Interface* **9,** 2749–2766 (2012).

31.   Niklas, K. J. *Plant biomechanics: An Engineering Approach to Plant Form and Function.* (The University of Chicago Press, 1992).

32.   Park, J. Y., Han, S. W. & Lee, I. H. Preparation of electrospun porous ethyl cellulose fiber by THF/DMAc binary solvent system. **13,** 1002–1008 (2007).

33.   Fratzl, P. Cellulose and collagen: from fibres to tissues. *Current Opinion in Colloid & Interface Science* **8,** 32–39 (2003).

34.   Vincent, J. F. From cellulose to cell. *The Journal of Experimental Biology* **202,** 3263–3268 (1999).

35.   Bidlack, J., Malone, M. & Benson, R. Molecular Structure and Component Integration of Secondary Cell Walls in Plants. *Proceedings of the Oklahoma Academy of Science* **72,** 51–56 (1992).

36.   Zimmermann, T., Bordeanu, N. & Strub, E. Properties of nanofibrillated cellulose from different raw materials and its reinforcement potential. *Carbohydrate Polymers* **79,** 1086–1093 (2010).

37.   Wang, J. *et al.* Anaerobic digestibility and fiber composition of bulrush in response to steam explosion. *Bioresource Technology* **101,** 6610–6614 (2010).

38.   Takashi, N., Ikuyo, M. & Hirao, K. All-Cellulose Composite. (2004). doi:10.1021/MA049300H

39.   Eichhorn, S. J. *et al.* Review: Current international research into cellulosic fibres and composites. *Journal of Materials Science* **36,** 2107–2131 (2001).

40.   Wang, B. & Sain, M. The effect of chemically coated nanofiber reinforcement on biopolymer based nanocomposites. *BioResources* **2,** 371–388 (2007).

41.   Fengel, D. & Wegener, G. *Wood : chemistry, ultrastructure, reactions.* (Walter de Gruyter, 1989).

42.   Mathew, A. P., Oksman, K. & Sain, M. The effect of morphology and chemical characteristics of cellulose reinforcements on the crystallinity of polylactic acid. *Journal of Applied Polymer Science* **101,** 300–310 (2006).

43.   Dybowski, U. Does polymerisation degree matter? *Manufacturing Chemist* **68,** 19–21 (1997).

44.   Thoorens, G., Krier, F., Leclercq, B., Carlin, B. & Evrard, B. Microcrystalline cellulose, a direct compression binder in a quality by design environment—A review. *International Journal of Pharmaceutics* **473,** 64–72 (2014).

45.   Gautam, S. P., Bundela, P. S., Pandey, A. K., Awasthi, M. K. & Sarsaiya, S. A review on systematic study of cellulose. *t* (2010).

46.   Timell, T. E. Recent progress in the chemistry of wood hemicelluloses. *Wood Science and Technology* **1,** 45–70 (1967).

47.   Hansen, C. M. M., Björkman, a. & Bjorkman, A. The Ultrastructure of Wood from a Solubility Parameter Point of View. *Holzforschung* **52,** 335–344 (1998).

48.   Peng, P. & She, D. Isolation, structural characterization, and potential applications of hemicelluloses from bamboo: A review. *Carbohydrate Polymers* **112,** 701–720 (2014).

49.   Hemsworth, G. R., Johnston, E. M., Davies, G. J. & Walton, P. H. Lytic Polysaccharide Monooxygenases in Biomass Conversion. *Trends in Biotechnology* **33,**

747–761 (2015).

50.   Peng, B. L., Dhar, N., Liu, H. L. & Tam, K. C. Chemistry and applications of nanocrystalline cellulose and its derivatives: A nanotechnology perspective. *Canadian Journal of Chemical Engineering* **89,** 1191–1206 (2011).

51.   Peng, F., Peng, P., Xu, F. & Sun, R. C. Fractional purification and bioconversion of hemicelluloses. *Biotechnology Advances* **30,** 879–903 (2012).

52.   Willför, S., Sundberg, K., Tenkanen, M. & Holmbom, B. Spruce-derived mannans – A potential raw material for hydrocolloids and novel advanced natural materials. *Carbohydrate Polymers* **72,** 197–210 (2008).

53.   Brandt, A. *et al.* Deconstruction of lignocellulosic biomass with ionic liquids. *Green Chemistry* **15,** 550 (2013).

54.   Crombie, H. J., Scott, C. & Reid, J. S. G. Detergent-Solubilization of a Homogalacturonan Galacturonsyltransferase from Mung Bean. *Advances in Pectin and Pectinase Research* **11,** 35–45 (2003).

55.   Fry, S. C. *The growing plant cell wall: chemical and metabolic analysis. The growing plant cell wall: chemical and metabolic analysis.* (Longman Group Limited, 1988).

56.   McNeil, M., Darvill, A. G., Fry, S. C. & Abersheim, P. Structure and Function of the Primary Cell Walls of Plants. *Annual Review of Biochemistry* **53,** 625–63 (1984).

57.   Hahn, M. G., Darvill, A. G. & Albersheim, P. Host-Pathogen Interactions '. 1161–1169 (1981).

58.   Jin, D. F. & West, C. A. Characteristics of Galacturonic Acid Oligomers as Elicitors of Casbene Synthetase Activity in Castor Bean Seedlings1. *Plant Physiology* **74,** 989–992 (1984).

59.   Nothnagel, E. A., McNeil, M., Albersheim, P. & Dell, A. Host-Pathogen Interactions '. *Plant Physiology* 916–926 (1983).

60.   Robertsen, B. Elicitors of the production of lignin-like compounds in cucumber hypocotyls. *Physiological and Molecular Plant Pathology* **28,** 137–148 (1986).

61.   Bishop, P. D., Pearce, G., Bryant, J. E. & Ryan, C. A. Isolation and Characterization of the Proteinase Inhibitor-inducing Factor from Tomato Leaves. *The Journal of Biological Chemistry* **259,** 13172–13177 (1984).

62.   Vorangen, A., Coenen, G.-J., Verhoef, R. P. & Schols, H. A. Pectin , a versatile polysaccharide present in plant cell walls. *Structural Chemistry* **20,** 263–275 (2009).

63.   Sjöström, E. in *Wood Chemistry* 71–89 (1993). doi:10.1016/B978-0-08-092589-9.50008-5

64.   Lupoi, J., Singh, S., Parthasarathi, R., Simons, B. A. & Henry, R. J. Recent innovations in analytical methods for the qualitative and quantitative assessment of

lignin. *Renewable and Sustainable Energy Reviews* **49,** 871–906 (2015).

65. Wardrop, A. B. & Harada, H. The Formation and Structure of the Cell Wall in Fibres and Tracheids. *Journal of Experimental Botany* **16,** 356–371 (1965).

66. Lanzalunga, O. & Bietti, M. Photo- and radiation chemical induced degradation of lignin model compounds. *Journal of Photochemistry and Photobiology B: Biology* **56,** 85–108 (2000).

67. Dence, C. W. & Lin, S. Y. in *Methods in Lignin Chemistry* (eds. Lin, S. Y. & Dence, C. W.) 3–19 (Springer Berlin Heidelberg, 1992). doi:10.1007/978-3-642-74065-7_1

68. Han, J. S. & Rowell, J. S. in *Paper and Composites from Agro-Based Resources* (eds. Rowell, R. M., Young, R. A. & Rowell, J. K.) (CRC Press Inc., 1997).

69. Schultz, T. P. & Nicholas, D. D. Naturally durable heartwood: evidence for a proposed dual defensive function of the extractives. *Phytochemistry* **54,** 47–52 (2000).

70. Albenne, C., Canut, H., Hoffmann, L. & Jamet, E. Plant Cell Wall Proteins: A Large Body of Data, but What about Runaways? *Proteomes* **2,** 224–242 (2014).

71. Canut, H., Albenne, C. & Jamet, E. in *Isolation of Plant Organelles and Structures: Methods and Protocols* (eds. Taylor, N. L. & Millar, A. H.) 171–185 (Springer New York, 2017). doi:10.1007/978-1-4939-6533-5_14

72. Sorek, N., Yeats, T. H., Szemenyei, H., Youngs, H. & Somerville, C. R. The Implications of Lignocellulosic Biomass Chemical Composition for the Production of Advanced Biofuels. *BioScience* **64,** 192–201 (2014).

73. Bischoff, V. *et al.* TRICHOME BIREFRINGENCE and its homolog AT5G01360 encode plant-specific DUF231 proteins required for cellulose biosynthesis in Arabidopsis. *Plant physiology* **153,** 590–602 (2010).

74. Seifert, G. J. & Roberts, K. The Biology of Arabinogalactan Proteins. *Annual Review of Plant Biology* **58,** 137–161 (2007).

75. Vassilev, S. V., Baxter, D., Andersen, L. K. & Vassileva, C. G. An overview of the chemical composition of biomass. *Fuel* **89,** 913–933 (2010).

76. Werkelin, J., Skrifvars, B.-J. & Hupa, M. Ash-forming elements in four Scandinavian wood species. Part 1: Summer harvest. *Biomass and Bioenergy* **29,** 451–466 (2005).

77. FitzPatrick, M., Champagne, P., Cunningham, M. F. & Whitney, R. A. A biorefinery processing perspective: Treatment of lignocellulosic materials for the production of value-added products. *Bioresource Technology* **101,** 8915–8922 (2010).

78. Kamm, B. & Kamm, M. Grüne Bioraffinerie. *Nachrichten aus Chemie, Technik und Laboratorium* **46,** 342–343 (1998).

79. Kamm, B. & Kamm, M. Biorefineries – Multi Product Processes. *Advanced Biochemical Engineering* **105,** 175–204 (2007).

80.   Kamm, B. & Kamm, M. Principles of biorefineries. *Applied Microbiology and Biotechnology* **64,** 137–145 (2004).

81.   Van Dyne, D. L., Blase, M. G. & Davis Clements, L. in *Perspectives on new crops and new uses* (ed. Janick, J.) 114–123 (ASHS Press, 1999).

82.   R., N., P., M. & C., R. Integrated production of biodegradable plastic, sugar and ethanol. *Applied Microbiology and Biotechnology* **57,** 1–5 (2001).

83.   Kamm, B., Kamm, M., Kromus, S. & Narodoslawsky, M. Green Biorefinery European Network for the Implementation of Biorefineries (NIB). *Brandenburgische Umwelt Berichte (BUB)* **8,** 251–259 (2000).

84.   Andersen, M. & Kiel, P. Integrated utilisation of green biomass in the green biorefinery. **11,** 129–137 (2000).

85.   Duarte, L. C., Esteves, M. P., Carvalheiro, F. & Gírio, F. M. Biotechnological valorization potential indicator for lignocellulosic materials. *Biotechnology Journal* **2,** 1556–1563 (2007).

86.   Sjöström, E. in *Wood Chemistry* 225–248 (1993). doi:10.1016/B978-0-08-092589-9.50014-0

87.   Sixta, H. in *Handbook of Pulp* (ed. Sixta, H.) 1–20 (WILEY‑VCH Verlag, 2006).

88.   Sixta, H., Potthast, A. & Krotschek, A. W. in *Handbook of Pulp* (ed. Sixta, H.) 109–229 (2006). doi:10.1002/9783527619887.ch4a

89.   Tayenthal, K. & Kleinert, T. Process of decomposing vegetable fibrous matter for the purpose of the simultaneous recovery both of the cellulose and of the incrusting ingredients. (1930).

90.   González, D., Campos, A. R., Cunha, A. M., Santos, V. & Parajó, J. C. Utilization of Fibers Obtained By Peroxyformic Acid Processing Of Broom as Reinforcing Agents for Biocomposites. *BioResources* **5,** 2591–2610 (2010).

91.   Blechschmidt, J. & Heinemann, S. in *Handbook of Pulp* (ed. Sixta, H.) 1079–1111 (WILEY‑VCH Verlag, 2006). at <http://www.masagroup.ir/Attach/165ff594-2680-4167-8424-b34bafdc0abdPulpingChemistryandTechnology.pdf#page=67>

92.   Sandelin, B., Trautwein, H. & Wundrak, R. in *Handbook of Pulp* (ed. Sixta, H.) 1073–1074 (WILEY‑VCH Verlag, 2006). doi:10.1094/APSnetFeature-2008-0308

93.   Ibarra, D. *et al.* Structural modification of eucalypt pulp lignin in a totally chlorine-free bleaching sequence including a laccase-mediator stage. *Holzforschung* **61,** 634–646 (2007).

94.   Bajpai, P. Biological Bleaching of Chemical Pulps. *Critical Reviews in Biotechnology* **24,** 1–58 (2004).

95.   Nelson, P. J. in *Environmentally Friendly Technologies for the Pulp and Paper Industry* (ed.

Young, R. A.) (John Wiley & Sons, Inc., 1998).

96.   Sullivan, M. J., McCaw, P. A., Holmes, R. L., Sewall, C. H. & Surgenor, S. D. Multiple exposure pathway risk assessment for dioxin at a bleached pulp mill. *Chemosphere* **20,** 1771–1778 (1990).

97.   LaFleur, L. *et al.* Studies on the mechanism of PCDD/PCDF formation during the bleaching of pulp. *Chemosphere* **20,** 1731–1738 (1990).

98.   Sjöström, E. in *Wood Chemistry* 114–164 (1993). doi:10.1016/B978-0-08-092589-9.50011-5

99.   Solomon, K. R., Hanson, M., Solomon, K. R. & Hanson, M. in *Handbook of Green Chemistry* (Wiley-VCH Verlag GmbH & Co. KGaA, 2012). doi:10.1002/9783527628698.hgc109

100.   Mateo, C., Chirat, C., Aït-Ouaret, R. & Jeunet, A. Nature and removal of the last colored chromophores in kraft pulps. *Nordic Pulp and Paper Research Journal* **16,** 385–388 (2001).

101.   Mateo, C., Chirat, C. & Lachenal, D. The Chromophores Remaining After Bleaching to Moderate Brightness. *Journal of Wood Chemistry and Technology* **24,** 279–288 (2005).

102.   Lachenal, D. *et al.* Influence of pulp colour on bleachability. Ways to improve the bleaching response of alkaline pulp. *ATIP. Association Technique de L'Industrie Papetiere* **59,** 6–11 (2005).

103.   Gierer, J. Chemistry of delignification. *Wood Science and Technology* **36,** 289–312 (1982).

104.   Süss, H. U., Schmidt, K. & Jakob, I. Peroxide application in ECF sequences: A description of the state-of-the-art. *Appita Journal* **53,** 116–121 (2000).

105.   Gellerstedt, G. & Pettersson, I. Chemical Aspects of Hydrogen Peroxide Bleaching. Part II the Bleaching of Kraft Pulps. *Journal of Wood Chemistry and Technology* **2,** 231–250 (1982).

106.   Süss, H. U. & Nimmerfroh, N. F. Hydrogen Peroxide in Chemical Pulp Bleaching. in *Meeting on Pulp Bleaching* 15 (Associação Brasileira Técnica de Celulose e Papel, 1996).

107.   Jones, P. W. & Williams, D. R. Chemical speciation simulation used to assess the efficiency of environment-friendly EDTA alternatives for use in the pulp and paper industry. *Inorganica Chimica Acta* **339,** 41–50 (2002).

108.   Pinto, I. S. S., Ascenso, O. S., Barros, M. T. & Soares, H. M. V. M. Pre-treatment of the paper pulp in the bleaching process using biodegradable chelating agents. *International Journal of Environmental Science and Technology* **12,** 975–982 (2015).

109.   Sabharwal, H. S. *et al.* Development of biological pulping processes for non-woody

plants. in *Proceedings of the 6th International Conference on Biotechnology in the Pulp and Paper Industry: Advances in Applied and Fundamental Research* (eds. Srebotnik, E. & Messner, K.) 233–236 (Facultas-Univ.-Verl., 1996).

110. Finell, M., Hedman, B. & Nilsson, C.-A. in *Cellulosic Pulps, Fibres and Materials* 261–266 (2000). doi:10.1533/9781845698546.261

111. Judt, M. Non-wood plant fibres, will there be a come-back in paper-making? *Industrial Crops and Products* **2,** 51–57 (1993).

112. Bledzki, A. . & Gassan, J. Composites reinforced with cellulose based fibres. *Progress in Polymer Science* **24,** 221–274 (1999).

113. Gutiérrez, A., Rodríguez, I. M. & del Río, J. C. Chemical composition of lipophilic extractives from sisal (Agave sisalana) fibers. *Industrial Crops and Products* **28,** 81–87 (2008).

114. Hunter & Neil. 'Fuels Plus' from the Forest. *Appita Journal: Journal of the Technical Association of the Australian and New Zealand Pulp and Paper Industry* **60,** 10 (2007).

115. Wong, A. & Chiu, C. *Pulping and Bleaching of Hemp (Cannabis Sativa). TAPPI Nonwood Plant Fiber Progress Report No. 22* (1995).

116. Alcaide, L. J., Baldovin, F. L. & Parra, I. S. Characterization of cellulose pulp from agricultural residues. *Tappi journal* **74,** 217–221

117. Zhao L.; Liu, D., X. . W. Effect of several factors on peracetic acid pretreatment of sugarcane bagasse for enzymatic hydrolysis. *Journal of Chemical Technology & Biotechnology* **82,** 1115–1121 (2007).

118. Uma Maheswari, C., Obi Reddy, K., Muzenda, E., Guduri, B. R. & Varada Rajulu, A. Extraction and characterization of cellulose microfibrils from agricultural residue – Cocos nucifera L. *Biomass and Bioenergy* **46,** 555–563 (2012).

119. Livča, S., Verovkins, A., Shulga, G., Neiberte, B. & Vitolina, S. Characteristics and Properties of Soda Lignin Obtained from Aspen Wood By-Products. *Latvian Journal of Chemistry* **51,** 421–427 (2012).

120. Pinto, P. C., Evtuguin, D. V. & Pascoal Neto, C. Chemical Composition and Structural Features of the Macromolecular Components of Plantation *Acacia mangium* Wood. *Journal of Agricultural and Food Chemistry* **53,** 7856–7862 (2005).

121. Pettersen, R. C. in 57–126 (1984). doi:10.1021/ba-1984-0207.ch002

122. Bertaud, F. & Holmbom, B. Chemical composition of earlywood and latewood in Norway spruce heartwood, sapwood and transition zone wood. *Wood Science and Technology* **38,** 245–256 (2004).

123. Jonoobi, M., Khazaeian, A., Tahir, P. M., Azry, S. S. & Oksman, K. Characteristics of cellulose nanofibers isolated from rubberwood and empty fruit bunches of oil palm using chemo-mechanical process. *Cellulose* **18,** 1085–1095 (2011).

124. Kopania, E., Wietecha, J. & Ciechańska, D. Studies on isolation of cellulose fibres from waste plant biomass. *Fibres and Textiles in Eastern Europe* **96,** 167–172 (2012).

125. Siqueira, G., Bras, J. & Dufresne, A. Cellulosic Bionanocomposites: A Review of Preparation, Properties and Applications. *Polymers* **2,** 728–765 (2010).

126. Iñiguez-Covarrubias, G., Lange, S. E. & Rowell, R. M. Utilization of byproducts from the tequila industry: Part 1: Agave bagasse as a raw material for animal feeding and fiberboard production. *Bioresource Technology* **77,** 25–32 (2001).

127. Urruzola, I., Robles, E., Serrano, L. & Labidi, J. Nanopaper from almond (Prunus dulcis) shell. *Cellulose* **21,** 1619–1629 (2014).

128. Abdul Khalil, H. P. S. *et al.* Production and modification of nanofibrillated cellulose using various mechanical processes: A review. *Carbohydrate Polymers* **99,** 649–665 (2014).

129. Samir, M. A. S. A., Alloin, F., Paillet, M. & Dufresne, A. Tangling Effect in Fibrillated Cellulose Reinforced Nanocomposites. *Macromolecules* **37,** 4313–4316 (2004).

130. Takagi, H. & Asano, A. Effects of processing conditions on flexural properties of cellulose nanofiber reinforced 'green' composites. *Composites Part A: Applied Science and Manufacturing* **39,** 685–689 (2008).

131. Yang, K.-K., Wang, X.-L. & Wang, Y.-Z. Progress in Nanocomposite of Biodegradable Polymer. *J . Ind . Eng . Chem* **13,** 485–500 (2007).

132. Rånby, B. G. Aqueous colloidal solutions of cellulose micelles. *Acta Chem. Scand.,* **3,** 649–650 (1949).

133. Bondeson, D., Mathew, A. & Oksman, K. Optimization of the isolation of nanocrystals from microcrystalline cellulose by acid hydrolysis. *Cellulose* **13,** 171–180 (2006).

134. Nakagaito, A. N., Fujimura, A., Sakai, T., Hama, Y. & Yano, H. Production of microfibrillated cellulose (MFC)-reinforced polylactic acid (PLA) nanocomposites from sheets obtained by a papermaking-like process. *Composites Science and Technology* **69,** 1293–1297 (2009).

135. Nakagaito, A. N. & Yano, H. The effect of morphological changes from pulp fiber towards nano-scale fibrillated cellulose on the mechanical properties of high-strength plant fiber based composites. *Applied Physics A: Materials Science & Processing* **78,** 547–552 (2004).

136. Nakagaito, A. N. & Yano, H. Novel high-strength biocomposites based on microfibrillated cellulose having nano-order-unit web-like network structure. *Applied Physics A* **80,** 155–159 (2005).

137. Lavoine, N., Desloges, I., Dufresne, A. & Bras, J. Microfibrillated cellulose - Its barrier properties and applications in cellulosic materials: A review. *Carbohydrate*

Polymers **90,** 735–764 (2012).

138.   Wuhrmann, K., Heuberger, A. & Mühlethaler, K. Elektronenmikroskopische Untersuchungen an Zellulosefasern nach Behandlung mit Ultraschall. *Experientia* **2,** 105–107 (1946).

139.   Turbak, A. F., Snyder, F. W. & Sandberg, K. R. Microfibrillated cellulose, a new cellulose product: properties, uses, and commercial potential. *Journal of Applied Polymer Science* **37,** Conference 9 (1983).

140.   Herrick, F. W., Casebier, R. L., Hamilton, J. K. & Sandberg, K. R. Microfibrillated Cellulose: Morphology, and Accessibility. *Journal of Applied Polymer Science* **28,** 797–813 (1983).

141.   Turbak, A. F., Snyder, F. W. & Sandberg, K. R. in *Proceedings of the Ninth Cellulose Conference, Applied Polymer Symposia* (ed. Sarko, A.) **37,** 815–827 (Wiley, 1983).

142.   Klemm, D. *et al.* Nanocelluloses: A New Family of Nature-Based Materials. *Angewandte Chemie International Edition* **50,** 5438–5466 (2011).

143.   Henriksson, M., Berglund, L. A., Isaksson, P., Lindström, T. & Takashi, N. Cellulose Nanopaper Structures of High Toughness. *Biomacromolecules* **9,** 1579–1585 (2008).

144.   Stenstad, P., Andresen, M., Tanem, B. S. & Stenius, P. Chemical surface modifications of microfibrillated cellulose. *Cellulose* **15,** 35–45 (2008).

145.   Brinchi, L., Cotana, F., Fortunati, E. & Kenny, J. M. Production of nanocrystalline cellulose from lignocellulosic biomass: Technology and applications. *Carbohydrate Polymers* **94,** 154–169 (2013).

146.   Henriksson, M., Henriksson, G., Berglund, L. A. & Lindström, T. An environmentally friendly method for enzyme-assisted preparation of microfibrillated cellulose (MFC) nanofibers. *European Polymer Journal* **43,** 3434–3441 (2007).

147.   Frone, A. N., Panaitescu, D. M. & Donescu, D. Some aspects concerning the isolation of cellulose micro- and nano- fibers. *UPB Scientific Bulletin, Series B: Chemistry and material science* **73,** 132–152 (2011).

148.   Siró, I. & Plackett, D. Microfibrillated cellulose and new nanocomposite materials: a review. *Cellulose* **17,** 459–494 (2010).

149.   Wang, Q. Q. *et al.* Morphological development of cellulose fibrils of a bleached eucalyptus pulp by mechanical fibrillation. *Cellulose* **19,** 1631–1643 (2012).

150.   Cheng, Q., Wang, S. & Rials, T. G. Poly(vinyl alcohol) nanocomposites reinforced with cellulose fibrils isolated by high intensity ultrasonication. *Composites Part A: Applied Science and Manufacturing* **40,** 218–224 (2009).

151.   Chen, P. *et al.* Concentration effects on the isolation and dynamic rheological

behavior of cellulose nanofibers via ultrasonic processing. *Cellulose* **20,** 149–157 (2013).

152. Jonoobi, M. *et al.* Different preparation methods and properties of nanostructured cellulose from various natural resources and residues: a review. *Cellulose* ASAP (2015). doi:10.1007/s10570-015-0551-0

153. Samir, M. A. S. A., Alloin, F. & Dufresne, A. Review of Recent Research into Cellulosic Whisker, Their Properties and Their Application in Nanocomposites Field. *Biomacromolecules* **6,** 612–626 (2005).

154. Andresen, M., Johansson, L.-S., Tanem, B. S. & Stenius, P. Properties and characterization of hydrophobized microfibrillated cellulose. *Cellulose* **13,** 665–677 (2006).

155. Lahiji, R. R. *et al.* Atomic Force Microscopy Characterization of Cellulose Nanocrystals. *Langmuir* **26,** 4480–4488 (2010).

156. Gindl, W. & Keckes, J. All-cellulose nanocomposite. *Polymer* **46,** 10221–10225 (2005).

157. Bondeson, D., Mathew, A. & Oksman, K. Optimization of the isolation of nanocrystals from microcrystalline cellulose by acid hydrolysis. *Cellulose* **13,** 171–180 (2006).

158. Brown, A. J. The Chemical action of Pure Cultivations of Bacterium Aceti. *Journal of the Chemical Society, Transactions* **49,** 172–187 (1864).

159. Lee, K., Buldum, G., Mantalaris, A. & Bismarck, A. More Than Meets the Eye in Bacterial Cellulose : Biosynthesis , Bioprocessing , and Applications in Advanced Fiber Composites a. *Macromolecular Bioscience* 10–32 (2014). doi:10.1002/mabi.201300298

160. Gardner, D. J., Oporto, G. S., Mills, R. & Azizi Samir, M. A. S. Adhesion and surface issues in cellulose and nanocellulose. *Journal of Adhesion Science and Technology* **22,** 545–567 (2008).

161. Heux, L., Chauve, G. & Bonini, C. Nonflocculating and Chiral-Nematic Self-ordering of Cellulose Microcrystals Suspensions in Nonpolar Solvents. *Langmuir* **16,** 8210–8212 (2000).

162. Hubbe, M. A., Rojas, O. J., Lucia, L. A. & Sain, M. CELLULOSIC NANOCOMPOSITES: A REVIEW. *BioResources* **3,** 929–980 (2008).

163. Kalia, S., Kaith, B. S. & Kaur, I. Pretreatments of natural fibers and their application as reinforcing material in polymer composites-A review. *Polymer Engineering & Science* **49,** 1253–1272 (2009).

164. Akil, H. M. *et al.* Kenaf fiber reinforced composites: A review. *Materials & Design* **32,** 4107–4121 (2011).

165. Goussé, C., Chanzy, H., Cerrada, M. L. & Fleury, E. Surface silylation of cellulose microfibrils: Preparation and rheological properties. *Polymer* **45,** 1569–1575 (2004).

166. Xu, S. H., Gu, J., Luo, Y. F. & Jia, D. M. Effects of partial replacement of silica with surface modified nanocrystalline cellulose on properties of natural rubber nanocomposites. *Express Polymer Letters* **6,** 14–25 (2012).

167. Raquez, J. M. *et al.* Surface-modification of cellulose nanowhiskers and their use as nanoreinforcers into polylactide: A sustainably-integrated approach. *Composites Science and Technology* **72,** 544–549 (2012).

168. Freire, C. S. R., Silvestre, A. J. D., Neto, C. P., Belgacem, M. N. & Gandini, A. Controlled heterogeneous modification of cellulose fibers with fatty acids: Effect of reaction conditions on the extent of esterification and fiber properties. *Journal of Applied Polymer Science* **100,** 1093–1102 (2006).

169. Saito, T., Kimura, S., Nishiyama, Y. & Isogai, A. Cellulose nanofibers prepared by TEMPO-mediated oxidation of native cellulose. *Biomacromolecules* **8,** 2485–2491 (2007).

170. Fält, S., Wågberg, L., Vesterlind, E. L. & Larsson, P. T. Model films of cellulose II - Improved preparation method and characterization of the cellulose film. *Cellulose* **11,** 151–162 (2004).

171. Malainine, M. E., Mahrouz, M. & Dufresne, A. Thermoplastic nanocomposites based on cellulose microfibrils from Opuntia ficus-indica parenchyma cell. *Composites Science and Technology* **65,** 1520–1526 (2005).

172. Njuguna, J., Pielichowski, K. & Desai, S. Nanofiller-reinforced polymer nanocomposites. *Polymers for Advanced Technologies* **19,** 947–959 (2008).

173. Kalia, S., Avérous, L., Njuguna, J., Dufresne, A. & Cherian, B. M. Natural fibers, bio- and nanocomposites. *International Journal of Polymer Science* **2011,** 2–4 (2011).

174. Biermann, C. J. *Essentials of pulping and papermaking. Essentials of pulping and papermaking.* (Academic Press, 1993).

175. Casey, J. P. *Pulp and paper : chemistry and chemical technology. Vol.3.* (Wiley, 1981).

176. Dunlop-Jones, N. in *Paper Chemistry* 98–119 (Springer Netherlands, 1996). doi:10.1007/978-94-011-0605-4_7

177. Bikerman, J. J. Causes of Poor Adhesion: Boundary Layers. *Industrial & Engineering Chemistry* **59,** 40–44 (1967).

178. Kalia, S. *et al.* Cellulose-Based Bio- and Nanocomposites: A Review. *International Journal of Polymer Science* **2011,** 1–35 (2011).

179. Oksman, K., Skrifvars, M. & Selin, J. F. Natural fibres as reinforcement in polylactic acid (PLA) composites. *Composites Science and Technology* **63,** 1317–1324 (2003).

180. Bondeson, D. & Oksman, K. Polylactic acid/cellulose whisker nanocomposites modified by polyvinyl alcohol. *Composites Part A: Applied Science and Manufacturing* **38,** 2486–2492 (2007).

181. Junior de Menezes, A., Siqueira, G., Curvelo, A. A. S. & Dufresne, A. Extrusion and characterization of functionalized cellulose whiskers reinforced polyethylene nanocomposites. *Polymer* **50,** 4552–4563 (2009).

182. Habibi, Y. *et al.* Bionanocomposites based on poly(ε-caprolactone)-grafted cellulose nanocrystals by ring-opening polymerization. *Journal of Materials Chemistry* **18,** 5002 (2008).

183. TAPPI T233 cm-06. in *Standard by Technical Association of the Pulp and Paper Industry* (2006).

184. Garcá, A. *et al.* Biorefining of lignocellulosic residues using ethanol organosolv process. *Chemical Engineering Transactions* **18,** (2009).

185. Gordobil, O., Egüés, I., Llano-Ponte, R. & Labidi, J. Physicochemical properties of PLA lignin blends. *Polymer Degradation and Stability* 1–9 (2014). doi:10.1016/j.polymdegradstab.2014.01.002

186. Li, H., Deng, Y., Ye, H., Xiao, L. & Qiu, X. Effect of Temperature on Polyelectrolyte Expansion of Lignosulfonate. *BioResources* **10,** 575–587 (2014).

187. Ibarra, D., Camarero, S., Romero, J., Martínez, M. J. & Martínez, A. T. Integrating laccase–mediator treatment into an industrial-type sequence for totally chlorine-free bleaching of eucalypt kraft pulp. *Journal of Chemical Technology & Biotechnology* **81,** 1159–1165 (2006).

188. Li, L., Lee, S., Lee, H. L. & Youn, H. J. Hydrogen peroxide bleaching of hardwood kraft pulp with adsorbed birch xylan and its effect on paper properties. *BioResources* **6,** 721–736 (2011).

189. TAPPI T257 sp-14. in *Standard by Technical Association of the Pulp and Paper Industry* (2014).

190. TAPPI T264. Tappi: Preparation of wood for chemical analysis. 3–5 (1993).

191. TAPPI T222 om-11. in *Standard by Technical Association of the Pulp and Paper Industry* (2011).

192. TAPPI T211 om-12. in *Standard by Technical Association of the Pulp and Paper Industry* (2012).

193. TAPPI T204 cm-07. in *Standard by Technical Association of the Pulp and Paper Industry* (2007).

194. TAPPI T207 cm-08. in *Standard by Technical Association of the Pulp and Paper Industry* (2008).

195. Arrazola, D. F. de M. Estudio del Contenido de Azúcares en la Piña del Agave

tequilana. (Universidad Autónoma de Puebla, 1969).

196. Espino, E. *et al.* Isolation and characterization of cellulose nanocrystals from industrial by-products of Agave tequilana and barley. *Industrial Crops and Products* **62,** 552–559 (2014).

197. Alonso-Gutiérrez, M. de la S. Valorisation de la bagasse de l'agave tequilana W. cv azul : caractérisation, étude de la digestibilité et de la fermentation des sucres. (Institut National Polythechnique de Toulouse, 2005).

198. Iñiguez-Covarrubias, G., Díaz-Teres, R., Sanjuan-Dueñas, R., Anzaldo-Hernández, J. & Rowell, R. M. Utilization of by-products from the tequila industry. Part 2: Potential value of Agave tequilana Weber azul leaves. *Bioresource Technology* **77,** 101–108 (2001).

199. Garside, P. & Wyeth, P. Identification of Cellulosic Fibres by FTIR Spectroscopy - Thread and Single Fibre Analysis by Attenuated Total Reflectance. *Studies in Conservation* **48,** 269–275 (2003).

200. Xu, F., Yu, J., Tesso, T., Dowell, F. & Wang, D. Qualitative and quantitative analysis of lignocellulosic biomass using infrared techniques: A mini-review. *Applied Energy* **104,** 801–809 (2013).

201. Watkins, D., Nuruddin, M., Hosur, M., Tcherbi-Narteh, A. & Jeelani, S. Extraction and characterization of lignin from different biomass resources. *Journal of Materials Research and Technology* **4,** 26–32 (2015).

202. Mosca Conte, A. *et al.* Role of Cellulose Oxidation in the Yellowing of Ancient Paper. *Physical Review Letters* **108,** 158301 (2012).

203. Castro, K. *et al.* Assessment of the weathering effects on cellulose based materials through a multianalytical approach. *Nuclear Instruments and Methods in Physics Research, Section B: Beam Interactions with Materials and Atoms* **269,** 1401–1410 (2011).

204. Yu, H. *et al.* Facile extraction of thermally stable cellulose nanocrystals with a high yield of 93% through hydrochloric acid hydrolysis under hydrothermal conditions. *Journal of Materials Chemistry A: Materials for Energy and Sustainability* **1,** 3938–3944 (2013).

205. Barbosa, A. *et al.* Cellulose Nanocrystal Membranes as Excipients for Drug Delivery Systems. *Materials* **9,** 1002 (2016).

206. Garcia de Rodriguez, N. L., Thielemans, W. & Dufresne, A. Sisal cellulose whiskers reinforced polyvinyl acetate nanocomposites. *Cellulose* **13,** 261–270 (2006).

207. Wang, B., Sain, M. & Oksman, K. Study of structural morphology of hemp fiber from the micro to the nanoscale. *Applied Composite Materials* **14,** 89–103 (2007).

208. von Smoluchowski, M. Contribution to the Theory of Electro-osmosis and Related Phenomena. *Bulletin International de l'Academie des Sciences de Cracovie* **3,** (1903).

209. Topalovic, T. *et al.* Analysis of the effects of catalytic bleaching on cotton. *Cellulose* **14,** 385–400 (2007).

210. Zeronian, S. H. & Inglesby, M. K. Bleaching of cellulose by hydrogen peroxide. *Cellulose* **2,** 265–272 (1995).

211. Hosemann, R. Crystallinity in high polymers, especially fibres. *Polymer* **3,** 349–392 (1962).

212. Ioelovich, M., Leykin, A. & Figovsky, O. Study of cellulose paracrystallinity. *BioResources* **5,** 1393–1407 (2010).

213. Segal, L., Creely, J. J., Martin, A. E. & Conrad, C. M. An Empirical Method for Estimating the Degree of Crystallinity of Native Cellulose Using the X-Ray Diffractometer. *Textile Research Journal* **29,** 786–794 (1959).

214. French, A. D. & Santiago Cintrón, M. Cellulose polymorphy, crystallite size, and the Segal Crystallinity Index. *Cellulose* **20,** 583–588 (2013).

215. Hult, E. L., Iversen, T. & Sugiyama, J. Characterization of the supermolecular structure of cellulose in wood pulp fibres. *Cellulose* **10,** 103–110 (2003).

216. Teeäär, R., Serimaa, R. & Paakkarl, T. Crystallinity of cellulose, as determined by CP/MAS NMR and XRD methods. *Polymer Bulletin* **17,** 231–237 (1987).

217. He, J., Cui, S. & Wang, S. Preparation and crystalline analysis of high-grade bamboo dissolving pulp for cellulose acetate. *Journal of Applied Polymer Science* **107,** 1029–1038 (2008).

218. Garvey, C. J., Parker, I. H. & Simon, G. P. On the Interpretation of X-Ray Diffraction Powder Patterns in Terms of the Nanostructure of Cellulose I Fibres. *Macromolecular Chemistry and Physics* **206,** 1568–1575 (2005).

219. Scardi, P., Leoni, M. & Beyerlein, K. R. On the modelling of the powder pattern from a nanocrystalline material. *Zeitschrift fur Kristallographie* **226,** 924–933 (2011).

220. Wada, M. & Okano, T. Localization of I α I α I α and I β I β I β phases in algal cellulose revealed by acid treatments. *Cellulose* **8,** 183–188 (2001).

221. Terinte, N., Ibbett, R. & Schuster, K. C. Overview on Native Cellulose and Microcrystalline Cellulose I Structure Studied By X-Ray Diffraction (Waxd): Comparison Between Measurement Techniques. *Lenzinger Berichte* **89,** 118–131 (2011).

222. Scherrer, P. Bestimmung der Größe und der inneren Struktur von Kolloidteilchen mittels Röntgenstrahlen. *Nachrichten von der Gesellschaft der Wissenschaften zu Göttingen, Mathematisch-Physikalische Klasse* **1918,** 98–100 (1918).

223. Langford, J. I. & Wilson, A. J. C. Scherrer after sixty years: A survey and some new results in the determination of crystallite size. *Journal of Applied Crystallography* **11,** 102–113 (1978).

224. Ungár, T. & Gubicza, J. Nanocrystalline materials studied by powder diffraction line profile analysis. *Zeitschrift für Kristallographie* **222,** 114–128 (2007).

225. Warren, B. *X-ray diffraction.* (Addison-Wesley Pub. Co., 1969).

226. Horikawa, Y. & Sugiyama, J. Localization of Crystalline Allomorphs in Cellulose Microfibril. *Biomacromolecules* **10,** 2235–2239 (2009).

227. Popa, N. C. & Balzar, D. Size-broadening anisotropy in whole powder pattern fitting. Application to zinc oxide and interpretation of the apparent crystallites in terms of physical models. *J. Appl. Cryst. J. Appl. Cryst* **41,** 615–627 (2008).

228. Park, S., Baker, J. O., Himmel, M. E., Parilla, P. A. & Johnson, D. K. Cellulose crystallinity index: measurement techniques and their impact on interpreting cellulase performance. *Biotechnology for biofuels* **3,** 10 (2010).

229. Boissou, F. *et al.* Transition of cellulose crystalline structure in biodegradable mixtures of renewably-sourced levulinate alkyl ammonium ionic liquids, γ-valerolactone and water. *Green Chemistry* **16,** 2463 (2014).

230. Isogai, A. & Atalla, R. H. Dissolution of Cellulose in Aqueous NaOH Solutions. *Cellulose* **5,** 309–319 (1998).

231. Abitbol, T., Kloser, E. & Gray, D. G. Estimation of the surface sulfur content of cellulose nanocrystals prepared by sulfuric acid hydrolysis. *Cellulose* **20,** 785–794 (2013).

232. Han, J., Zhou, C., Wu, Y., Liu, F. & Wu, Q. Self-Assembling Behavior of Cellulose Nanoparticles during Freeze- Drying: E ff ect of Suspension Concentration, Particle Size, Crystal Structure, and Surface Charge. (2013).

233. Tonoli, G. H. D. *et al.* Cellulose micro/nanofibres from Eucalyptus kraft pulp: Preparation and properties. *Carbohydrate Polymers* **89,** 80–88 (2012).

234. Lee, C. M. *et al.* Cellulose polymorphism study with sum-frequency-generation (SFG) vibration spectroscopy: identification of exocyclic CH2OH conformation and chain orientation. *Cellulose* **20,** 991–1000 (2013).

235. Fernandes, A. N. *et al.* Nanostructure of cellulose microfibrils in spruce wood. *Proceedings of the National Academy of Sciences of the United States of America* **108,** E1195-203 (2011).

236. Yuan, Z., Kapu, N. S., Beatson, R., Chang, X. F. & Martinez, D. M. Effect of alkaline pre-extraction of hemicelluloses and silica on kraft pulping of bamboo (Neosinocalamus affinis Keng). *Industrial Crops and Products* **91,** 66–75 (2016).

237. Bordeanu, N., Eyhozler, C. & Zimmermann, T. Surface modified cellulose nanofibrils. **1,** 1–18 (2010).

238. ASTM E1131-08. *Standard Test Method for Compositional Analysis by Thermogravimetry.* (2014).

239. Owens, D. K. & Wendt, R. C. Estimation of the surface free energy of polymers. *Journal of Applied Polymer Science* **13,** 1741–1747 (1969).

240. Rabel, W. Einige Aspekte der Benetzungstheorie und ihre Anwendung auf die Untersuchung und Veränderung der Oberflächeneigenschaften von Polymeren. *Farbe und Lack* **77,** 997–1005 (1971).

241. Kaelble, D. H. Dispersion-Polar Surface Tension Properties of Organic Solids. *The Journal of Adhesion* **2,** 66–81 (1970).

242. Paunikallio, T., Suvanto, M. & Pakkanen, T. T. Viscose fiber/polyamide 12 composites: Novel gas-phase method for the modification of cellulose fibers with an aminosilane coupling agent. *Journal of Applied Polymer Science* **102,** 4478–4483 (2006).

243. Liu, H. & Zhang, L. Silylation of Cellulose with Trichlorosilane and Triethoxysilane in Homogeneous LiCl/N,n-Dimethylacetamide Solution. *Chinese Journal of Polymer Science* **18,** 161–168 (2000).

244. Thanomchat, S. & Schlarb, A. K. Morphology and Crystallization of Polypropylene / Microfibrillated Cellulose Composites. **7,** 23–34 (2014).

245. Shabir, Q. *et al.* Medically Biodegradable Hydrogenated Amorphous Silicon Microspheres. *Silicon* **3,** 173–176 (2011).

246. Linck, C. *et al.* Corrosion behavior of silicon oxycarbide-based ceramic nanocomposites under hydrothermal conditions. *International Journal of Materials Research* **103,** 31–39 (2012).

247. Çetin, N. S. *et al.* Acetylation of cellulose nanowhiskers with vinyl acetate under moderate conditions. *Macromolecular Bioscience* **9,** 997–1003 (2009).

248. Missoum, K., Bras, J. & Belgacem, M. N. Organization of aliphatic chains grafted on nanofibrillated cellulose and influence on final properties. *Cellulose* **19,** 1957–1973 (2012).

249. Roche, V. *et al.* Tracking the fate of ??-aminopropyltriethoxysilane from the sol state to the dried film state. *Thin Solid Films* **518,** 3640–3645 (2010).

250. Fadeev, A. Y. & McCarthy, T. J. Trialkylsilane monolayers covalently attached to silicon surfaces: Wettability studies indicating that molecular topography contributes to contact angle hysteresis. *Langmuir* **15,** 3759–3766 (1999).

251. Dankovich, T. A. & Gray, D. G. Contact Angle Measurements on Smooth Nanocrystalline Cellulose (I) Thin Films. *Journal of Adhesion Science and Technology* **25,** 699–708 (2011).

252. Jandas, P. J., Mohanty, S. & Nayak, S. K. Surface treated banana fiber reinforced poly (lactic acid) nanocomposites for disposable applications. *Journal of Cleaner Production* **52,** 392–401 (2013).

253. Garlotta, D. A Literature Review of Poly (Lactic Acid). **9,** (2002).

254. Han, S. O. *et al.* Understanding the Reinforcing Mechanisms in Kenaf Fiber/PLA and Kenaf Fiber/PP Composites: A Comparative Study. *International Journal of Polymer Science* **2012,** 1–8 (2012).

255. Auras, R. a., Harte, B., Selke, S. & Hernandez, R. Mechanical, Physical, and Barrier Properties of Poly(Lactide) Films. *Journal of Plastic Film and Sheeting* **19,** 123–135 (2003).

256. Jamshidian, M., Tehrany, E. A., Imran, M., Jacquot, M. & Desobry, S. Poly-Lactic Acid: Production, applications, nanocomposites, and release studies. *Comprehensive Reviews in Food Science and Food Safety* **9,** 552–571 (2010).

257. Kowalczyk, M., Piorkowska, E., Kulpinski, P. & Pracella, M. Mechanical and thermal properties of PLA composites with cellulose nanofibers and standard size fibers. *Composites Part A: Applied Science and Manufacturing* **42,** 1509–1514 (2011).

258. Bondeson, D. & Oksman, K. Polylactic acid/cellulose whisker nanocomposites modified by polyvinyl alcohol. *Composites Part A: Applied Science and Manufacturing* **38,** 2486–2492 (2007).

259. Zhang, W., Zhang, X., Liang, M. & Lu, C. Mechanochemical preparation of surface-acetylated cellulose powder to enhance mechanical properties of cellulose-filler-reinforced NR vulcanizates. *Composites Science and Technology* **68,** 2479–2484 (2008).

260. Frone, A. N., Berlioz, S., Chailan, J. F. & Panaitescu, D. M. Morphology and thermal properties of PLA-cellulose nanofibers composites. *Carbohydrate Polymers* **91,** 377–384 (2013).

261. ASTM E96/E96M-14. *Standard Test Methods for Water Vapor Transmission of Materials.* (2014).

262. Cho, M.-J. & Park, B.-D. Tensile and thermal properties of nanocellulose-reinforced poly(vinyl alcohol) nanocomposites. *Journal of Industrial and Engineering Chemistry* **17,** 36–40 (2011).

263. Sehaqui, H., Zhou, Q., Ikkala, O. & Berglund, L. a. Strong and tough cellulose nanopaper with high specific surface area and porosity. *Biomacromolecules* **12,** 3638–3644 (2011).

264. Sehaqui, H., Allais, M., Zhou, Q. & Berglund, L. A. Wood cellulose biocomposites with fibrous structures at micro- and nanoscale. *Composites Science and Technology* **71,** 382–387 (2011).

265. Salaberria, A. M., Diaz, R. H., Labidi, J. & Fernandes, S. C. M. Role of chitin nanocrystals and nanofibers on physical, mechanical and functional properties in thermoplastic starch films. *Food Hydrocolloids* **46,** 93–102 (2015).

266. Entsar I. Rabea, †, Mohamed E.-T. Badawy, †, Christian V. Stevens, *,‡, Guy

Smagghe, † and & Steurbaut†, W. Chitosan as Antimicrobial Agent: Applications and Mode of Action. (2003). doi:10.1021/BM034130M

267. Kong, L.-A. *et al.* Different Chitin Synthase Genes Are Required for Various Developmental and Plant Infection Processes in the Rice Blast Fungus Magnaporthe oryzae. *PLoS Pathogens* **8,** e1002526 (2012).

268. Krajewska, B., Wydro, P. & Jańczyk, A. Probing the Modes of Antibacterial Activity of Chitosan. Effects of pH and Molecular Weight on Chitosan Interactions with Membrane Lipids in Langmuir Films. *Biomacromolecules* **12,** 4144–4152 (2011).

269. Krajewska, B., Wydro, P. & Kyzioł, A. Chitosan as a subphase disturbant of membrane lipid monolayers. The effect of temperature at varying pH: I. DPPG. *Colloids and Surfaces A: Physicochemical and Engineering Aspects* **434,** 349–358 (2013).

270. Salaberria, A. M., Fernandes, S. C. M., Diaz, R. H. & Labidi, J. Processing of α-chitin nanofibers by dynamic high pressure homogenization: Characterization and antifungal activity against A. niger. *Carbohydrate Polymers* (2014). doi:10.1016/j.carbpol.2014.04.047

271. Ziani, K., Fernández-Pan, I., Royo, M. & Maté, J. I. Antifungal activity of films and solutions based on chitosan against typical seed fungi. *Food Hydrocolloids* **23,** 2309–2314 (2009).

272. Shen, D. K. & Gu, S. The mechanism for thermal decomposition of cellulose and its main products. *Bioresource Technology* **100,** 6496–6504 (2009).

273. Rodionova, G., Lenes, M., Eriksen, Ø. & Gregersen, Ø. Surface chemical modification of microfibrillated cellulose: Improvement of barrier properties for packaging applications. *Cellulose* **18,** 127–134 (2011).

274. Wijesena, R. N., Tissera, N., Perera, R. & de Silva, K. M. N. Side selective surface modification of chitin nanofibers on anionically modified cotton fabrics. *Carbohydrate Polymers* **109,** 56–63 (2014).

275. Robles, E., Salaberria, A. M., Herrera, R., Fernandes, S. C. M. & Labidi, J. Self-bonded composite films based on cellulose nanofibers and chitin nanocrystals as antifungal materials. *Carbohydrate Polymers* **144,** 41–49 (2016).

276. Standard, T., Standard, O., Method, O. T. & The, T. Water absorptiveness of sized (non-bibulous) paper , paperboard , and corrugated fiberboard (Cobb test). *Tappi* 1–6 (2009).

277. Box, P. O. & Wageningen, A. D. Water uptake and freeze stability test. 1–9 (2013).

278. EN 622-1:2004. in *European Comitee for Standarization* (2010).

279. Alvarez-López, C., Rojas, O. J., Rojano, B. & Gañán, P. Development of Self-Bonded Fiberboards from Fiber of Leaf Plantain: Effect of Water and Organic Extractives Removal. *BioResources* **10,** 672–683 (2014).

280. Nonaka, S., Umemura, K. & Kawai, S. Characterization of bagasse binderless particleboard manufactured in high-temperature range. *Journal of Wood Science* **59,** 50–56 (2013).

281. Mejía, E. H., Quintana, G. C. & Ogunsile, B. O. Development of Binderless Fiberboards from Steam- exploded and Oxidized Oil Palm Wastes. *Bioresources.com* **9,** 2922–2936 (2014).

282. Zheng, Y., Pan, Z., Zhang, R., Jenkins, B. M. & Blunk, S. Properties of medium-density particleboard from saline Athel wood. *Industrial Crops and Products* **23,** 318–326 (2006).

283. Tabarsa, T., Ashori, A. & Gholamzadeh, M. Evaluation of surface roughness and mechanical properties of particleboard panels made from bagasse. *Composites Part B: Engineering* **42,** 1330–1335 (2011).

284. Nielsen, N. P. K., Gardner, D. J. & Felby, C. Effect of extractives and storage on the pelletizing process of sawdust. *Fuel* **89,** 94–98 (2010).

285. Kowaluk, G. PROPERTIES OF LIGNOCELLULOSIC COMPOSITES CONTAINING REGENERATED CELLULOSE FIBERS. **9,** 5339–5348 (2014).

286. Kowaluk, G., Fuczek, D., Beer, P. & Grześkiewicz, M. Influence of the raw materials and production parameters on chosen standards properties for furniture panels of biocomponents from fibrous chips. *BioResources* **6,** 3004–3018 (2011).

287. Ali, I., Jayaraman, K. & Bhattacharyya, D. Implications of fiber characteristics and mat densification on permeability, compaction and properties of kenaf fiber panels. *Industrial Crops and Products* **61,** 293–302 (2014).

Appendices

Appendix A: Reagents and equipments used

Reagents used

1.1   Sodium Hydroxide pellets (NaOH) M = 40.00, PanReac AppliChem (Germany).

1.2   Acetic Acid glacial, for synthesis (CH_3CO_2H) 99.5%, M = 60.05, PanReac AppliChem (Germany).

1.3   Sodium Chlorite solution for synthesis ($NaClO_2$) 25% w/w, M = 90.44, PanReac AppliChem (Germany).

1.4   Ethanol absolute (C_2H_5OH), 99.99 % v/v, M = 46.07, Sharlab (Spain).

1.5   Magnesium sulfate ($MgSO_4$) 97%, M = 120.36, Acros organics (Belgium).

1.6   Diethylenetriaminepentaacetic acid ($C_{14}H_{23}N_3O_{10}$) 98%, M = 393.35, Alfa Aesar (USA).

1.7   Hydrogen Peroxide for analysis (H_2O_2), 30 % w/v, M = 34.01, PanReac AppliChem (Germany).

1.8   Pyridine-2,6-dicarboxylic acid ($C_7H_5NO_4$), 98 %, M = 167.12, Alfa Aesar (USA).

1.9   Sulfuric Acid for analysis (H_2SO_4) 96 %, M = 98.08, PanReac AppliChem (Germany).

1.10   Hydrochloric Acid (HCl) 37 %, M = 36.46, PanReac AppliChem (Germany).

1.11   (3-Aminopropyl)triethoxysilane ($C_9H_{23}NO_3Si$) 98 %, M = 221.37, Alfa Aesar (USA).

1.12   Dodecanoyl chloride ($C_{12}H_{23}ClO$), 97.5 %, M = 218.76, Fluka® Analytical (Germany).

1.13   Toluene (C_7H_8) 99.5 %, M = 92.14, Fisher Scientific (England).

1.14   Pyridine (C_5H_5N), 99 %, M = 79.1, Fisher Scientific (England).

Reactors

1.15   EL0723 4 L batch stainless steel reactor, Iberfluid Instruments (Spain).

Filtration systems

1.16   6274 Stainless Steel Pressure Filter Holder with Barrel, Sartoruis Stedim (Germany).

Homogenizing equipments

1.17 R100S-D Overhead stirrer, CAT Scientific (USA).

1.18 Silent Crusher M, Heidolph (Germany).

1.19 NS1001L Panda laboratory homogenizer, Niro Soavi (Italy).

1.20 Elmasonic S 70 (H) Sonication bath, Elma Schmidbauer (Germany).

1.21 Sonoplus S3200 Ultrasonic homogenizer, Bandelin (Germany).

1.22 Vibra-Cell™ VC 750 Ultrasonic Liquid Processor, Sonics & Materials (USA).

Centrifuges

1.23   Meditronic BL-S with 7001087 rotor, Selecta (Spain).

Pressing systems

1.24   PH-1LP25 hydraulic press (500x500), ZUP-NYSA (Poland).

1.25   PH-1P125 hydraulic press (500x500), ZUP-NYSA (Poland).

1.26   200 t, 4 pillars hydropneumatic molding press (600x600), Santec (India).

1.27   5-932 hydraulic press (600x600), Siempelkamp (Germany).

Extrusion systems

1.28   Haake Minilab twin-screw extruder

Microscopes

1.29   Eclipse E600, Nikon Corporation (Japan).

1.30   Dino-Lite Digital Microscope, AnMo Electronics Corporation (Taiwan).

1.31   Multimode TM-AFM with NanoScope IIIa controller; Digital instruments Inc. (USA), Veeco Instruments Inc. (USA), Bruker (Germany).

1.32   Dimension Icon® Atomic Force Microscope System with NanoScope V controller; Digital instruments Inc. (USA), Bruker (Germany).

1.33   S-3400N Scanning electron microscope, Hitachi (Japan).

1.34   JSM-6400 F Scanning electron microscope, JEOL (Japan).

Cell counting devices

1.35   Cellometer® Mini, Nexcelom Bioscience LLC (USA).

Colorimeters

1.36   MiniScan XE Plus reflection colorimeter, HunterLab (USA).

1.37   504 spectrodensitometer, X-Rite (USA).

Spectrometers

1.38   16 PC FT-IR fourier transform infrared spectrophotometer with a MKII Golden Gate™ Single Reflection ATR System; Perkin-Elmer (USA), Specac (England).

1.39   Spectrum Two FT-IR Spectrometer with a L1050231 Universal Attenuated Total Reflectance accessory, Perkin-Elmer (USA).

1.40   AVANCE-500 Digital NMR spectrometer, Bruker (Germany).

Dynamic light scattering devices

1.41   BI-200SM Laser Light Scattering System, Brookhaven Instruments Corporation (USA).

1.42   Zetasizer Nano ZS, Malvern (England).

X-ray diffractometers

1.43   X'Pert PRO multipurpose diffractometer, PANalytical (Netherlands).

Mechanical testing machines

1.44   MTS 10 Insight material testing system, MTS Systems Corporation, (USA).

1.45   3369 Dual column universal testing system, Instron (USA).

1.46   Autoline tearing tester, Lorentzen & Wettre (Sweden).

1.47   Autoline Bursting Strength meter, Lorentzen &Wettre (Sweden).

1.48   PPS 78 Parker Print-Surf tester, Messmer Büchel BV (Britain).

1.49   RM.01 Kodak-Pathè type stiffness tester, Creusot-Loire Instrumentation/Adamel Lhomargy instrument, (France).

Thermal calorimeters

1.50   TGA/SDTA851e Thermogravimetric Analyzer, Mettler-Toledo (Switzerland).

1.51   DSC822e Differential Scanning Calorimeter, Mettler-Toledo (Switzerland).

1.52   Pyris 6. Perkin Elmer thermogravimetric analyzer

Contact angle systems

1.53   PGx Portable contact angle meter, Henniker Plasma (United Kingdom).

1.54   OCA20 Contact angle system, DataPhysics (Germany).

1.55   Phoenix 300 Touch contact angle, Surface Electro Optics (Korea).

Permeability systems

1.56   OX-TRAN 2/21 OTR test system, MOCON (USA).

Densitometers

1.57   DA-X direct scanning X-ray densitometer, Grecon (Germany).

List of Figures

apparition of new signals at ~10, 25 and 40 ppm correspond to the propyl and ethyl carbons of ATS.

List of Tables

The possibility of evolving traditional industry to full-developed bioindustries represents both a responsibility and a challenge for any scientist, as in ancestral customs and techniques it can be found the future, but is with integral approaches that agroindustry would be a fundamental part of human industrial chains, it is for this reason that the present work was done, to provide final products based in value-added agroindustrial side-streams, therefore showing the feasibility to obtain diverse materials with diverse applications starting from the smallest particles present in plant cell-wall, cellulose nanostructures are here extracted and modified, in an exciting quest to give them new properties and to face then against their nature by modifying their surface with silanes and with fatty acids. I hope the reader will find this pages of scientific interest, but also as a tale of one man finding himself in this world that is the academic world.

Eduardo ROBLES

eman ta zabal zazu

Universidad
del País Vasco

Euskal Herriko
Unibertsitatea

Donostia 2017